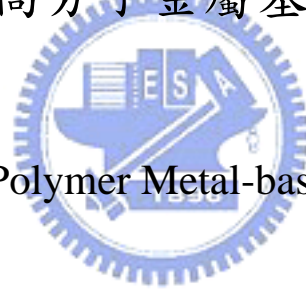


國立交通大學

物理研究所

博士論文

垂直式高分子金屬基極電晶體



Vertical Polymer Metal-base Transistor

研究生：趙宇強

指導教授：孟心飛 教授

中華民國九十七年七月

垂直式高分子金屬基極電晶體

Vertical Polymer Metal-base Transistor

研究生：趙宇強

Student : Yu-Chiang Chao

指導教授：孟心飛

Advisor : Hsin-Fei Meng

國立交通大學

物理研究所

博士論文



Submitted to Institute of Physics

College of Science

National Chiao Tung University

in partial Fulfillment of the Requirements

for the Degree of

Doctor of Philosophy

in

Physics

July 2008

Hsinchu, Taiwan, Republic of China

中華民國九十七年七月

垂直式高分子金屬基極電晶體

學生：趙宇強

指導教授：孟心飛 教授

國立交通大學物理研究所博士班

摘 要

本論文旨在實現新穎有機電子元件並且探討其特性。本論文展示了高分子熱載子電晶體與高分子空間電荷限制電晶體這兩種垂直式高分子金屬基極電晶體，以及一種發光高分子空間電荷限制電晶體。首先將討論具有不同射極材料的高分子熱載子電晶體。當熱載子電晶體使用具有高能隙之高分子為射極材料時，共射電流增益為 25。當元件使用具有低能隙之高分子為射極材料時，共射電流增益為 31 且輸出電流密度為 31 mA/cm^2 。當元件的射極材料是混合有低能隙與高能隙的高分子時，電流密度可以達到 428 mA/cm^2 。使用此電晶體去驅動高分子發光二極體時，可以達到 3000 cd/m^2 的亮度。接著將討論高分子空間電荷限制電晶體的操作原理與特性。柵極上的孔洞大小與孔洞密度可以控制空間電荷限制電晶體的操作特性。在高真空下退火與增加絕緣層於柵極旁更可提升高分子空間電荷限制電晶體的特性。目前高分子空間電荷限制電晶體的最大輸出電流密度是 27 mA/cm^2 ，開關比為 428，電流增益約為 10^4 。最後將討論由上發光高分子發光二極體垂直堆疊於高分子空間電荷限制電晶體所製成之發光高分子空間電荷限制電晶體。當柵極電壓調變於 -0.9 伏到 0.9 伏時，發光強度將可以被調變並且最亮可達 1208 cd/m^2 。此發光高分子空間電荷限制電晶體的電流效率為 10 cd/A 。由於向上發出的光將不會被在下方的高分子金屬基極電晶體所阻擋，當電晶體與發光二極體面積相同時，基本上可以達到 100 % 的開口率。

Vertical Polymer Metal-base Transistor

student : Yu-Chiang Chao

Advisors : Dr. Hsin-Fei Meng

Institute of Phycis
National Chiao Tung University

ABSTRACT

This dissertation aims to realize and characterize novel organic electronic devices. Two vertical polymer metal-base transistors, namely polymer hot-carrier transistor and polymer space-charge-limited transistor, and one light-emitting polymer space-charge-limited transistor are demonstrated. First, polymer hot-carrier transistors with various emitter materials are discussed. For the metal-base hot-carrier transistor with high bandgap emitter, common-emitter current gain of 25 is obtained. For the metal-base hot-carrier transistor with low bandgap emitter, common-emitter current gain of 31 and the current density as high as 31 mA/cm^2 are obtained. Furthermore, for the device using blend of high and low bandgap polymer as the emitter, the current density 428 mA/cm^2 is achieved. The brightness of 3000 cd/m^2 is obtained as a polymer light-emitting diode is driven by the hot-carrier transistor. Second, operation principles and electrical properties of the polymer space-charge-limited transistor are studied. The characteristics of the transistor can be tuned by the diameters and the density of the openings on the grid. Annealing in high vacuum as well as adding insulator on grid metal can further enhance the performance of the polymer space-charge-limited transistor. So far, output current density is about 27 mA/cm^2 , on/off ratio is 428, and current gain is around 10^4 . Finally, a light-emitting polymer space-charge-limited transistor is realized by vertically stacking a top-emitting polymer light-emitting diode on a polymer space-charge-limited transistor. As the grid base voltage varies from -0.9 V to 0.9 V , the light emission is turned on and off with on luminance up to 1208 cd/m^2 . The current efficiency of the light-emitting transistor is 10 cd/A . The aperture ratio is basically 100 % because the light emitted upward is not shielded by the vertical metal-base transistor underneath with roughly the same area.

Acknowledgments

I would like to express my sincere appreciation to my thesis advisor, *Professor Hsin-Fei Meng*, for providing me countless opportunities, original thinking, extensive supports, and helpful guidance throughout this research work. I am grateful for his commitment in providing his students effective environment and broad experience. He was always willing to encourage me to conquer obstacles. Numerous critical discussions are also appreciated.

Professor Sheng-Fu Horng, Professor Chain-Shu Hsu, Professor Yu-Tai Tao, Professor Ray-Nien Kwo, Professor Hsiao-Wen Zan, and Professor Heh-Nan Lin are appreciated for their suggestions and comments on this thesis.

I would like to express my gratitude to all current and former PhD and Master students who cooperated with me throughout my past four years. Especially for those who have had a positive influence on my work.

Finally, I especially thank my family members for their unconditional support and patience. I feel a deep sense of gratitude for my parents. They have always been supportive to me at their best in my life. I now realize how much I still have to learn from their admirable tenacity.

Thank you all. ~~

Yu-Chiang Chao

July 9, 2008

Contents

Abstract	viii
Acknowledgements	x
Contents	xi
List of Figures	xv
1 Introduction	1
1.1 Organic materials.....	2
1.1.1 Polymers.....	2
1.1.2 Small molecular weight materials.....	5
1.2 Fundamental organic electronics.....	8
1.2.1 Organic light-emitting diodes.....	8
1.2.2 Organic photovoltaics.....	11
1.2.3 Organic field-effect transistors.....	14
1.3 Motivation.....	17
1.4 Overview of the thesis.....	19
2 Theoretical background	21
2.1 Semiconducting polymer.....	21
2.1.1 Molecular orbital and bonding.....	21
2.1.2 Electronic excitations.....	25
2.2 Metal/organic interface.....	28
2.2.1 Energy band diagram.....	28
2.2.2 Image-force lowering.....	30
2.3 Carrier injection and transport.....	32
2.3.1 Injection limitation at the contact.....	32

2.3.2	Transport limitation in the bulk.....	34
2.4	Recombination and emission process.....	39
2.4.1	Exciton formation and decay.....	39
2.4.2	Quantum efficiency.....	40
2.5	Operation principles of related devices.....	42
2.5.1	Field-effect transistors.....	42
2.5.2	Bipolar junction transistors.....	43
2.5.3	Metal-base transistors.....	45
2.5.4	Permeable-base transistors.....	46
2.5.5	Static-induction transistors.....	48
2.5.6	Vacuum tube triodes.....	51
3	Polymer hot-carrier transistor	53
3.1	Introduction.....	53
3.1.1	Background.....	53
3.1.2	Organization of this chapter.....	55
3.2	Polymer hot-carrier transistor with high bandgap emitter.....	55
3.2.1	Motivation.....	55
3.2.2	Device structure and fabrication.....	56
3.2.3	Electrical characteristics.....	59
3.2.4	Summary of section 3.2.....	61
3.3	Polymer hot-carrier transistor with low bandgap emitter.....	61
3.3.1	Motivation.....	61
3.3.2	Device structure and fabrication.....	63
3.3.3	The effect of the insulating layer thickness.....	65
3.3.4	The effect of the emitter-base diode current density.....	67
3.3.5	Electrical characteristics.....	68
3.3.6	Frequency response.....	69
3.3.7	Summary of section 3.3.....	70
3.4	Polymer hot-carrier transistor with a blend of low and high bandgap materials as emitter.....	71
3.4.1	Motivation.....	71

3.4.2	Device structure and fabrication.....	71
3.4.3	Electrical characteristics.....	72
3.4.4	Connection between the polymer hot-carrier transistor and a polymer light-emitting diode.....	72
3.4.5	Summary of section 3.4.....	74
3.5	Summary of chapter 3.....	74
4	Polymer space-charge-limited transistor	76
4.1	Introduction.....	76
4.1.1	Background.....	76
4.1.2	Organization of this chapter.....	78
4.2	Polymer space-charge-limited transistor with low current density.....	78
4.2.1	Motivation.....	78
4.2.2	Device structure and fabrication.....	79
4.2.3	Spin-coated polystyrene spheres as shadow mask.....	82
4.2.4	Device characteristics.....	83
4.2.5	The effect of the opening diameter and density.....	85
4.2.6	Summary of section 4.2.....	86
4.3	Polymer space-charge-limited transistor with high current density.....	87
4.3.1	Motivation.....	87
4.3.2	Device structure and fabrication.....	87
4.3.3	High density polystyrene spheres as shadow mask.....	89
4.3.4	Electrical characteristics.....	90
4.3.5	Operation mechanism.....	94
4.3.6	Summary of section 4.3.....	97
4.4	Summary of chapter 4.....	97
5	Light-emitting polymer space-charge-limited transistor	99
5.1	Introduction and motivation.....	99
5.2	Device structure and fabrication.....	101
5.3	Electrical and optical characteristics.....	104
5.3.1	High performance polymer space-charge-limited transistor...	104
5.3.2	Light-emitting polymer space-charge-limited transistor.....	106

5.4 Summary of chapter 5.....	108
6 Conclusions	110
References	113



List of Figures

1.1	Molecular structure of widely used conjugated polymers.....	4
1.2	Molecular structure of widely used small molecular weight materials.....	7
1.3	Structure of a single-layer polymer electroluminescent diode.....	10
1.4	Schematic energy level diagram for an ITO/PPV/Al LED.....	10
1.5	Evolution of organic light-emitting diode structures.....	10
1.6	Four device architectures of conjugated polymer-based photovoltaic cells.....	12
1.7	Schematic of the bottom-gate organic field-effect transistors with various structures.....	15
1.8	Crystallite structure in polythiophenes.....	16
2.1	Structures of trans- and cis-polyacetylene.....	22
2.2	sp^2 -hybridized atom.....	23
2.3	Formation of σ bond and π bond.....	23
2.4	The energy levels of a π -conjugated molecule.....	24
2.5	Period doubling in dimerized chain.....	25
2.6	Schematic form of a neutral soliton on a trans-polyacetylene chain.....	26
2.7	Electronic structure leading to various charge and spin state of a soliton.....	26
2.8	Schematic energy band diagrams for polarons and bipolarons.....	27
2.9	Energy band diagram of a metal-semiconductor contact.....	29
2.10	Energy band diagrams of rectifying metal / n-type semiconductor contact.....	29
2.11	The energy band diagram for the interface between a metal surface and a vacuum.....	31
2.12	Basic steps of electroluminescence.....	40
2.13	A schematic representation of the elementary processes.....	41
2.14	A p-n-p bipolar transistor.....	44
2.15	Energy-band diagram of a metal-base transistor.....	46

2.16	Structures of a permeable-base transistor.....	47
2.17	Energy-band diagrams of a permeable-base transistor.....	48
2.18	Various schemes for the structure of static-induction transistor.....	49
2.19	Energy-band diagram from source to drain in the middle of the channel between gates.....	50
2.20	Structure of a vacuum-tube triode.....	52
3.1	The structures and energy band diagram of polymer hot-carrier transistor with high bandgap emitter.....	57
3.2	The I-V curves of emitter-base and base-collector diodes.....	60
3.3	The characteristics of the polymer hot-carrier metal-base transistor in common-emitter configuration.....	60
3.4	The characteristics of the polymer hot-carrier metal-base transistor in common-emitter configuration.....	61
3.5	The structures and energy band diagram of polymer hot-carrier transistor with low bandgap emitter.....	64
3.6	The current gain β as a function of LiF thickness of the hot-carrier transistor.....	66
3.7	The AFM image of Al base on P3HT.....	66
3.8	The current gain β as a function of EB diode current density at 4 V.....	68
3.9	The base voltage of various devices with different emitter thickness.....	68
3.10	The characteristics of the polymer hot-carrier transistor in common emitter configuration.....	69
3.11	Frequency response of the hot-carrier transistor.....	70
3.12	The characteristics of the polymer hot-carrier transistor in common emitter configuration.....	73
3.13	Connection between hot-carrier transistor and polymer light-emitting diode.....	73
3.14	The luminance of the polymer light-emitting diode driven by the polymer hot-carrier transistor.....	74
4.1	Device structure and energy band diagram of the polymer space-charge-limited transistor.....	80
4.2	The potential profile of the transistor.....	81
4.3	The AFM images of the Al grid.....	83
4.4	Collector current I_C and grid current I_G as a function of collector voltage V_C at different grid bias V_G of device with 2000 Å openings	

on Al grid.....	84
4.5 $(-I_c)^{1/2}$ against $-V_c$ when $V_G = 0.5$ V.....	85
4.6 The characteristics of the polymer space-charge-limited transistor.....	86
4.7 Device structure and energy band diagram of polymer space-charge-limited transistor with an Al grid with random submicron openings.....	88
4.8 Al grid with various opening diameter.....	91
4.9 The electric characteristics of the polymer space-charge-limited transistor with various grid voltages applied.....	93
4.10 The device structure near one opening and operation principle of polymer space-charge-limited transistor.....	96
5.1 Device structure of the polymer space-charge-limited transistor.....	102
5.2 Device structure of the top-emitting polymer light-emitting transistor....	103
5.3 Energy profile of the top-emitting polymer light-emitting transistor.....	103
5.4 The electric characteristics of the polymer space-charge-limited transistor with 2000 Å openings on Al grid.....	105
5.5 The efficiency and luminance of the top-emitting polymer light-emitting diode.....	107
5.6 The electric characteristics of the polymer light-emitting transistor with 1000 Å and 2000 Å openings on Al grid.....	107

Chapter 1

Introduction

The goal of this introductory chapter is to provide the reader with a concise introduction of organic materials and devices. Material properties and optoelectronic properties of organic electronic materials, including small molecular weight materials and polymer, are introduced and discussed. Benefits and drawbacks of current state-of-the-art in organic devices and processing technology are also surveyed. Its intention is not to provide a complete description of organic materials and devices, but rather, it aims to provide springboards for further reading through the references that are cited.

In Section 1.1, many organic electronic materials and organic semiconductors will be introduced. Development history of the organic materials is also provided in this section.

In Section 1.2, the current state-of-the-art in organic electronics is summarized and the remaining challenges are outlined. Discussion in this section is focus on organic light-emitting diodes, organic photovoltaics, and organic field-effect transistors. The techniques utilized for fabricating organic electronics and photonic devices are briefly introduced. In addition to commonly used preparation methods, some aspects that make organic electronics unique are also included in this section.

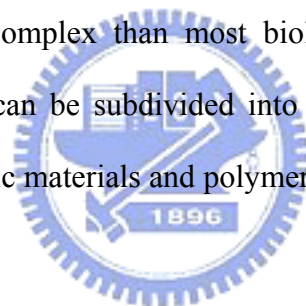
After introducing various organic materials and devices, in Section 1.3, a

summary of the challenges and motivations of this research work is present.

Finally, in Section 1.4, we overview the topics present in this thesis for various reader's interests.

1.1 Organic materials

Every living organism is made of organic chemicals. The food you eat; the medicines you take; and the wood, paper, plastics, and fibers that make modern life possible are all organic chemicals. However, only those molecules have pronounced optical and electrical qualities can be utilized for electronics. In general, the organic electronic materials that find use in organic electronics are more complex than simple organic materials, but less complex than most biological materials. The class of organic electronic materials can be subdivided into two clearly distinct categories: small molecular weight organic materials and polymers.



1.1.1 Polymers

The conventional polymer is largely used due to their plastic deformability, mechanical strength, low weight, and usually high resistivity. These characteristics allowed plastic materials enter every sector of our civilization, from low cost simple utilities to highly sophisticated technologies such as aircraft construction. Ever since the polymer became important in technology, their usefulness can be significantly enhanced if their conductivity could be raised. Metal could then be replaced by light and easily processible materials.

At the beginning of the 1970s, the Japanese chemist Shirakawa found that it was possible to synthesize polyacetylene $(CH)_n$ in a new way. Shirakawa synthesized trans-polyacetylene by accidentally adding “a thousand-fold too much catalyst” to the reaction vessel. To Shirakawa's surprise, this time a beautiful silvery film appeared.

Shirakawa was stimulated by this discovery. The corresponding reaction at another temperature gave a copper-colored film instead, and it appeared to consist of almost pure *cis*-polyacetylene. Around the same time chemist Alan G. MacDiarmid and physicist Alan J. Heeger were experimenting with a metallic-looking film of the inorganic polymer sulphur nitride, (SN)_x. When MacDiarmid heard about Shirakawa's discovery at a seminar in Tokyo, he invited Shirakawa to the University of Pennsylvania in Philadelphia. After Shirakawa and MacDiarmid modified polyacetylene by oxidation with iodine vapor, they knew that the optical properties changed in the oxidation process and asked Heeger to have a look at the films. After measured the conductivity of the iodine-doped *trans*-polyacetylene, the incredible increase of ten million times the original conductivity was discovered. In the summer of 1977, Alan Heeger, Alan MacDiarmid and Hideki Shirakawa, and co-workers, published their discovery in the article "Synthesis of electrically conducting organic polymers: Halogen derivatives of polyacetylene (CH)_n" in The Journal of Chemical Society, Chemical Communications.[1] The discovery was considered a major breakthrough, and Alan Heeger, Alan MacDiarmid and Hideki Shirakawa have been awarded the Nobel Prize in Chemistry in the year 2000 for showing how plastic can be made to conduct electric current.[2] Since then the field has grown immensely, and also given rise to many new and exciting applications.

The properties of a polymer are strongly related to the physical arrangement of monomers along the backbone of the chain. Polymers which contain only one type of monomer are known as homopolymers, while polymers containing a mixture of monomers are known as copolymers.

The conducting conjugated polymer consists of a long chain of carbon atoms with alternating single and double bonds between them, each with one hydrogen atom. The structure of polyacetylene is shown in Fig. 1.1(a) as a typical example.

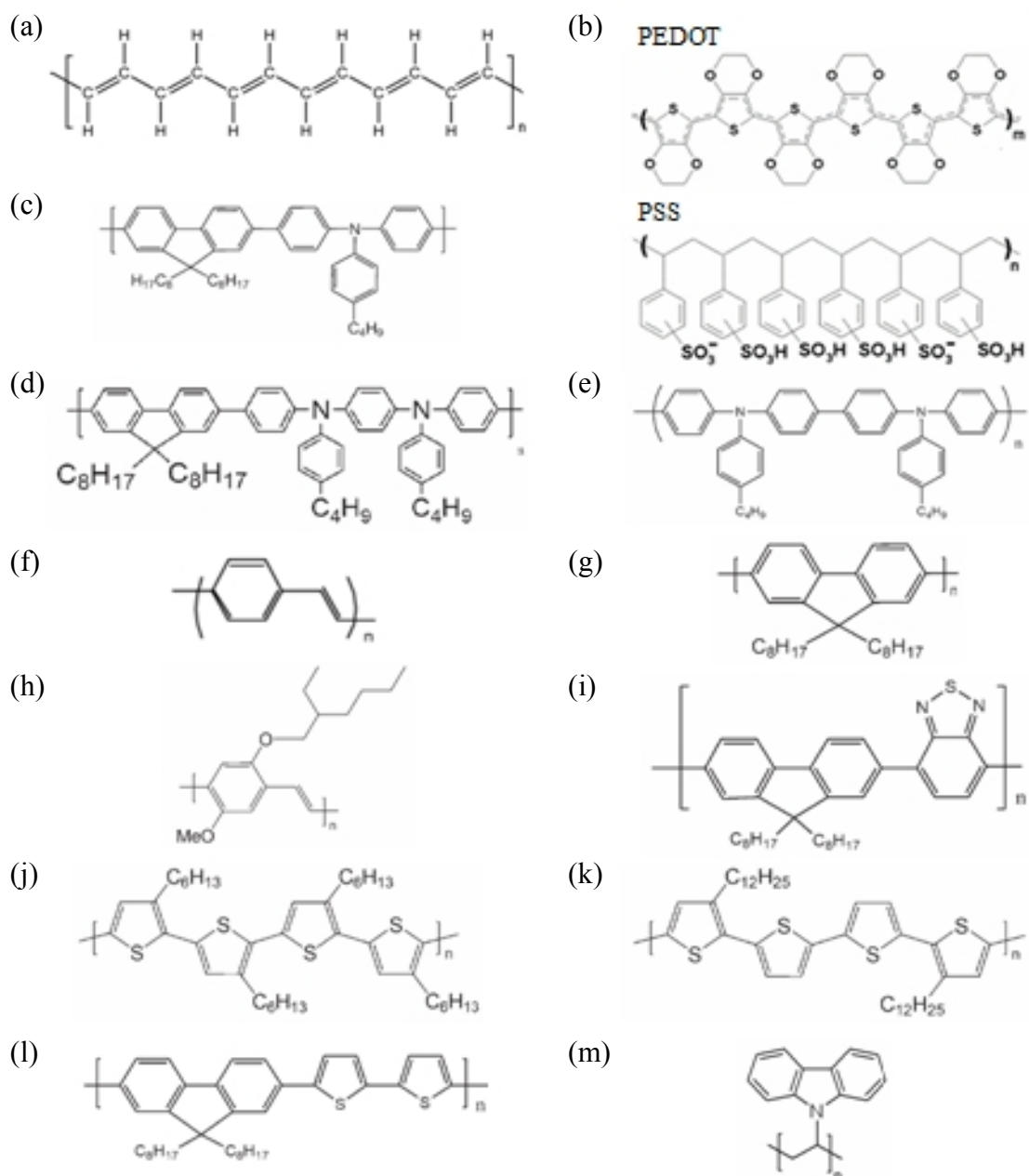


Figure 1.1 Molecular structure of widely used conjugated polymers: (a) polyacetylene; (b) poly(3,4-ethylenedioxythiophene) : poly(styrenesulfonate) (PEDOT:PSS); (c) poly(9,9-dioctylfluorene-co-N-(4-butylphenyl)diphenylamine) (TFB); (d) poly(9,9-dioctylfluorene-co-bis-N,N-(4-butylphenyl)-bis-N,N-phenyl-1,4-phenylenediamine) (PFB); (e) poly[N,N'-bis(4-butylphenyl)-N,N'-bis(phenyl)-benzidine] (polyTPD); (f) poly(p-phenylenevinylene) (PPV); (g) poly[9,9-dioctylfluorenyl-2,7-diyl] (PFO); (h) poly-[2-methoxy,(5-2'-ethyl-hexyloxy)-p-phenylenevinylene] (MEH-PPV); (i) poly(9,9-dioctylfluorene-co-benzothiadiazole) (F8BT); (j) poly[3-hexylthiophene] (P3HT); (k) poly[5,5'-bis(3-alkyl-2-thienyl)-2,2'-bithiophene] (PQT); (l) poly[(9,9-dioctylfluorene-co-bithiophene)] (F8T2); (m) poly(9-vinylcarbazole) (PVK).

Polyacetylene is usually prepared in the cis- form which can be converted into the thermodynamically more stable trans- form by thermal isomerization.

Other semiconducting conjugated polymers shown in Fig. 1.1 are commonly used in organic light-emitting diodes (OLEDs), organic field-effect transistors (FETs), and organic solar cells. As shown in Fig. 1.1(b), PEDOT:PSS is a water-soluble transparent conducting polymer, which enabled the fabrication of all plastic polymer light-emitting diodes (PLEDs). PEDOT:PSS can be used as a transparent anode. Currently, it serves as the hole transport layer to develop PLEDs for commercial products.

Structures of PPV and PPV derivatives (MEH-PPV) are shown in Fig. 1.1(f) and 1.1(h). The most commonly used PPV is typically deposited by spin coating a precursor polymer, and then thermal treatment is used to convert the precursor to PPV. PPV also used as hosts for low gap emitter.[3] PFO is also the material used in the blue PLEDs as shown in Fig. 1.1(g). Following the first blue PFO-based PLED was developed in 1991 [4], efforts was conducted on developing commercially viable devices based on these polymer.

Polythiophenes and P3HT-based PLEDs and FETs are widely studied.[5,6] Due to it relatively low gap, the polythiophenes are red emitters. However, the relatively poor lifetime of polythiophene-based PLEDs inhibits their commercialization. On the other hand, P3HT is a commonly used material in FETs. Under proper treatment, the mobility can be increased and the performance of the FETs can be optimized.

1.1.2 Small molecular weight materials

The phenomenon of organic electroluminescence was first discovered by Pope in 1963.[7] But, the development of organic light-emitting diode actually began in the late 1970s by Tang and coworkers. Their research led eventually to the discovery of

the first efficient multi-layered organic electroluminescent device.[8] Since then, tremendous progress has been made in the field of organic electroluminescence. Among all efforts to improve the performance of organic light-emitting diode, the continuing discovery of new and improved electroluminescent materials is the most essential one.

Small molecular weight materials consist of molecules with several to a few hundred atoms. Small molecular weight materials were the initial focus of physicists and engineers who seeking to understand the optoelectronics properties of organic materials. Structure of some small molecular weight materials are shown in Fig. 1.2.

Fig. 1.2(a) shows the structure of CuPC which is widely used as an hole transport layer. However, depending on the other layer, it may inhibit hole injection [9] or enhance it [10]. TPD is another material commonly used as hole transport layer as shown in Fig. 1.2(b). But, its relatively low glass transition temperature around 65°C causes a failure of OLED as TPD recrystallized. The recrystallization may be suppressed by adding guest molecule such as rubrene. However, it may result in red electroluminescence from rubrene. Hence, NPB is developed with a structure similar to TPD but the methylphenyl groups are replaced by naphthylphenyls. The modification significantly enhance the stability of the OLED due to the increased glass transition temperature around 95°C.

Alq3 is the most widely used electron-transport and host emitting material in OLEDs. It is still one of the most robust electron-transport backing layers in OLED, particularly with the help of the hole blocking layer to trap the hole carriers from injecting into Alq3.[11] It is not only commonly used as a green emitter, but also as a host for lower-gap emitter guest molecules. It has been found by the time-of-flight technique that the drift mobility of electrons in Alq3 is increased by about two orders of magnitude (to 10^{-4} cm²/Vs) as the deposition rate decreased from 0.7 to 0.2 nm/s.

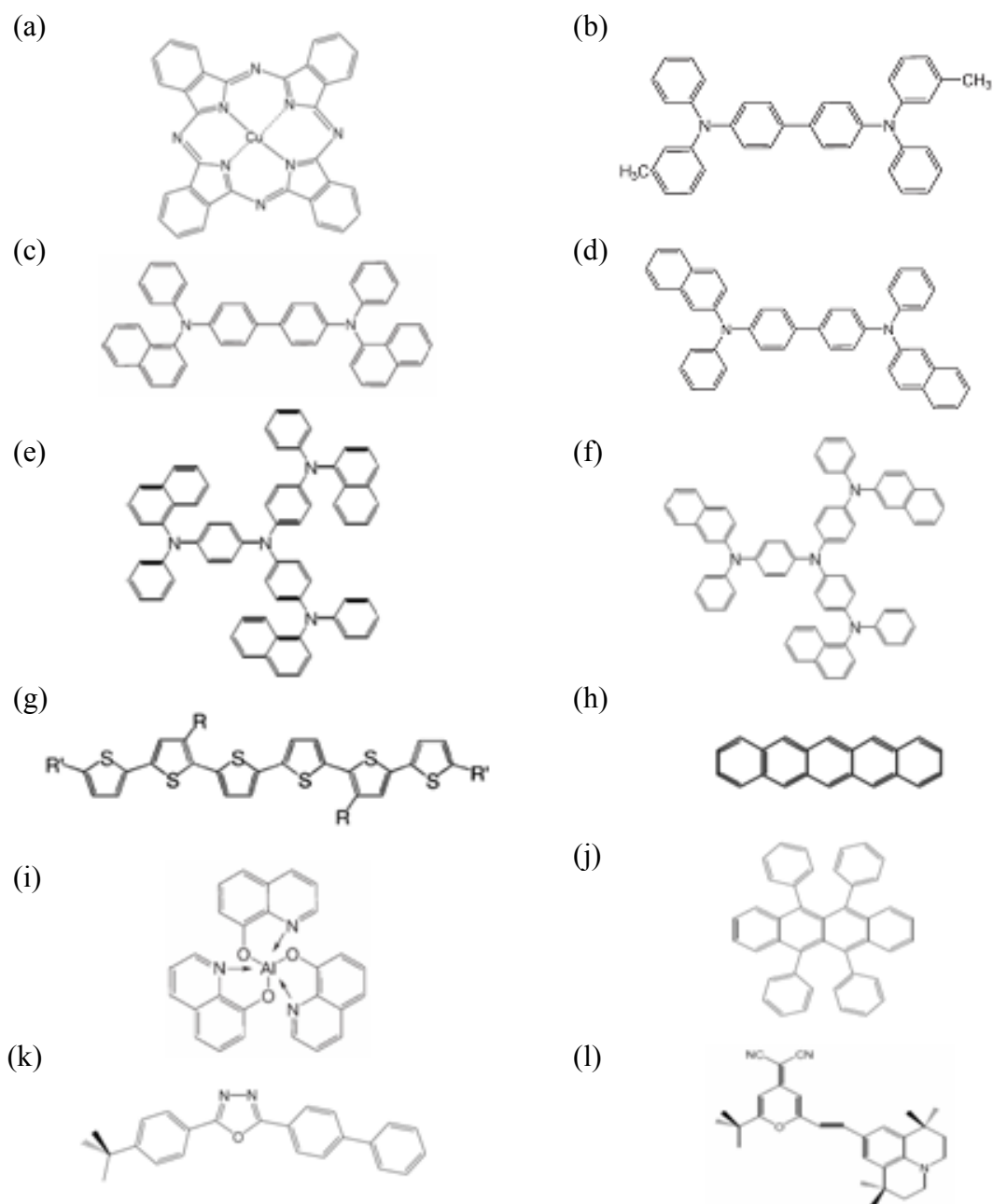


Figure 1.2 Molecular structure of widely used small molecular weight materials: (a) copper phthalocyanine (CuPC); (b) N,N'-Bis(3-methylphenyl)-N,N'-bis(phenyl)-benzidine (TPD); (c) N,N'-bis(1-naphthalenyl)-N,N'-bis(phenylbenzidine) (α -NPB); (d) N,N'-bis(2-naphthalenyl)-N,N'-bis(phenylbenzidine) (β -NPB); (e) 4,4',4''-Tris(N-(1-naphthyl)-N-phenyl-amino)triphenylamine (1T-NATA); (f) 4,4',4''-Tris(N-(2-naphthyl)-N-phenyl-amino)triphenylamine (2T-NATA); (g) α -sexthiophene (α -6T); (h) Pentacene; (i) Tris(8-hydroxyquinoline) Aluminum (Alq3T); (j) (5,6,11,12)-Tetraphenylnaphthacene (Rubrene); (k) 2-(4-Biphenyl)-5-(4-tert-butylphenyl)-1,3,4-oxadiazole (PBD); (l) 4-(Dicyanomethylene)-2-tert-butyl-6-(1,1,7,7-tetramethyljulolidin-4-yl-vinyl)-4H-pyran (DCJTb).

1.2 Fundamental organic electronics

Inorganic silicon and gallium arsenide semiconductors have been the backbone of the semiconductor industry for the past forty years. Now, a research area named organic electronics is growing with improved conducting, semiconducting, and light-emitting properties. Through novel synthesis and self-assembly techniques, performance of the organic electronics has been improved to a large extent. Unique technologies and new applications are expected because of the ability to process these organic materials at low temperatures over large areas on materials such as plastic or paper.

Organic transistor circuits are being investigated for a number of low-cost, large-area applications. The utilization of organic materials opens up several possibilities to develop integrated circuit technologies based on organic transistors. [12] Organic field-effect transistors have been developed for applications such as display drivers, radio-frequency identification tags [13], and sensors [14]. Organic transistors have also been integrated with optical devices for optoelectronics.[15-18]

In this section we introduce several research areas and concepts that are important for our discussion of electronic devices in the following chapters.

1.2.1 Organic light-emitting diodes

During the past two decades, organic light-emitting diodes (OLEDs) have attracted considerable interest owing to their promising applications in flat-panel displays by replacing cathode ray tube or liquid crystal displays. Another promising usage of OLEDs is for general white lighting. Electroluminescence is the emission of light from materials in an electric field. An important breakthrough was achieved in 1987 by Kodak scientist.[8] They discovered that sending an electrical current

through an organic compound caused these materials to glow. Another important development was achieved at University of Cambridge.[19] Electroluminescence from conjugated polymers was first reported in 1990, using poly(p-phenylene vinylene), PPV, as the single semiconductor layer between metallic electrodes, as is illustrated in Fig. 1.3. A schematic energy-level diagram for a PPV LED under forward bias is shown in Fig. 1.4. Based on these important findings, many companies and institutions start to pursue display applications with organic materials. Research continues to focus on perfecting materials to produce better color, require less power and last longer. The key advantages of OLEDs for flat-panel display applications are their self-emitting property, high luminous efficiency, full color capability, wide viewing angle, high contrast, low power consumption, low weight, and flexibility.

The historical evolution of OLED architectures is shown in Fig. 1.5. Initially, a simple monolayer structure is utilized, as in Fig. 1.3. The ITO layer functions as a transparent electrode, and allows the light generated within the diode to leave the device. The top electrode is formed by thermal evaporation of a metal. Electroluminescence is achieved when the diode is biased sufficiently to achieve injection of positive and negative charge carriers from opposite electrodes. Recombination of oppositely charged carriers within the region of the polymer layer can then result in photon emission.

Since the breakthrough of the Kodak group, more and more layer layers have been used with various functions. As shown in Fig. 1.5, it has been demonstrated that the electroluminescence efficiency of OLEDs can be increased by carrier or exciton confinement within a multilayer device.[20] Another promising approach for low-power display technology is to combine electrically doped transport layers and a phosphorescent-doped emitting layer in a diode structure called a p-i-n junction.[21] Multilayer PLED made by solution process are also realized.[22]

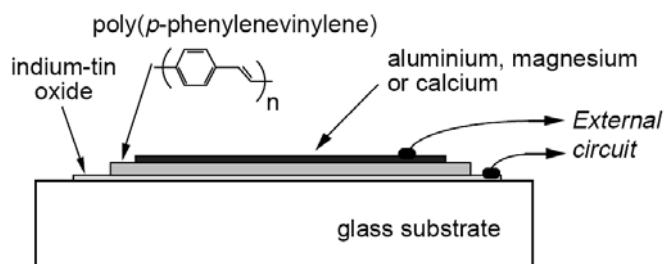


Figure 1.3 Structure of a single-layer polymer electroluminescent diode. From Ref. [3].

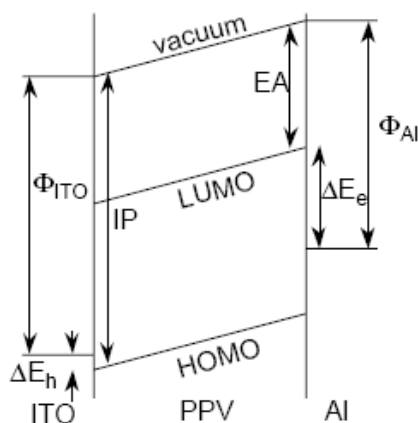


Figure 1.4 Schematic energy level diagram for an ITO/PPV/Al LED, showing the ionization potential (IP) and electron affinity (EA) of PPV, the work functions of ITO and Al (ϕ_{ITO} and ϕ_{Al}), and the barriers to injection of electrons and holes (ΔE_e and ΔE_h). From Ref. [3]

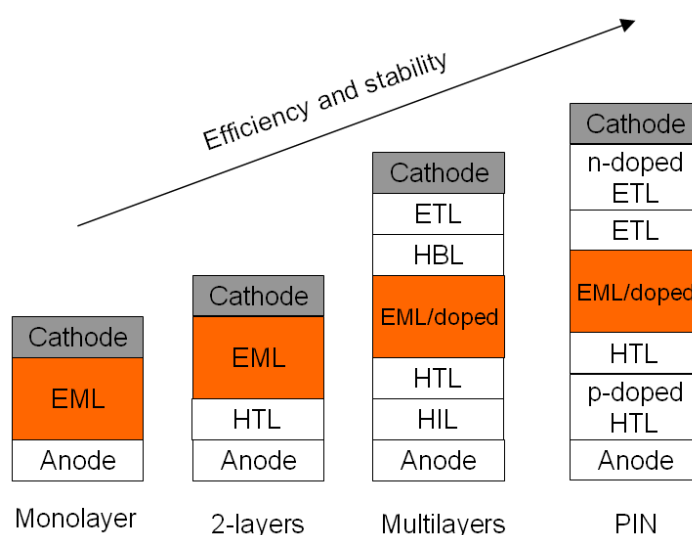


Figure 1.5 Evolution of organic light-emitting diode structures (HIL=hole injecting layer, HTL=hole transporting layer, EML=emitting layer, HBL=hole blocking layer, ETL=electron transporting layer).

1.2.2 Organic photovoltaics

Solar energy is a possible alternative to fossil fuels. Even solar energy presently generate only a small fraction of the world's electricity, that fraction is projected to grow to 10% or more by 2040. There are three main types of silicon solar cells in production: silicon wafer based, compound crystalline, and thin-film solar cells. Currently, crystalline silicon solar cells are the predominant technology which accounting for 80-85% of all cells manufactured. However, for silicon solar cells, significant fraction of the cost of solar cells comes from the photoactive materials and sophisticated processing technologies.

Recently, it has been shown that the inorganic materials utilized in solar cells can be replaced by semiconducting polymers which is capable of achieving reasonably high power conversion efficiencies. These polymers are inexpensive and can be solution-processed with high throughput. These organic solar cells could provide electricity at a lower cost than crystalline silicon solar cells if a reasonable power efficiency and lifetime could be achieved.

One of the first organic solar cells based on conjugated polymer is made by a spin coated polymer film sandwiched between two metal electrodes with different work functions, as shown in Fig. 1.6(a).[23] In most cases the open-circuit voltage was roughly equal to the work function difference between the top and bottom electrodes divided by the charge of an electron. Since the exciton diffusion length for most organic solar cell materials is below 20 nm, only those excitons generated in a small region within 20 nm from the contacts contribute to the photocurrent. Although single-layer solar cells are easy to fabricate, its photocurrent is very low.

Figure 1.6(b) shows a bilayer device, a donor and an acceptor material are stacked together with a planar interface. The bilayer is sandwiched between two

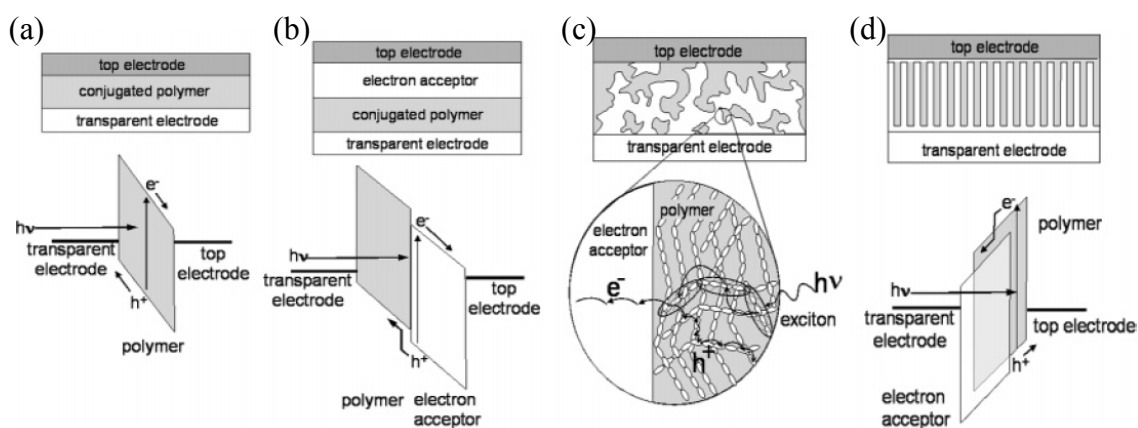


Figure 1.6 Four device architectures of conjugated polymer-based photovoltaic cells: (a) single-layer PV cell; (b) bilayer PV cell; (c) disordered bulk heterojunction; (d) ordered bulk heterojunction. From Ref. [24]

electrodes matching the highest occupied molecular orbital (HOMO) of donor and the lowest unoccupied molecular orbital (LUMO) of acceptor, for efficient extraction of the corresponding charge carriers.[25] The charge separation occurs in the interface which has a large potential drop between donor and acceptor. Upon photon absorption in the donor, excitons generated within a few nanometers of the heterojunction and excitons could diffuse to the interface. If an acceptor molecule is in close proximity, the electron may be transferred to the LUMO of acceptor. This process of forward charge transfer led to the spatial separation of the electron and hole, thereby preventing direct recombination and allowing the transport of electrons to one electrode and holes to the other. However, the carrier transit time to electrode is long if the organic layer is thick or the mobility of the organic material is low.

To circumvent the problem of low exciton diffusion length, the bulk heterojunction device is developed to intimately mix the donor and acceptor components in a bulk volume so that each donor–acceptor interface is within a distance less than the exciton diffusion length of each absorbing site.[26] The bulk heterojunction device is similar to the bilayer device with respect to the donor-acceptor concept, but it exhibits a largely increased interfacial area where

charge separation occurs. Due to the interface being dispersed throughout the bulk, no loss due to too small exciton diffusion lengths is expected, because ideally all excitons will be dissociated within their lifetime.[24] Though in the bilayer heterojunction the donor and acceptor phase contact the anode and cathode selectively, the bulk heterojunction requires percolated pathways for the hole and electron transporting phases to the contacts. Therefore, the bulk heterojunction devices are much more sensitive to the nanoscale morphology in the blend, which will be discussed in more detail below.

Another kind of bulk heterojunction solar cell that has recently received attention is the conjugated polymer-titania (TiO_2) solar cell. Although TiO_2 does not absorb visible light, it indeed have some potential advantages as an electron-accepting material. The most attractive aspect of using TiO_2 with a conjugated polymer in a solar cell is the fact that the TiO_2 can be patterned into a continuous network for electron transport.[27,28] A continuous network for electron transport should allow a fairly high volume fraction of the conjugated polymer to be used in films, as long as the TiO_2 and polymer can be structured so that excitons can be dissociated effectively. Other reasons to use TiO_2 are that it is nontoxic, many molecules can be attached to its surface, and it has been used to make dye-sensitized solar cells with up to 10% power efficiency.

In solar cells made from conjugated polymers and TiO_2 , it is generally the case that electrons are transported to the transparent bottom electrode. Similarly, holes are transported to the top electrode. In these cells it is advantageous to use a high-work-function metal such as gold as the top electrode to provide an ohmic contact to the HOMO of the polymer. Besides, the method of making a thin nanoporous TiO_2 film and then filling it in with conjugated polymer has the advantage of producing two truly bicontinuous phases in the solar cell.

1.2.3 Organic field-effect transistors

The beginning of the electronics age was marked by cathode ray tube, vacuum rectifier, and vacuum-tube triode. The triode, includes a grid between the anode and the cathode, transformed the rectifier into an amplifier, and made the radio communication and long-distance telephone come true. However, the vacuum-tube triode was fragile, slow, and difficult to miniaturize.

Replacing the triode with a solid-state device offering an alternative to the thermionic principle is thus a good idea for solving problems of triode. This concept was successfully demonstrated with Bardeen and Brattain's point-contact transistor and Shockley's bipolar transistor. After material technology research for more than forty years, the performance of metal-oxide-semiconductor field-effect transistor (MOSFET) is optimized. Today, MOSFETs dominated almost every electronic device.

Recently, organic field-effect transistors (OFETs) based on solution-processible polymeric as well as small molecular semiconductors have obtained impressive improvements in their performance. Even an all polymer transistor has been reported.[29] Initially, because of the poor performance of these initial devices, interest in organic transistors remained limited. Following a continuing effort, the carrier mobility was improved. Several review papers and books describing the materials, operating principles, and fabrication processes have been published for comprehensive understanding.[30-37]

Organic field-effect transistors have been developed to realize low-cost, large-area electronic devices. OFETs have been developed with various device geometries as depicted in Figure 1.7. The most commonly used device geometry is bottom gate with top contact partly because of using thermally grown Si/SiO₂ oxide as gate dielectric. Devices based on glass substrate are also demonstrated for possible

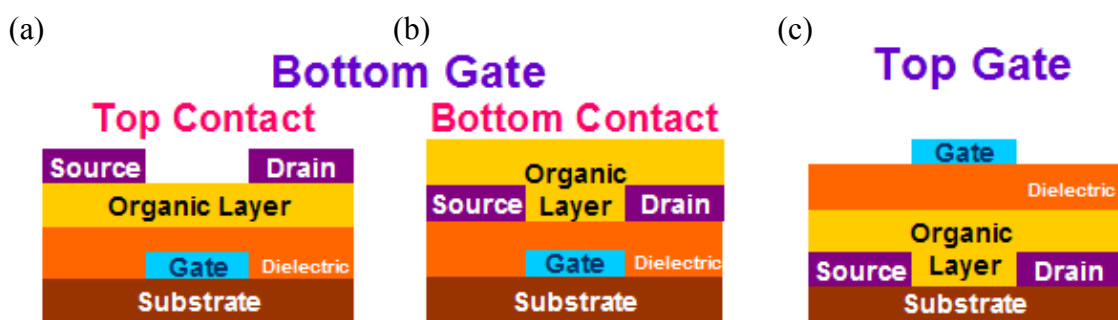


Figure 1.7 Schematic of the bottom-gate organic field-effect transistors with (a) top contact or (b) bottom contact structures. (c) Schematic diagram of a (c) top-gate with bottom contact transistor using a standard TFT device structures.

integration with organic light-emitting diodes. Another immediate opportunity is to use organic dielectric for the top-gate structured OFET. The solution for the organic dielectric can be properly chosen such that it will not destroy the underlying organic semiconductors. Top-gate bottom contact structure devices allow patterning the bottom source-drain electrodes on top of any flexible or rigid substrate first. Take the most commonly used OFET device configuration as example. The organic semiconductor is deposited on top of a dielectric with an underlying gate electrode. Current between source and drain electrodes is measured when no voltage is applied between the gate and source electrodes (off state). When a voltage is applied to the gate, electrons or holes can be induced at the semiconductor-dielectric interface and the source-drain current increases.

Carrier mobilities in organic semiconductors are limited by the hopping process between the molecules in disordered regions of the material. Many research works have examined the effects of modifying molecular parameters (regioregularity [38], molecular weight [39], and side-chain length [40]) and processing conditions (film thickness [41], doping level [42], thermal annealing [43], and the film-forming method [44]). Studies of semiconductor/insulator interface phenomena (such as surface-mediated molecular ordering, surface dipoles, semiconductor alignment using

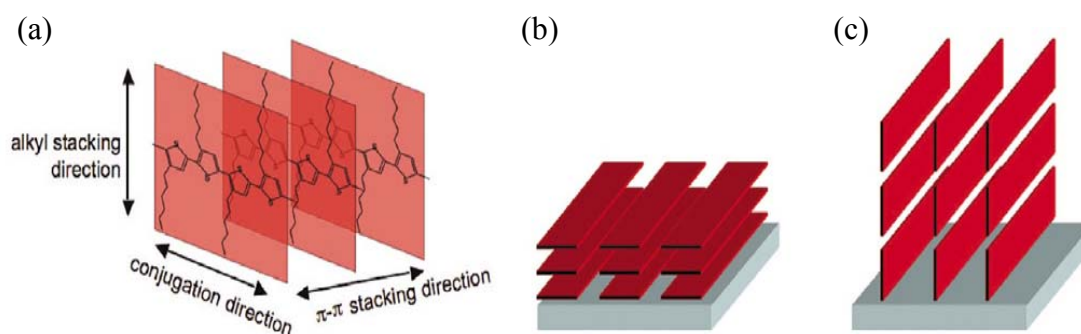


Figure 1.8 (a) Crystallite structure in polythiophenes. The conjugation direction and the π - π stacking direction are fast charge transport directions. Charge transport in the alkyl stacking direction is slower. (b) Plane-on and (c) edge-on texture of polymeric crystallites. In the plane-on texture, the alkyl stacking direction is in the plane of the substrate, which is bad for the current density in TFTs. From Ref. [31]

self-assembled monolayers (SAMs), physical treatment, and photoalignment) are also receiving attention for enhancing the electrical properties of organic semiconductors. SAMs are highly ordered, two-dimensional structures that form spontaneously on a variety of surfaces. Tuning of the interfacial surface can be achieved by varying the rigidity, length, and terminal functional group of the molecule, which in turn affects the uniformity, packing, conformation, polarity, and charge density of the surface.

Fluorene copolymers and polythiophenes have a relatively rigid backbone with attached alkyl chains for solubility, and are able to crystallize. Mobility is highly anisotropic as a result of chain packing in the crystallites. Charge transport is fastest in the conjugation direction as shown in Fig. 1.8(a). When chains pack, the π -orbitals belonging to different polymer chains are stacked cofacially, and this partial overlap between π -orbitals assists interchain charge transfer. However, in another direction, the insulating alkyl chains impede charge transport so that mobility in this direction is the lowest. Such anisotropy has been experimentally verified by comparing the electrical characteristics of TFTs and diodes. Because of this pronounced anisotropy, texture and relative orientation of crystallites are expected to play an important role in controlling the electrical properties of these materials.

1.3 Motivation

One of the key components of the flexible electronics is FET, a horizontal device with source and drain electrodes on the same plane. The current ratio in the on and off states (on/off ratio) and the field-effect mobility are two parameters to characterize the organic field-effect transistors. So far the organic FET shows low current output because of the intrinsically low carrier mobility due to the weak wavefunction overlaps between the molecules and the disorder in the thin film. The low mobility also strongly limits the operation speed to be under 100 kHz. Furthermore, the organic FET is unstable because the conduction channel is confined to a few monolayers at the semiconductor-dielectric interface where the adsorbed oxygen, moisture, and other chemicals have huge effect on the transistor characteristics. To obtain a desired current output, its operating voltage usually exceeds 20 volts. A great deal of effort was made in to improve the performance of the field-effect transistors by increasing the mobility, reducing the gate dielectrics thickness, and reducing the channel lengths.

For new material developments, many new organic molecules have been designed and synthesized.[45-51] Pentacene represents one of the most studied molecule for FET application. Under favorable fabrication conditions, mobilities as high as $5 \text{ cm}^2\text{V}^{-1}\text{s}^{-1}$ have been reported.[45] Much progress has also been made in polymeric materials.[52,53] So far the highest mobility for polymer is about $1 \text{ cm}^2\text{V}^{-1}\text{s}^{-1}$. [52] While these values are still far below that offered by inorganic semiconductors, some are appropriate for some low-end applications. One way to reduce the operating voltage is utilizing a self-assembled monolayer (SAM) as gate dielectric with gate current densities as low as 10^{-9} Acm^{-2} . [54,55] With these dielectrics, the transistor can be operated with voltages of 2 V. The devices is however sensitive to the pin-holes in SAM and not highly reproducible. Lithography

upon SAM is also difficult. Organic field-effect transistors with submicron channel lengths made by electron-beam lithography [56], nanoimprint lithography [57] and soft contact lamination [58] have been demonstrated. Vertical organic field-effect transistors, whose channel length was determined by the thickness of an insulating layer between source and drain, have been made by solid-state embossing [59], excimer laser [60] and photolithography [61]. However, these procedures to reduce the channel length are complicated and expensive. So far the organic FET still suffers from low mobility, high voltage and low speed. The unique promises of organic materials such as low-cost and large-area solution process not yet realized by high-performance field-effect transistors.

Vertical non-field-effect transistors with multilayer sandwich structures give another route to circumvent the limits of organic field-effect transistors. In vertical non-field-effect transistors, the channel length can be made small easily because of it is defined by the thickness of the organic layers. The current is modulated by a conductive metal layer embedded in the organic materials. Various device operating principles were proposed with different types of conductive layers such as a thin metal film [62,63], a strip-type metal film [64,65], a mesh gate electrode [66-68], and a porous conducting polymer network.[69] The remaining problems are the low current density, low on/off ratio as well as the complex fabrication process.

In order to tackle the major challenge for organic transistors, that is, low mobility of most organic materials, molecular or polymeric, we have invented two new metal-base organic transistors with vertical structure. One is based on the concept of hot carrier ballistic transport in the base [70,71], and another one is a solid-state analogy of vacuum tube which we call space-charge-limited transistor [72,73]. Operation principles and device structures of these two vertical metal-base organic transistors are discussed below. They show good performance including low voltage,

high current output and high speed with easy fabrication. The polymer light-emitting transistor is also realized by vertically stacking a top-emitting polymer light-emitting diode on a polymer space-charge-limited transistor. Uniform luminance is achieved and the aperture ratio is basically 100%. Detail descriptions will be given in the following chapters.

1.4 Overview of the thesis

The main theme of this thesis is the characterization of two metal-base transistors with vertical structure. A polymer light-emitting transistor, which is realized by vertically stacking a top-emitting polymer light-emitting diode on a polymer space-charge-limited transistor, is also characterized.

In Chapter 2, useful information which serves as a reference materials for the remainder of this thesis are provided. Physics of conjugated organic materials are reviewed in Section 2.1. How charge carriers inject into the materials through metal/organic interface and how charge carriers transport in the organic molecules are discussed in Section 2.2 and Section 2.3 respectively. For devices with opposite charged carriers, exciton formation and the luminous efficiency are introduced in Section 2.4. Other relevant devices and device physics are reviewed in Section 2.5. Many useful references are cited.

Polymer hot-carrier transistors with various emitter materials are discussed in Chapter 3. For the emitter material with high band gap, electrical properties and fabrication procedures are described in Section 3.2, while Section 3.3 discusses the hot-carrier transistors with low band gap emitter. The properties of the hot-carrier transistor with a blend polymer as emitter are described in Section 3.4. Optical response of a polymer light-emitting diode connected to the hot-carrier transistor are

also shown in Section 3.4

Polymer space-charge-limited transistors with different fabrication procedures and properties are discussed in Chapter 4. The electrical properties of the transistor with low opening density is described in Section 4.2, while Section 4.3 describe the electrical properties of transistor with high opening density. Fabrication procedure of the grid electrode is also described in detail.

Light-emitting polymer space-charge-limited transistor is described in Chapter 5. It is realized by vertically stacking a top-emitting polymer light-emitting diode on a polymer space-charge-limited transistor. Fabrication procedures, electrical response and optical response are discussed in Section 5.3 and Section 5.4 respectively.

In the final Chapter, the results of our experiments are concluded. Suggestions are also given for further studies on vertical metal-base transistors.



Chapter 2

Theoretical background

We are interested in the invention and fabrication of novel organic devices with all kinds of operation principles. In this chapter, fundamental polymer physics and device physics required for this thesis are introduced. Section 2.1 introduces molecular orbital and electronic excitations. Information about the interface is discussed in Section 2.2. Section 2.3 discusses the charge injection and transport. After opposite charged carrier injected into the semiconductor, the formation of exciton and the quantum efficiency are discussed in Section 2.4. Operation principles of related devices are described in Section 2.5.

2.1 Semiconducting polymers

2.1.1 Molecular orbital and bonding

The bonding in organic semiconductors is fundamentally different from inorganic semiconductors. Organic molecular crystals are van der Waals bonded solids implying a considerably weaker intermolecular bonding as compared to covalently bonded semiconductors such as Si or GaAs. Polyacetylene $(CH)_n$ is composed of a chain of repeating CH units. Since polyacetylene is the simplest polymer, it is used as an example here. Structures of trans-polyacetylene and

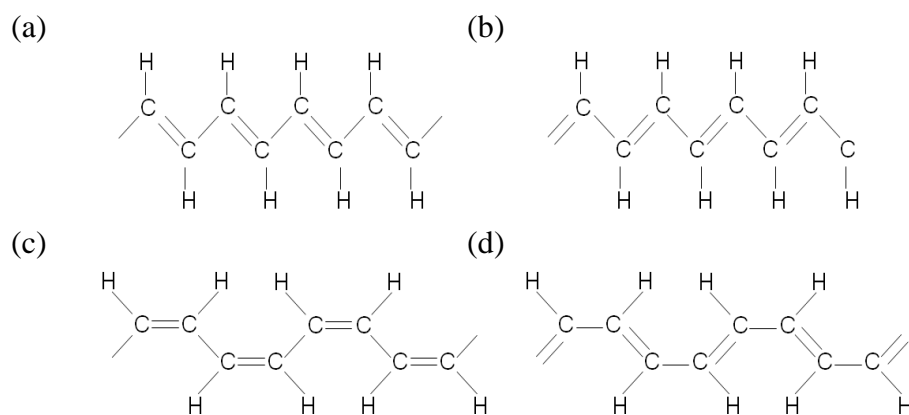


Figure 2.1 (a) Structures of *trans*-polyacetylene. (b) The counterpart of *trans*-polyacetylene with single and double bond exchanged. (c) Structures of *cis*-polyacetylene. (d) The counterpart of *cis*-polyacetylene with single and double bond exchanged.

cis-polyacetylene are shown in Fig. 2.1(a) and 2.1 (c), respectively. The structure of *trans*-polyacetylene and the structure obtained by interchanging the single and double bonds is energetically degenerate. While for the structure of *cis*-polyacetylene and the structure obtained by interchanging the single and double bonds, they are not energetically degenerate.

There are four valence electrons in carbon's outer shell. Three of these electrons form a hybridized sp^2 orbital, which is a linear combination of the spherical s orbital and two dumbbell shaped p orbitals as shown in Fig. 2.2. An sp^2 -hybridized atom has three equivalent sp^2 orbitals, each with $1/3$ s and $2/3$ p character, and one unadulterated p orbital. The sp^2 orbitals are 120° apart. Two of them form σ bonds with the two adjacent carbon atoms and the third bonds with the hydrogen atom. The trigonal planar nature of the sp^2 orbitals gives *trans*-polyacetylene its zigzag backbone structure.

The fourth valence electron of each of the carbon atoms resides in a p_z orbital that is perpendicular to the plane of the sp^2 orbitals. The electronic wavefunctions of the p_z orbitals on adjacent carbons overlap and form the delocalized π bond as

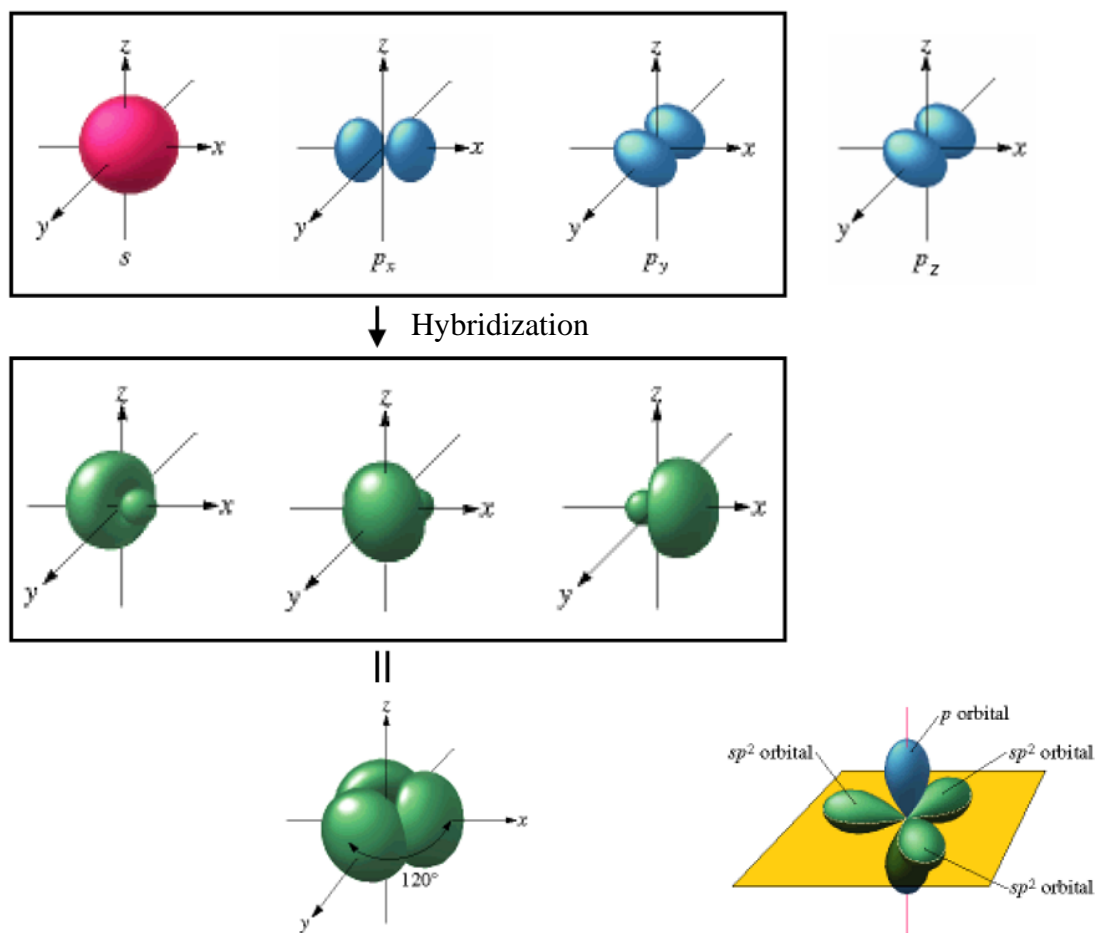


Figure 2.2 An sp^2 -hybridized atom has three equivalent sp^2 orbitals, each with $1/3$ s and $2/3$ p character, and one unadulterated p orbital.

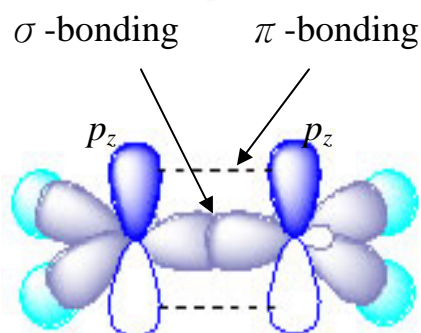


Figure 2.3 Formation of σ bond and π bond.

shown in Fig. 2.3. The presence of the π electron is the important difference between conjugated polymers and non-conjugated polymers. Since the π band between the carbon atoms are weaker than σ bond, the orbitals appear at higher energies. The electrons in the σ bonds form the backbone of the chain while the π

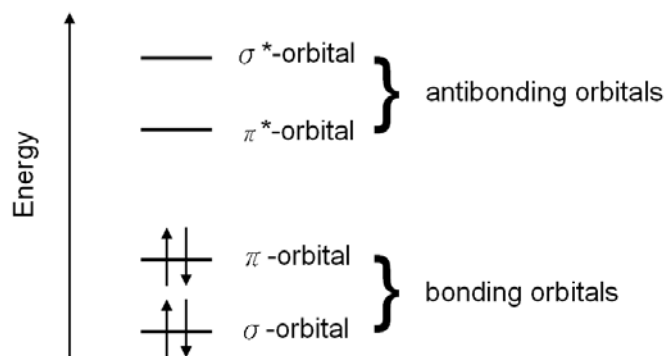


Figure 2.4 The energy levels of a π -conjugated molecule. The lowest electronic excitation is between the bonding π -orbital and the antibonding π^* -orbital.

electrons delocalize along the chain. The π electron delocalization and the weak interchain bonding give polyacetylene and other members of the class of conjugated polymer a quasi-one dimensional nature and give rise to strong anisotropies when the macromolecules are chain extended and chain aligned.

When atomic orbitals form molecular orbitals, these orbitals are often divided into bonding orbitals and antibonding orbitals as shown in Fig. 2.4. The lowest electronic excitation is between the bonding π -orbital and the antibonding π^* -orbital. The σ bonds form completely filled low lying energy bands that have a much larger ionization potential than the π -electrons and thus do not contribute in a major way to the electrical or optical properties. As the intermolecular interaction is increased, the π and π^* bands become broader, and the energy gap between the highest occupied molecular orbital (HOMO) and lowest unoccupied molecular orbital (LUMO) is lowered.

According to the Peierls' Instability, the one-dimensional polyacetylene is unstable against a doubling of the unit cell which will lead to alternating bond lengths as well as to an energy gap. The chain of evenly spaced carbon atoms spontaneously distorts to a chain with alternating bond lengths, called a "dimerized" chain as shown in Fig. 2.5. The bond length alternates between single and double bonds. Dimerization

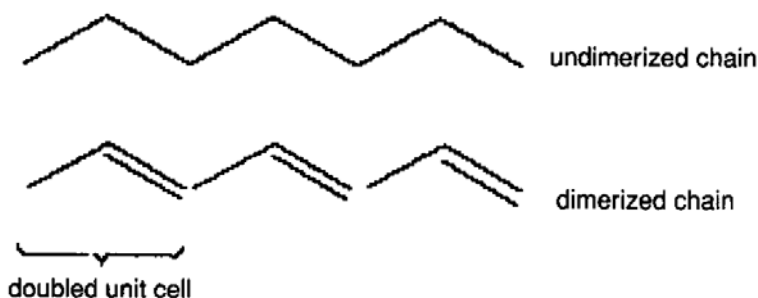


Figure 2.5 Period doubling in dimerized chain. From Ref. [74].

doubles the period of the lattice, making the HOMO completely filled. As a result, polyacetylene is a semiconductor. [74]

2.1.2 Electronic excitations

The electronic excitations in quasi-one-dimensional materials are different from those in conventional semiconductors. Assuming that a linear chain model without inter-chain interactions can be applied to polymers with degenerate ground state, two excitations are expected, namely the solitons and the polarons. In the case of polymers with non-degenerate ground state, the soliton is clearly not a stable excitation in these polymers, since the high-energy form can only exist over a finite length of chain. The charged excitations of a non-degenerate ground state polymer are termed polarons and bipolarons, which represent localized charges on the polymer chain with an accompanying local bonding rearrangement. However, if the inter-chain interaction has taken into account, then polarons may be unstable. Hence the excited carriers are expected to be electrons or holes as in conventional semiconductors.[75]

Solitons can be viewed as bond-alternation domain walls in trans-polyacetylene, and is illustrated for a neutral defect in Fig. 2.6. It separates a segment of polymer chain that alternates single bond, double bond; and a segment that alternates double bond, single bond. Trans-polyacetylene may or may not contain a soliton depending on the number of carbon atoms. The polymer chain contain an even number of carbon

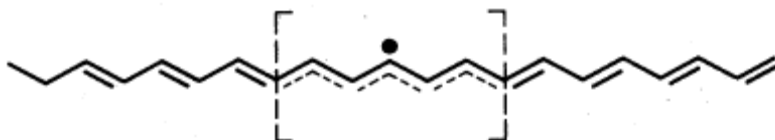


Figure 2.6 Schematic form of a neutral soliton on a trans-polyacetylene chain. From Ref. [76].

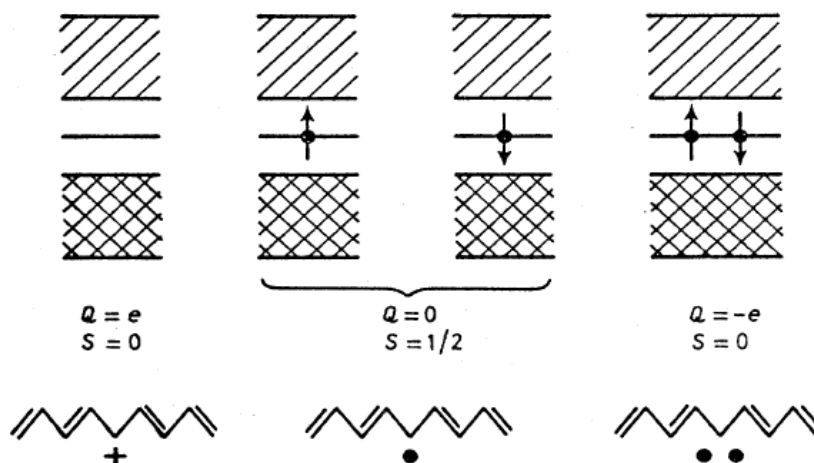


Figure 2.7 Electronic structure leading to various charge and spin state of a soliton. The localized chemical shorthand for these delocalized structures is sketched. From Ref. [76].

atoms does not contain a soliton, while in odd-numbered chains a neutral soliton is incorporated for topological and energetic reasons. Thermal excitation will create additional solitons, but only in pairs on a chain. Upon doping either charged solitons or polarons are formed initially due to charge transfer from the dopant to odd chains and even numbered chains. The soliton can be neutral with spin $1/2$ (one electron in the state at midgap) and charged positively or negatively with spin zero (corresponding to zero or two electrons in the midgap level) as shown in Fig. 2.7.

Formation of a polaron requires a sufficient separation between electron and hole so that they do not interact to form an exciton. When an electron is added to a conjugated polymer, the chain deforms around the charge in order to put the charge in a lower electronic energy state. The competition between elastic deformation energy and electronic energy determines the size of the lattice deformation. The added charge

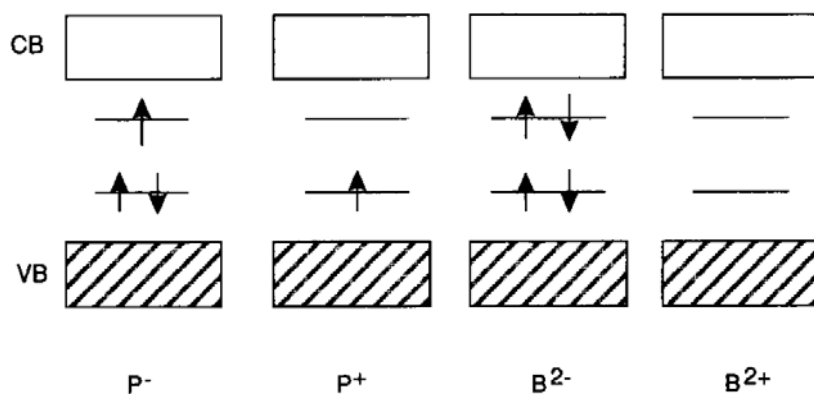


Figure 2.8 Schematic energy band diagrams for polarons and bipolarons. From Ref. [74].

on the polymer chain is thus not a free electron, but an electron that interacts with the polymer chain by deforming the chain around itself. The charge and the resulting deformation (phonon) constitute a polaron.[74] Polarons are formed similarly on all other conducting polymers.

Bipolarons are similar to polarons but they are doubly charged. Instead of being a single electron that distorts the lattice, there are two electrons or holes, with opposite spins, bound together within the same conjugation length. Although these electrons or holes repel one another via the Coulomb interaction, they remain bound together by their common lattice deformation.[77]

For the energy states located in the energy gap of the polymer as shown in Fig. 2.8. The polaron has two subgap states of which one is doubly occupied for a negatively charged polaron (P^-) and the other is singly occupied for a positively charged polaron (P^+). The doubly charged bipolaron has its subgap states either completely filled for a negative bipolaron (B^{2-}) or completely empty for a positive bipolaron (B^{2+}). A significant difference between polarons and bipolarons is their spin signatures. Polarons have charge ± 1 and spin $1/2$, while bipolarons are spinless and doubly charged.

2.2 Metal/organic interface

The choice of contacts in organic electronics is an area of critical importance. Unlike inorganic semiconductors, such as Si and GaAs, the Schottky energy barrier formed at a metal contact depends weakly on the choice of metal.[78] In organic transistors, contacts can affect the output current density. In organic electroluminescence devices, contacts can affect minority and majority current flow, and hence recombination rates and efficiency. In fact, the operation of organic light-emitting diodes depends on the asymmetry of the barrier heights at the two contacts. In this section, we consider some of the models adopted from inorganic semiconductor theory that have been used to describe the energy band diagram of a metal/organic structure.

2.2.1 Energy band diagram

When metal and n-type semiconductor are brought into contact, their Fermi levels must be equal at the interface in order to achieve thermodynamic equilibrium. In general, this requires a charge transfer between the metal and the semiconductor. Electrons from the semiconductor flow into the metal, leaving behind positive ionized donors in the semiconductor. The bands bend as shown in Fig. 2.9(b) and a Schottky barrier is formed. The band diagrams under different bias conditions are shown in Fig. 2.10. If p-type semiconductor is in contact with metal, electrons are injected from the metal into the semiconductor, causing a build-up of negative charge in the semiconductor, and consequently the bands bend the other way. The barrier heights to electron and hole injection, ϕ_{bn} and ϕ_{bp} , can be calculated as follows:

$$e\phi_{bn} = e(\phi_m - \chi_c) \quad (2.1)$$

$$e\phi_{bp} = E_g - e\phi_{bn} \quad (2.2)$$

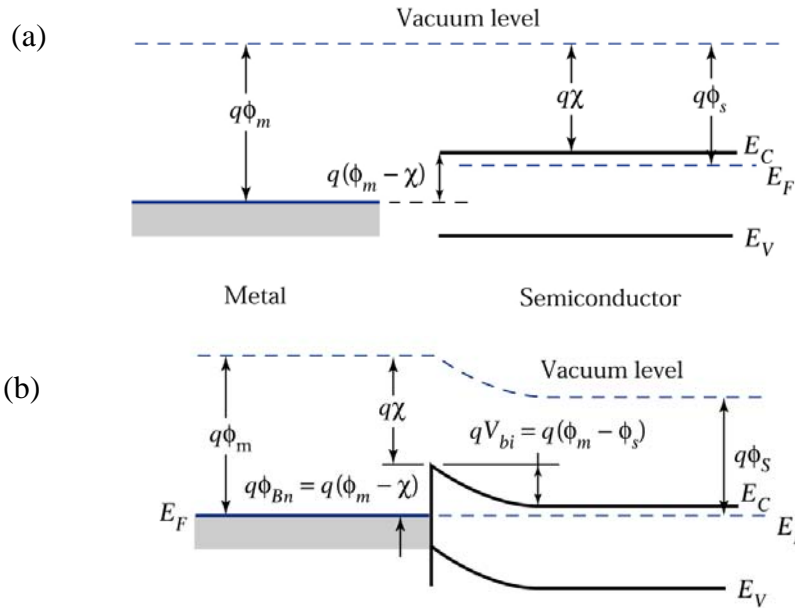


Figure 2.9 (a) Energy band diagram of an isolated metal adjacent to an isolated n-type semiconductor under thermal non-equilibrium condition. (b) Energy band diagram of a metal-semiconductor contact in thermal equilibrium. From Ref. [78].

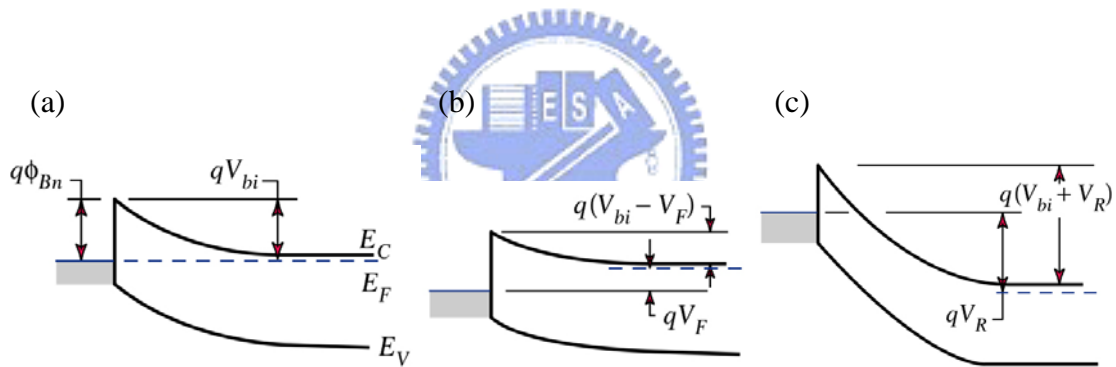


Figure 2.10 Energy band diagrams of rectifying metal / n-type semiconductor contact at (a) thermal equilibrium, (b) forward bias, and (c) reverse bias. From Ref. [78].

An ohmic contact can also be formed at a metal/semiconductor junction. One method is not to form a carrier injection barrier by use a metal with a work function which is smaller than that of the semiconductor for n-type semiconductors, or greater than that of the semiconductor for p-type semiconductors. However, this approach is not usually followed because the barrier height may be pinned by the high interface state density at the contact.[79] Another method is to use a heavily doped semiconductor at the interface to cause a significant band bending and a narrow

barrier for carrier tunneling through. However, for organic semiconductor, increase the free charge-carrier density by adding dopants is difficult. Therefore, so far, the common method is to minimize the barrier height by choosing appropriate contact materials.

2.2.2 Image-force lowering

Image-force lowering is also known as the Schottky effect. It occurs in a metal/nonmetal interface. In such junctions, a barrier exists that controls the emission of carriers from the metal to nonmetal layer. The image force lowering reduces the barrier height, and a larger current flow may occur.

In simulations, the charge carrier injection barrier heights at the contacts are assumed to be field independent. However, in reality, this is not the case. The injection barrier height is reduced under applied bias due to the image force of the carrier as shown in Fig. 2.11. Consider a metal-vacuum system first. When an electron is at a distance x from the metal, a positive image charge will be induced on the metal surface. The force of attraction between the electron and the image charge is equivalent to the attractive force between the electron and the equal positive charge located at $-x$. The attractive image force, called the image force, is then given by the following expression:

$$F = \frac{-q^2}{4\pi(2x)2\epsilon_0} = \frac{-q^2}{16\pi\epsilon_0 x^2}. \quad (2.3)$$

The potential energy of an electron at a distance x from the metal surface is given by:

$$U_e(x) = \int_{\infty}^x F dx = \frac{q^2}{16\pi\epsilon_0 x}. \quad (2.4)$$

When an external field E is applied, the total potential energy as a function of distance is given by:

$$U(x) = \frac{q^2}{16\pi\epsilon_0 x} + qEx. \quad (2.5)$$

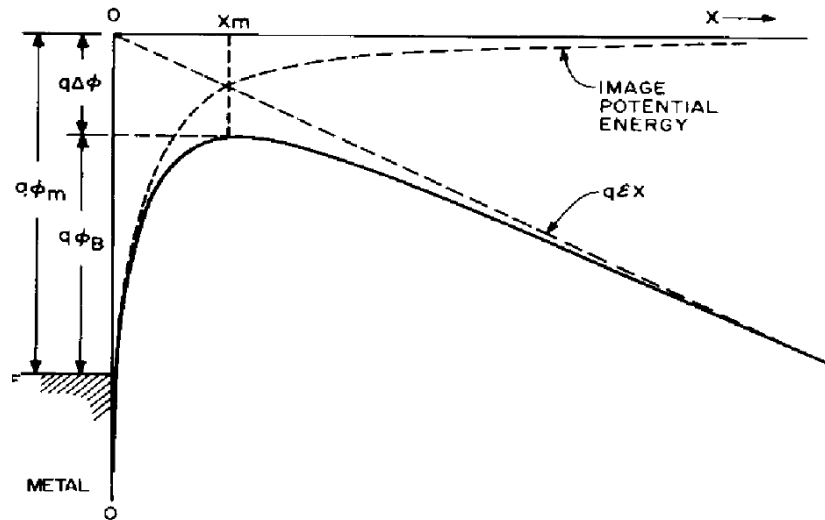


Figure 2.11 The energy band diagram for the interface between a metal surface and a vacuum. The metal work function is $q\phi_m$. The effective energy barrier is lowered when an electric field is applied to the surface. The lowering is due to the combined effects of the field and the image force. From Ref. [80].

The maximum barrier location x_m

$$x_m = \sqrt{\frac{q}{16\pi\epsilon_0 E}} \text{ cm} \quad (2.6)$$

The image force lowering $\Delta\phi$:

$$\Delta\phi = \sqrt{\frac{q^3 E}{4\pi\epsilon_0}} \text{ V.} \quad (2.7)$$

These results can also be applied to metal-semiconductor systems. In organic semiconductors, the free-space permittivity ϵ_0 should be replaced by an appropriate permittivity ϵ_s characterizing the semiconductor medium. Hence, the $\Delta\phi$:

$$\Delta\phi = \sqrt{\frac{q^3 E}{4\pi\epsilon_s}} \text{ V.} \quad (2.8)$$

In organic semiconductors, the values of ϵ_s around $3\epsilon_0$ is much lower than inorganic semiconductors. Therefore, the importance of image-force lowering term is increased. This contribution must be included for any device model to have a successful calculation.[81]

2.3 Carrier injection and transport

The theory of charge injection from a metal into an organic semiconductor and the carrier transport in organic semiconductor has been important topics for a long time. There are many theoretical research works available in the analysis of experimental data. Theoretical calculations based on different assumption and simplifications are not all suitable for organic materials. In this section we will review the commonly used formulations describing charge injection and transport in organic electronics.

Discussions are divided according to two limiting regimes of device operation, namely injection limitation and transport limitation of the current. The occurrence of maximum possible space-charge limited currents requires that at least one contact has good injecting properties. In contrast, injection limitation occurs if the injection barrier is so large that the injection current from the contact into the organic materials is insufficient to become the space-charge limited currents.

2.3.1 Injection limitation at the contact

There are two main possible mechanisms describing charge carrier injection, which are the thermionic emission and the tunnel emission. Both concepts are under certain conditions in inorganic semiconductors. The disorder in organic semiconductors poses an obstacle to be overcome. The process of injection into a disordered hopping system has been studied by many researchers, and these important references are cited for readers interested in this topic.

Thermionic emission

At any finite temperature T , the carrier density at any finite energy is not zero. There are always carriers above the barrier height. The thermally generated carriers

are no longer confined by the triangular barrier and these carriers contribute to the thermionic emission current. The total net current is given by

$$J = \frac{4\pi q k_B m^*}{h^3} T^2 \exp(-q\phi_b / k_B T) [\exp(qV / k_B T) - 1] , \quad (2.9)$$

$$= A^* T^2 \exp(-q\phi_b / k_B T) [\exp(qV / k_B T) - 1]$$

Where ϕ_b is the barrier height, k_B is the Boltzmann constant, V is the applied voltage, and A^* is the effective Richardson constant. However, this calculation is not totally correct in the amorphous organic semiconductor where the electronic states are highly localized and charge transport is by hopping. For semiconductor with low mobility, it is necessary take into account the carrier diffusion within the barrier back toward the contact. The analysis is complicated, and depends on the type of barrier. Detail description can be found in Ref. [80], [81], and [82].

Tunnel emission

Tunnel emission, which is also called Fowler-Nordheim tunneling injection, is intrinsically quantum mechanical, with free carrier tunneling from states at the metal Fermi level directly into continuum states through a triangular barrier. The current flow is described by

$$J = \frac{A^* q^2 E^2}{\phi_B \alpha^2 k_B^2} \exp\left(-\frac{2\alpha\phi_B^{3/2}}{3qE}\right) \quad (2.10)$$

with $\alpha = \frac{4\pi\sqrt{2m^*}}{h}$.

E is the external field. The tunneling current can be analyzed by a Fowler-Nordheim plot, where $\log(J/E^2)$ is plotted against $1/E$ to give a straight line. The gradient of the line can be used to extract the barrier height. The characteristic of field emission for a Schottky barrier is that the current strongly dependent on the applied field. The current expressions for the Schottky barrier and thermally assisted tunneling are complicated. Detail description can also be found in Ref. [80], [81], and [82].

2.3.2 Transport limitation in the bulk

As the contact is able to supply sufficient carrier density which is higher than the material has in thermal equilibrium without carrier injection, the total current will be limited by the space charge within the semiconductor. In this circumstance, the current is limited by the material properties rather than the contact. The space-charge-limited current has been treated in various situations.[83] Here, we introduce some results under different conditions.

In vacuum

The magnitude of the current density J is given by

$$J = \rho v \quad \text{amp/m}^2 \quad (2.11)$$

where v is the drift velocity, and ρ is the charge density. Both v and ρ are functions of the distance from the origin. At the carrier injecting electrode, the velocity of the electrons is very small, and hence the charge density is very large. While at the carrier collecting electrode the velocity is a maximum, the charge density is a minimum. From the assumption that the initial velocity can be neglected, the velocity of the carrier at any point can be determined from the equation

$$\frac{1}{2}mv^2 = eV. \quad (2.12)$$

Hence, from Eq. 2.12, the Poisson's equation

$$\frac{d^2V}{dx^2} = \frac{\rho}{\epsilon_0} = \frac{J}{v\epsilon_0} = \frac{J}{[2(e/m)]^{1/2}\epsilon_0} V^{-1/2} = kV^{-1/2} \quad (2.13)$$

where

$$k = \frac{J}{[2(e/m)]^{1/2}\epsilon_0}. \quad (2.14)$$

Define

$$y = \frac{dV}{dx} \quad (2.15)$$

equation 2.13 becomes

$$\frac{dy}{dx} = kV^{-1/2} \quad (2.16)$$

$$dy = kV^{-1/2} dx = kV^{-1/2} \frac{dV}{y} \quad (2.17)$$

$$y dy = kV^{-1/2} dV \quad (2.18)$$

Equation 2.18 can be integrated to

$$\frac{y^2}{2} = 2kV^{1/2} + C_1 \quad (2.19)$$

Since $V = 0$ at the carrier injecting electrode, and $y = dV/dx = 0$, the constant of integration C_1 is zero. By taking the square root of Eq. 2.19, the equation becomes

$$y = \frac{dV}{dx} = 2k^{1/2} V^{1/4} \quad (2.19)$$

$$V^{-1/4} dV = 2k^{1/2} dx \quad (2.20)$$

This equation integrates to

$$\frac{4}{3} V^{3/4} = 2k^{1/2} x + C_2 \quad (2.21)$$

Since $V = 0$ at $x = 0$, the constant of integration C_2 is zero. Finally,

$$V = \left(\frac{3}{2}\right)^{4/3} k^{2/3} x^{4/3} \quad (2.22)$$

$$J = \frac{4}{9} \left(2 \frac{e}{m}\right)^{1/2} \varepsilon_0 \frac{V^{3/2}}{x^2} \quad (2.23)$$

Therefore, the current varies as the three-half power of the potential. This equation can be used to describe the space-charge-limited current in vacuum diode. The space-charge-limited current dose not depends on the temperature or the work function of the carrier injecting electrode. The geometry of the tube and the potential applied will determine the maximum current under the condition that the electron supply from the electrode is sufficient.[84]

In trap-free materials with field-independent mobility

For a trap-free material without traps and intrinsic carriers, and while the diffusion current is neglected and the mobility is field-independent, the space-charge-limited current can be derived as below.

The drift current is given by

$$J = e\mu nE \quad (2.24)$$

Start from the equation

$$\frac{\varepsilon_s}{e} \frac{dE}{dx} = n \quad (2.25)$$

and from Eq. 2.24

$$\frac{\varepsilon_s}{e} \frac{dE}{dx} = \frac{J}{e\mu E} \quad (2.26)$$

$$E \frac{dE}{dx} = \frac{J}{\varepsilon_s \mu} \quad (2.27)$$

$$EdE = \frac{J}{\varepsilon_s \mu} dx \quad (2.28)$$

This differential equation can be integrated to give

$$\frac{1}{2} E^2 = \frac{J}{\varepsilon_s \mu} x + C_1 \quad (2.29)$$

According to the boundary condition $E(0) = 0$, Eq. 2.29 becomes

$$\frac{1}{2} E^2 = \frac{J}{\varepsilon_s \mu} x \quad (2.30)$$

$$E = \left(\frac{2J}{\varepsilon_s \mu} \right)^{1/2} (x)^{1/2} \quad (2.30)$$

Therefore

$$V = \int_0^L Edx = \left(\frac{2J}{\varepsilon_s \mu} \right)^{1/2} \frac{L^{3/2}}{3/2} = \left(\frac{8J}{9\varepsilon_s \mu} \right)^{1/2} L^{3/2} \quad (2.31)$$

$$J = \frac{9}{8} \varepsilon_s \mu \frac{V^2}{L^3} = \frac{9}{8} \varepsilon_r \varepsilon_0 \mu \frac{V^2}{L^3} \quad (2.32)$$

Equation 2.32 is referred to as the trap-free square law, the Mott-Gurney square law,

and Child's law for solid.[83] This condition is analog to the thermionic vacuum diode, but there are no thermal free carriers and trapping states in the solid. The importance of the trap-free space-charge-limited current is that it is the maximum possible unipolar current in this kind of materials.

The boundary condition $E(0) = 0$ leads to an infinitely high carrier density at the contact. The problem of infinite carrier concentration can be resolved by including the diffusion term, but this makes an analytic solution impossible. More discussion can be found in Ref. [85], [86], and [87].

In the very low applied voltage condition, the number of injected charge carriers is negligible compared to the number of thermally generated free carriers, the current is described by Ohm's law

$$J = q\mu n \frac{V}{d} \quad (2.33)$$

where d is the material thickness.

In materials with traps and field-independent mobility

If there is a single set of shallow traps situated at certain energy below the conduction band, the total charge is

$$\rho_f + \rho_t \quad (2.34)$$

and the ratio θ is

$$\theta = \frac{\rho_f}{\rho_f + \rho_t} \quad (2.35)$$

The ρ_f and the ρ_t are free carrier density and trapped carrier density, respectively. The θ is equal to the ratio of free carriers to the total number of carriers. The current density is given by

$$J = \mu\rho_f E \quad (2.36)$$

Equations becomes

$$\frac{dE}{dx} = \frac{\rho_f + \rho_t}{\varepsilon_r \varepsilon_0} \quad (2.37)$$

and hence

$$J = \frac{9}{8} \theta \varepsilon_r \varepsilon_0 \mu \frac{V^2}{L^3} \quad (2.38)$$

The existence of unfilled traps modifies the transport mechanism by capturing the injected carriers. More information can be found in Ref. [88].

However, if traps are distributed in energy, they will be gradually filled with increasing electric field. The current will increase faster than quadratic until all traps are filled. One of numerous calculations is the trap-charge limited current.[82,83,87]

$$J = N_c \mu q \left(\frac{\varepsilon \varepsilon_0 l}{N_t q (l+1)} \right)^l \left(\frac{2l+1}{l+1} \right)^{l+1} \frac{V^{l+1}}{d^{2l+1}} \quad (2.39)$$

Furthermore, if the injected charge density is high enough that the traps are completely filled, the density of charge in traps becomes negligible compared to the injected charge, and the trap-filled space-charge-limited current comes back to the trap-free value as shown in Eq. 2.32.

In materials with traps and field-dependent mobility

There have been many calculation results discussing the energy distribution form of traps and field-dependent mobility on the current density. The commonly used energy distribution form is the Gaussian distribution and exponential distribution. One example is given here.

Considering the Poole-Frenkel mobility

$$\mu_{eff}(F) = \mu_0 \exp(\beta \sqrt{F})$$

$$\text{where } \beta = \frac{\sqrt{q/\pi\varepsilon}}{kT} \quad (2.40)$$

and the trap-filling effect, that is the hopping-type mobility

$$\mu_{eff}(E_t) = \mu_0 \exp\left(-\frac{E_t}{kT}\right) \quad (2.40)$$

the current density for unipolar carrier transport can be given by

$$J = N_C \mu_{eff} (E_t, F) q \left(\frac{\varepsilon m}{N_t q (m+1)} \right)^m \left(\frac{2m+1}{m+1} \right)^{m+1} \frac{V^{m+1}}{d^{2m+1}} \quad (2.41)$$

where the effective mobility may take the form

$$\mu_{eff} (E_t, F) = \mu_0 \exp(-m + \beta \sqrt{F}), \quad (2.41)$$

where $m = T_t/T$, and E_t is trap depth.[83,89]

2.4 Recombination and emission process

When there are two kinds of carriers, namely electrons and holes, injected into the device, they may subsequently form excitons by electron-hole capture. The output light is determined by competition between radiative and nonradiative decay. In this section, charge carrier recombination and emission process will be discussed.

2.4.1 Exciton formation and decay

Figure 2.12 shows the basic steps of electroluminescence, such as the charge carrier injection, transport, exciton formation, and radiative recombination. The drawing is simplified to ignore the disorder nature of the organic materials. Once charge carriers are injected into the organic materials, polarons are formed. Positive and negative polarons are transport in the field towards the counter electrode. During the transport, they may be trapped in trap states originate form impurities or structural traps. Finally, positive and negative polarons are recombined to form neutral, bound excitons, either spin singlet or triplet. The total spin of exciton is either $S = 0$, or $S = 1$. The $S = 0$ spin wavefunction is antisymmetric

$$\sigma_- = \frac{1}{\sqrt{2}} \{ \uparrow (1) \downarrow (2) - \downarrow (1) \uparrow (2) \} \quad (2.42)$$

where \uparrow and \downarrow represent the possible spin states of each carrier. The carriers are

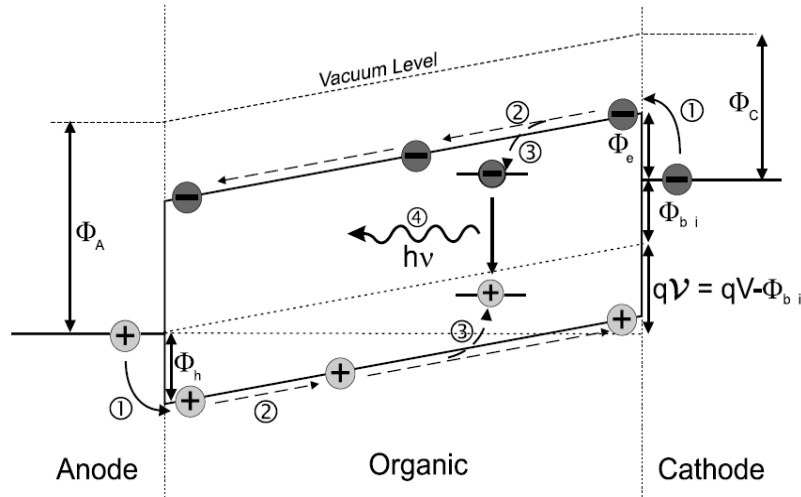


Figure 2.12 Basic steps of electroluminescence: (1) charge carrier injection, (2) charge carrier transport, (3) exciton formation, (4) radiative exciton decay. Polaronic effects and a distribution of transport states due to disorder are neglected. From Ref. [87].

signified by (1) and (2), and σ is spin wavefunction. The $S = 1$ spin wavefunctions are symmetric

$$\sigma_+ = \frac{1}{\sqrt{2}} \{ \uparrow(1) \downarrow(2) + \downarrow(1) \uparrow(2) \} \quad (2.43)$$

$$\sigma_+ = \uparrow(1) \uparrow(2) \quad (2.44)$$

$$\sigma_+ = \downarrow(1) \downarrow(2) \quad (2.45)$$

The $S = 0$ state is known as a singlet, and the $S = 1$ is a triplet.

2.4.2 Quantum efficiency

The efficiency of organic light-emitting diodes is characterized by its quantum efficiency, the current efficiency, and the luminous efficiency. For the quantum efficiency, two parameters need to be mentioned are the external quantum efficiency (η_{ext}) and the internal quantum efficiency (η_{int}). These two parameters are connected by the factor η_c .

$$\eta_{ext} = \eta_{int} \eta_c = \gamma \eta_r \phi_f \eta_c \quad (2.46)$$

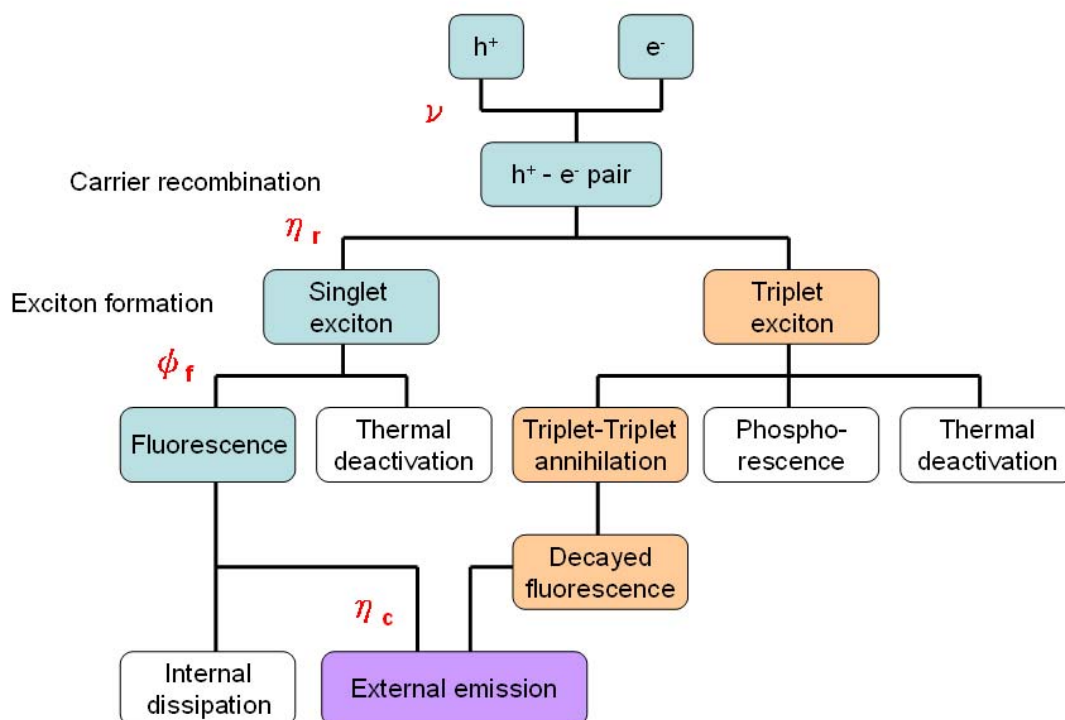


Figure 2.13 A schematic representation of the elementary processes for charge carrier recombination, production of molecular excitons, emission, and external emission. Redrawn from Ref. [90].

External quantum efficiency (η_{ext}) is the ratio of the number of photons emitted by the organic-light emitting diodes into the viewing direction to the number of electron injected. The internal quantum efficiency (η_{int}) is the ratio of the total number of photons generated within the structure to the number of electrons injected.[91] The connection factor η_c is the fraction of the light emitted at the surface relative to the light produced in the bulk, and η_c is determined by the device structure and the refractive indices of the composed layers.

The variable γ is the probability that holes and electrons recombine to form excitons. In order to maximize γ , a good balance between electrons and holes is desired, and hence γ is called the charge-balance factor.

The quantity η_r is the efficiency of production for singlet excitons. The carrier recombination creates both singlet (S) and triplet (T) excitons at a ratio of 1 to 3:



Furthermore, the triplet-triplet annihilation creates both of S and T [90]:



According to spin statistics, only relaxations of singlet excitons conserve spin and generate fluorescence. Nevertheless, it has been proved that almost 100% excitons in devices contain heavy atom can produce light.

The quantity ϕ_f is the ratio of radiative transition from the singlet excitons. It is also called the quantum efficiency of fluorescence, and its value is approximately 1.[92]

The current efficiency η_L , expressed in cd/A, is the ratio of the luminance to the current density. The luminous efficiency η_p , expressed in lm/W is the ratio of the optical flux to the electrical input. The device with high η_p has to combine high current efficiency and low working voltage.[93]

2.5 Operation principles of related devices

2.5.1 Field-effect transistors

The charge transport properties and the electrical properties of the metallic contacts are needed to be included in the device model of an organic field-effect transistor. Charge density, electric field dependence of the carrier mobility, and the contact interface electronic structure are also important properties that need to be taken into account. To date, organic field-effect transistors have been analyzed using inorganic thin-film transistor models that use electric field and charge density independent mobilities and neglect the details of the contacts.

$$I_d = \frac{Z}{L} \mu C_i \left\{ \left(V_g - 2\phi_b - \frac{V_d}{2} \right) V_d - \frac{2}{3} \frac{\sqrt{2\varepsilon_s q N_a}}{C_i} \left[(V_d + 2\phi_b)^{3/2} - (2\phi_b)^{3/2} \right] \right\} \quad (2.49)$$

Eq. 2.49 predicts that for a given gate voltage, the drain current first increases linearly with the drain voltage (linear regime), then gradually levels off to a constant value (saturation regime). It also predicts that the drain current increases when the gate voltage increases.[94]

For a small V_d , Eq. 2.49 reduces to

$$I_d = \frac{Z}{L} \mu C_i (V_g - V_t) V_d \quad (2.50)$$

where

$$V_t = 2\phi_b + \frac{\sqrt{2\varepsilon_s q N_a} (2\phi_b)}{C_i} . \quad (2.50)$$

The channel conductance g_d and the transconductance g_m are

$$g_d = \left. \frac{\partial I_d}{\partial V_d} \right|_{V_g = \text{const}} = \frac{Z}{L} \mu C_i (V_g - V_t) \quad (2.51)$$

$$g_m = \left. \frac{\partial I_d}{\partial V_g} \right|_{V_d = \text{const}} = \frac{Z}{L} \mu C_i V_d . \quad (2.52)$$

In the saturation regime, the drain current and transconductance are

$$I_{d,sat} = \frac{Z}{2L} \mu C_i (V_g - V_t)^2 \quad (2.53)$$

$$g_m = \frac{Z}{L} \mu C_i (V_g - V_t) \quad (2.54)$$

2.5.2 Bipolar junction transistors

The bipolar junction transistor contains both types of carriers. It is also called the junction transistor since its structure has two p-n junctions back to back. The bipolar transistor can be an n-p-n or p-n-p structure. Fig. 2.14 shows only the p-n-p structure. The arrows indicate the direction of current flow under normal operation, which are

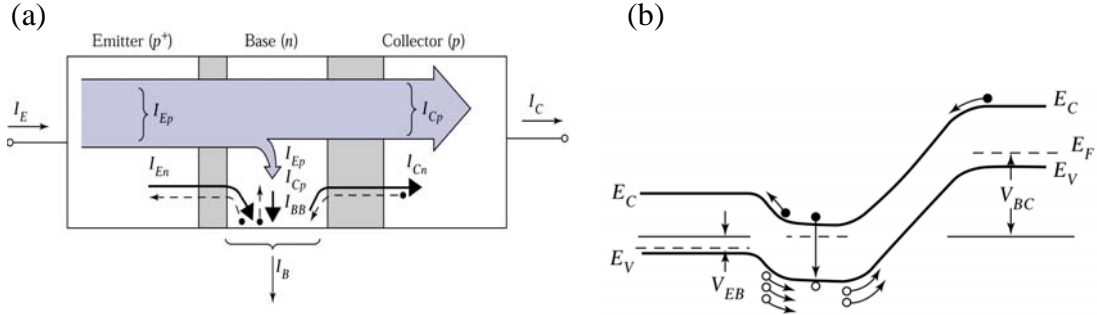


Figure 2.14 (a) A p-n-p transistor connected in common-base configuration for amplifier application. (b) Energy-band diagram under normal operating conditions. From Ref. [78].

forward-biased emitter junction and reverse-biased collector junction. Fig. 2.14(a) is a schematic of a p-n-p bipolar junction transistor in common-base configuration.[80] Fig. 2.14 (b) shows the corresponding band diagram under normal operating condition.

The emitter current as a function of the applied voltages is:

$$\begin{aligned}
 I_E &= AJ_p(x=0) + AJ_n(x=-x_E) \\
 &= Aq \frac{D_B p_B}{L_B} \coth\left(\frac{W}{L_B}\right) \left[(e^{qV_{EB}/kT} - 1) - \frac{1}{\cosh\left(\frac{W}{L_B}\right)} (e^{qV_{CB}/kT} - 1) \right] \\
 &\quad + Aq \frac{D_E n_E}{L_E} (e^{qV_{EB}/kT} - 1)
 \end{aligned} \tag{2.55}$$

and for the total collector current

$$\begin{aligned}
 I_C &= AJ_p(x=W) + AJ_n(x=x_C) \\
 &= Aq \frac{D_B p_B}{L_B} \frac{1}{\sinh\left(\frac{W}{L_B}\right)} \left[(e^{qV_{EB}/kT} - 1) - \coth\left(\frac{W}{L_B}\right) (e^{qV_{CB}/kT} - 1) \right] \\
 &\quad - Aq \frac{D_C n_C}{L_C} (e^{qV_{CB}/kT} - 1)
 \end{aligned} \tag{2.56}$$

The difference between these two currents is small and appears as the base current:

$$I_B = I_E - I_C \tag{2.57}$$

The common-base current gain α_0 is defined as

$$\alpha_0 = \frac{\partial I_C}{\partial I_E} = \frac{\partial I_{pE}}{\partial I_E} \frac{\partial I_{pC}}{\partial I_{pE}} \frac{\partial I_C}{\partial I_{pC}} = \gamma \alpha_T M \quad (2.58)$$

The first term, $\partial I_{pE}/\partial I_E$, is defined as the emitter efficiency γ . The second term, $\partial I_{pC}/\partial I_{pE}$, is called the base transport factor α_T . The third term, $\partial I_C/\partial I_{pC}$, is the collector multiplication factor M .

The common-emitter current gain β_0 is defined as

$$\beta_0 = \frac{\partial I_C}{\partial I_B} \quad (2.59)$$

and the α_0 and β_0 are related to each other by

$$\beta_0 = \frac{\alpha_0}{1 - \alpha_0} \quad (2.60)$$

Since the value of α_0 is close to unity, β_0 is generally much larger than 1.[80]

2.5.3 Metal-base transistors

The metal-base transistor is also called semiconductor-metal-semiconductor transistor. The device made by inorganic semiconductors is used as an example. The energy-band diagram of device made by epitaxial silicides on Si is shown in Fig. 2.15(a). The thickness of CoSi_2 base is critical. Thicker base are known to produce rough and discontinuous film, while thinner base are more prone to pinholes.[95]

Figure 2.15(b) shows the device under normal operation that the emitter-base junction is forward biased while the collector-base junction is reverse biased. The forward current is due to thermionic emission which is discussed in Section 2.3.1. The injected electrons may be able to go through the base and collected by the collector. However, the loss of electrons contributes to the base current under many loss mechanisms.

$$\begin{aligned} J_{nC} &= \alpha_T J_{nE} \\ &= \alpha_B \alpha_{BC} \alpha_C J_{nE} \end{aligned} \quad (2.61)$$

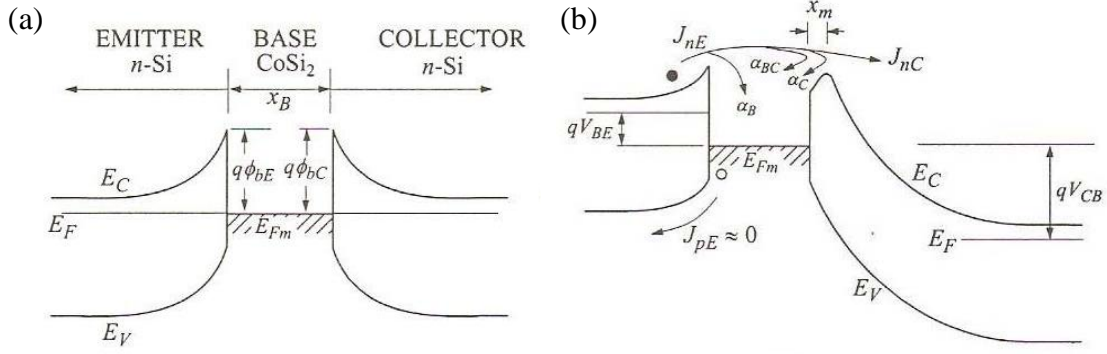


Figure 2.15 (a) Energy-band diagram of a metal-base transistor under thermal equilibrium. (b) Energy-band diagram of a metal-base transistor under normal biases. x_m is the field reversal region from image-force lowering. From Ref. [95].

where α_T is the base transport factor. α_B is due to electron scattering in the metal base, given by

$$\alpha_B = \exp\left(-\frac{x_B}{l_{mB}}\right) \quad (2.62)$$

where l_{mB} is the carrier mean free path in the metal base. α_{BC} is due to quantum-mechanical reflection at the base-collector interface

$$\alpha_{BC} \approx 1 - \left[\frac{1 - \sqrt{1 - (q\phi_{bC}/E)}}{1 + \sqrt{1 - (q\phi_{bC}/E)}} \right]^2 \quad (2.63)$$

E is the electron energy with respect to the metal Fermi level, and it is approximately equal to emitter-base barrier height $q\phi_{bE}$. For a device with $E \approx q\phi_{bE} \approx q\phi_{bC}$, and α_{BC} approaches zero. For $q\phi_{bE} > q\phi_{bC}$, the α_{BC} can be enhanced. The collector efficiency α_C is due to back-scattering of electrons within the distance x_m of the image-force lowering

$$\alpha_C = \exp\left(-\frac{x_m}{l_{mC}}\right) \quad (2.64)$$

where l_{mC} is the carrier mean free path in the collector.[95]

2.5.4 Permeable-base transistors

Then permeable-base transistor is basically a metal-semiconductor field-effect

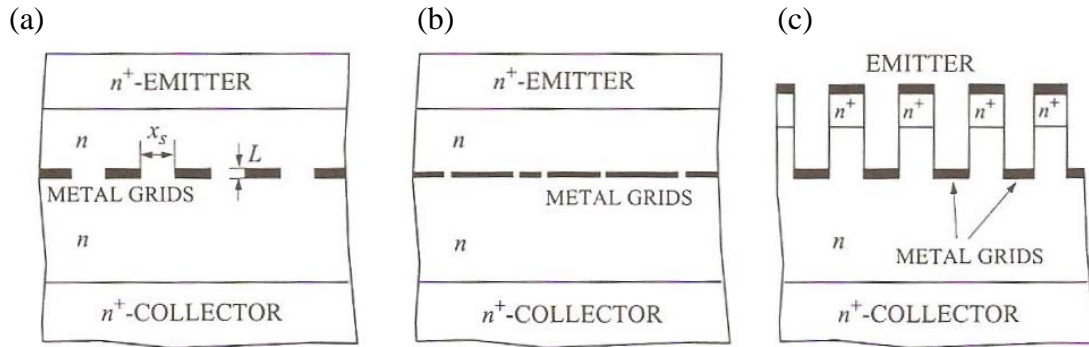


Figure 2.16 Structures of a permeable-base transistor. (a) Metal grids are defined by photolithography and embedded in semiconductor. (b) Metal grids with random pinholes are embedded in semiconductor. (c) Metal grids are deposited on semiconductor trenches. From Ref. [95].

transistor in vertical architecture. Three main structures of permeable-base transistor which have been developed in the past few decades are shown in Fig. 2.16. The structure with a completely embedded metal grid is shown in Fig. 2.16(a). The metal grids are defined by lithography and etching. The device is usually designed for operating in enhancement mode, so that the depletion width surrounding the metal grids at zero base voltage is large than half the spacing between the metal strips (x_s).

$$\sqrt{\frac{2\varepsilon_s\psi_{bi}}{qN_D}} > \frac{x_s}{2} \quad (2.65)$$

The metal should yield high Schottky-barrier height to minimize forward-bias leakage. Fig. 2.16(b) shows another structure, the metal grids with random pinholes are embedded in the semiconductor. Since the channel openings are random pinholes, the operation regime will be different. Fig. 2.16(c) shows the third structure which trenches made by photolithography. Metal grids are connected together in a different plane.[95]

Under normal operation, the transistor behaves like a metal-semiconductor field-effect transistor with a very short channel length. The channels are gaps between the metal grids. When the depletion regions are merged together, the channel is cut

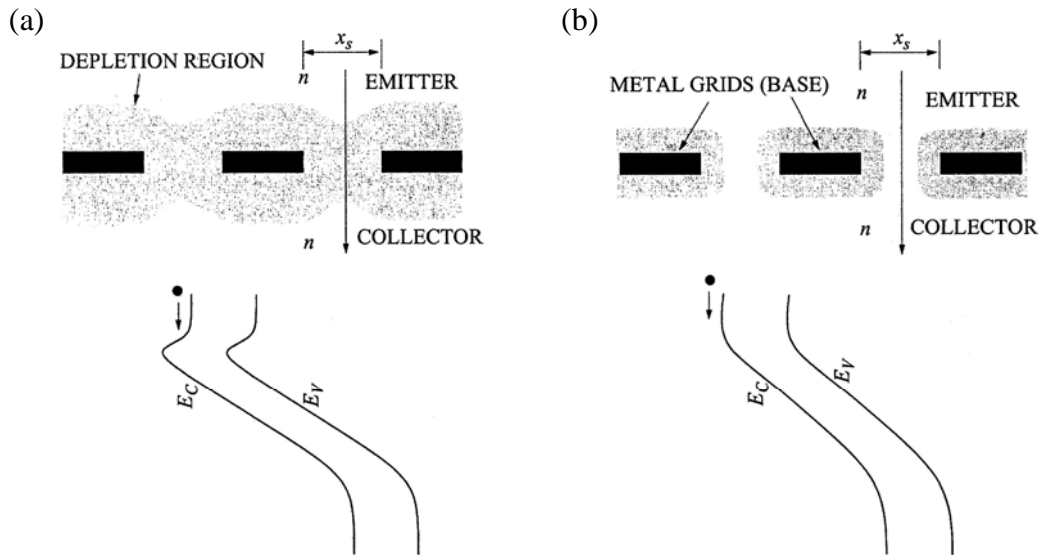


Figure 2.17 Grey area is depletion regions. Energy-band diagrams show that a potential barrier for electrons exists only when depletion regions merge. (a) Device is off. (b) Device is on. From Ref. [95].

off, as shown in Fig. 2.17(a). When the depletion width is reduced by a forward base bias, a channel can exist and the transistor is turned on. The output current in the linear region is described by

$$I_{in} \approx \frac{G_0}{2V_P} (V_B - V_T) V_C \quad (2.66)$$

where

$$G_0 = \frac{q\mu_n N_D x_s W}{L} \quad (2.67)$$

The output current in the saturation region is

$$V_{C,sat} \approx L \left(\frac{v_{sat}}{\mu_n} \right) \quad (2.68)$$

2.5.5 Static-induction transistors

The static-induction transistor features nonsaturating I-V characteristics with increasing drain voltage because the barrier for carriers is lowered by electrostatic induction from the drain. Different structures for the static-induction transistor are

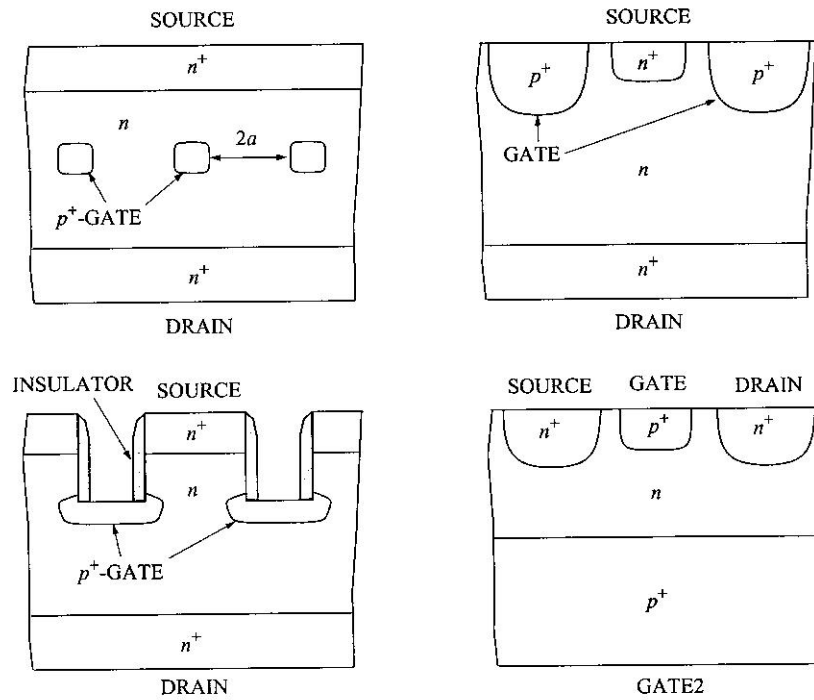


Figure 2.18 Various schemes for the structure of static-induction transistor. (a) Buried gate. (b) Planar gate. (c) Recessed gate. (d) Planar gate with lateral current flow. From Ref. [95].

shown in Fig. 2.18. Compared to the analog transistor proposed in 1952, one difference between static-induction transistor and analog transistor is that the current of analog transistor is limited by space-charge-limited current which have a power-law dependence on drain bias while the current of static-induction transistor have an exponential dependence on drain bias. Besides, the main difference between static-induction transistor and permeable-base transistor is the device operation regime. Most static-induction transistors are designed normally-on, the depletion regions from the gates do not merge and exists a channel opening. The depletion regions around the gates do not pinch off the gap completely

$$\sqrt{\frac{2\varepsilon_s\psi_{bi}}{qN_D}} < a \quad (2.69)$$

where ψ_{bi} is the built-in potential of the p-n junction from the gate,

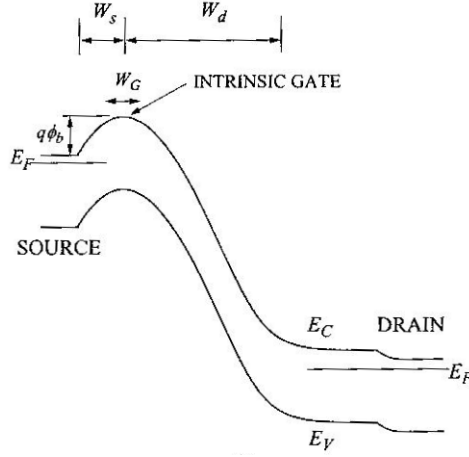


Figure 2.19 Energy-band diagram from source to drain in the middle of the channel between gates. From Ref. [95].

$$\psi_{bi} = \phi_T \ln \left(\frac{N_A N_D}{n_i^2} \right) . \quad (2.70)$$

When negative gate bias, the depletion regions widen, pinch off the channel, and electrons from the source start to see a potential barrier as shown in Fig. 2.19. The current of a static-induction transistor is pinched off is

$$J = qN_D^+ \left(\frac{D_n}{W_G} \right) \exp \left(\frac{-q\phi_b}{kT} \right) \quad (2.71)$$

where N_D^+ is the doping concentration in the source, and D_n/W_G is the carrier diffusion velocity. When the effective thickness of the barrier W_G becomes small, carriers are limited by the thermal velocity.[95]

$$J = qN_D^+ \left(\sqrt{\frac{kT}{2\pi m^*}} \right) \exp \left(\frac{-q\phi_b}{kT} \right) \quad (2.71)$$

When there is a negligible barrier, the injected electrons are comparable to the doping level N_D . The current is controlled by the space-charge-limited current

$$J = \frac{9}{8} \epsilon_s \mu_n \frac{V_D^2}{L^3} \quad (2.72)$$

and

$$J = 2\varepsilon_s v_{sat} \frac{V_D}{L^2} . \quad (2.73)$$

in the mobility regime and velocity saturation regime. Since gate bias also controls the barrier and hence the current, V_D in Eq. 2.72 and 2.73 can be replaced by $V_D + \alpha V_G$.

2.5.6 Vacuum-tube triodes

The electrodes in vacuum-tube triodes are surrounded by vacuum as shown in Fig. 2.20. The cathode is the electron emitter which is heated to high temperature for sufficient electron emission. The operation of a vacuum tube is based on the thermionic emission of electrons from metal to vacuum. [95]

$$J = AT^2 \exp\left(\frac{-q\phi}{kT}\right) . \quad (2.74)$$

In a vacuum tube, the medium has very low conductivity, hence the current can be described by the Child-Langmuir law

$$J = \frac{4}{9} \left(2 \frac{e}{m}\right)^{1/2} \varepsilon_0 \frac{V^{3/2}}{L^2} \quad (2.74)$$

where L is the spacing between the cathode and the plate.

For a triode, there are three electrodes, the grid electrode placed between the cathode and the plate is utilized to modulate the current. The plate current can be described by

$$I_p = C_1 (\mu V_G + V_p)^{3/2} \quad (2.75)$$

where μ is called the amplification factor and V_G is the grid voltage. [95] If the electron in a retarding field, it cannot reach the plate. If the grid voltage is made more positive, current will flow only in the region midway between the grid wires. Since the grid is much closer to the cathode than the plate, a given change in potential of the grid has a much greater effect on the field intensity at the cathode than does the same change in potential of the anode. The exact dependence of the amplification factor is not known.

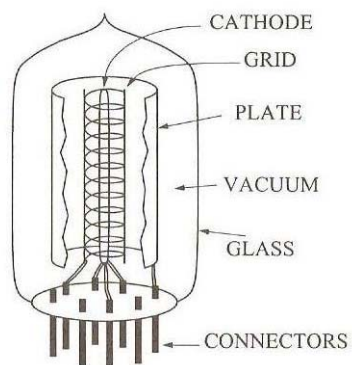
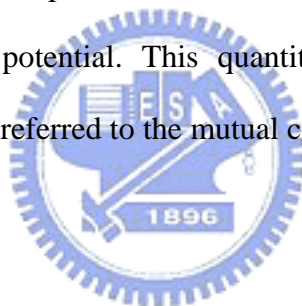


Figure 2.20 Structure of a vacuum-tube triode. From Ref. [95].

The quantity

$$\frac{\partial I_{plate}}{\partial V_{grid}} \quad (2.76)$$

gives the ratio of an increment of plate current to the corresponding increment in grid potential for constant plate potential. This quantity is known as the plate-grid transconductance. This is also referred to the mutual conductance and is designated by the symbol g_m . [96]



Chapter 3

Polymer hot-carrier transistor

3.1 Introduction

3.1.1 Background

Polymer-based organic transistors provide a promising future for large-area and low-cost applications in display technology, sensors, and radio frequency identification cards from the perspectives of their easy solution process as well as the potential integration with organic optoelectronics.[15,17,18,97] Polymer field-effect transistors (FETs) are mostly horizontal devices in which source and drain electrodes lie in the same plane of the substrate. The highest polymer hole mobility of about $0.1 \text{ cm}^2 / \text{V s}$ is reported for poly(3-hexylthiophene) (P3HT) FET [15,16] a few years ago. Beyond this value little progress has been made. Due to the limited mobility, such horizontal devices are not candidates for high current and high frequency application unless the channel length is made submicron. Consequently, how to shrink the channel length in polymer FET has been a demanding issue. Though the well developed technology of submicron lithography can be directly applied to reduce the polymer FET channel length, this strategy is in opposition to the advantages of low-cost and large-area solution process unique to conjugated polymers.

Aside from FET, the bipolar junction transistor (BJT) is a successful vertical device with high current and high frequency for inorganic semiconductors. BJT consists of two back-to-back pn junctions formed by heavily doped base (B), emitter (E) and collector (C). In principle this device structure can be applied to conjugated polymer using multiply spin coating. The thickness and therefore the effective channel length can be reduced down to 10 nm. However, the major problem is that the base layer needs to have low resistance in order to maintain a uniform voltage throughout the active area and reduce the emitter-to-collector transient time. Even for heavily doped conducting polymer, the resistivity is too large to serve as the base material. Despite of its vertical nature, polymer BJT is quite unlikely to succeed.

Polymer FET with vertical channel has been proposed to achieve submicron channel length. For vertical polymer FET the channel length is defined by the thickness of the layer. However, in order to realize a vertical FET channel one usually needs to employ an unreliable mechanical method like embossing.[59] There are another type of polymer transistor, namely the vertical metal-based transistor.[64,68-73,95,99,106,107] Due to its potential to overcome the limit of FET recently metal-base organic transistors, including the space-charge-limited transistor [72,73] and hot-carrier transistor [70,71], gain more and more attention for both polymer and small molecules.[64,68,106-110] In this chapter we present a vertical polymer hot-carrier transistor with metal base, which combines the advantage of short effective channel length, low base resistivity, and easy large-area solution process. Similar to BJT, in hot-carrier transistor the carriers are injected from the emitter into the base. Because of the large energy barrier at the emitter-base junction, they become hot carriers in the metal. Assuming the metal is thinner than the mean free path of the carrier, most of the injected carriers will be collected by the collector. The loss of the carrier to the base contributes to the base current. The ratio is called the transport

factor α , which plays the same role as the transport factor in BJT. Large current amplification results from α close to one. Current gain β is defined as $\alpha/(1-\alpha)$. An ideal hot-carrier transistor has a high collector current and small base current.

3.1.2 Organization of this chapter

In this chapter, the vertical polymer hot-carrier transistors with metal base are demonstrated. For the emitter material with high band gap, electrical properties and fabrication procedures are described in Section 3.2, while Section 3.3 discusses the hot-carrier transistors with low band gap emitter. The properties of the hot-carrier transistor with a blend polymer as emitter are described in Section 3.4. Optical response of a polymer light-emitting diode connected to the hot-carrier transistor are also shown in Section 3.4

3.2 Polymer hot-carrier transistor with high bandgap emitter



3.2.1 Motivation

For silicon BJT, the replacement of semiconductor base by metal was proposed in the early 1960s.[98] However, since silicon is a nearly perfect crystal, the backscattering of carrier at the base-collector junction is severe as the interface varies abruptly. The current gain β is therefore usually poor. A similar idea of using C60 as the emitter but still utilizing silicon as the collector is recently reported.[62,99] But such device turns out to be a permeable base transistor instead of the hot-carrier one. Because of the disorder of polymer and that the interface does not vary so abruptly, we expect the backscattering in our polymer hot-carrier transistor will not be as severe as in silicon hot-carrier transistor and higher β is expected. Indeed we found that high

current gain with low operation voltage can be realized in polymer hot-carrier transistor. Interestingly, in addition to the base for hot-carrier transistor, metal sandwiched between organic semiconductors has been shown to exhibit current memory effect [100], and transistor-like device can be made based on such an effect.[101]

3.2.2 Device structure and fabrication

The multilayer structure of the polymer metal-base transistor is indium tin oxide (ITO) glass/P3HT/Al/LiF/PVK/Au. P3HT is used as the collector because of the small Schottky barrier with Al and high mobility. PVK is poly(9-vinylcarbazole), which is used as emitter because of the large Schottky barrier with Al. Fig. 3.1 shows the structure and energy band profile of hot-carrier transistor in the active mode, i.e., the base-emitter (BE) junction is forward biased while the base-collector (BC) junction reverse biased. The hot carrier in our device is hole. In order to illustrate the picture of hole, the negative of all the energy levels is shown. The work function of Au and Al are 5.1 and 4.3 eV, respectively. The lowest unoccupied molecular orbital (LUMO) and highest occupied molecular orbital (HOMO) for PVK are 2.3 and 6.1 eV below the vacuum level, and those for P3HT are 3 and 5.1 eV, respectively. Note that LUMOs of the polymers are irrelevant to the device operation and not shown. The resultant energy barrier between base and emitter is as large as 1.8 eV, which enables the holes to be far above the Fermi level (i.e., hot carrier) when passing through the thin metal base. The hot holes are expected to have such a high kinetic energy that they are easily injected into the collector since the collector-base barrier is less than that of emitter-base by 1 eV. In addition to the energy level requirements, the base layer thickness must be less than the mean free path for the hot hole in the base in order to reduce the probability of hole capture by the base through inelastic

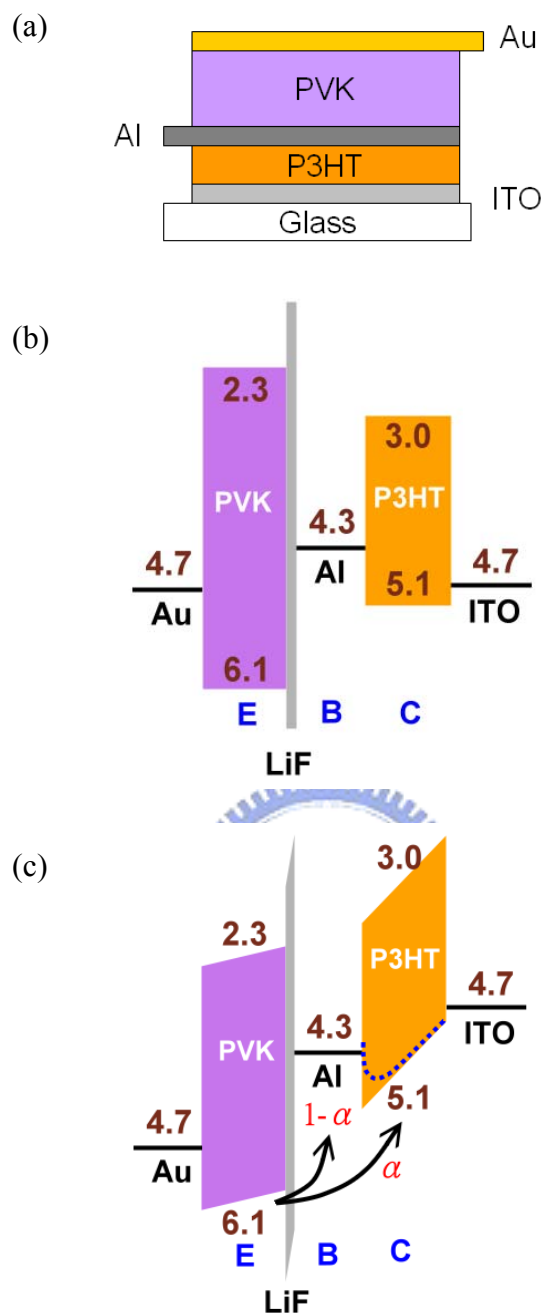


Figure 3.1 (a) The structures of polymer hot-carrier transistor with high bandgap emitter. (b) The energy band profile of metal-base hot-carrier transistor with high bandgap emitter. (c) The energy band profile of metal-base hot-carrier transistor in the active mode. The negatives of the actual energy are shown in order to illustrate the picture of holes better. The energies are indicated in eV.

scattering.[95] The mean free path of Al is about 100 Å.[102] The unwanted electron current is negligible because the electron injection barrier from Al to PVK is 2 eV, and 1.7 eV from ITO to P3HT. Under active mode bias, holes are injected into the

HOMO of PVK from the Au electrode, followed by tunneling through the LiF layer and passing ballistically across the base high above the Fermi level. Because P3HT is not crystalline, the quantum mechanical reflection at the base-collector interface which has plagued the inorganic hot-carrier transistor will not happen here. The LiF layer between emitter and base is intended to provide two advantages. First, the voltage drop across LiF lowers the Al Fermi level relative to HOMO of PVK and further increases the energy difference between PVK and P3HT. Hence the holes have higher kinetic energy in base with LiF. Second, the LiF layer serves as a protection layer which prevents the P3HT from possible dissolution when spin coating PVK. Indeed, the insertion of LiF layer enhances the device stability and reproducibility. The I-V curve of EB and BC junctions shown in Fig. 3.2 demonstrate good diode characteristic with rectification ratio of about 103 and 105, respectively.

The device is fabricated on patterned ITO glass substrate cleaned by de-ionized water, acetone and 2-propanol consecutively in ultrasonic bath. Fourteen hundred angstroms of P3HT is spun cast from chloroform solution (1.2 wt %) onto the substrate, followed by a thin aluminum film of 90 Å evaporated as the base at 0.2 Å/s through a shadow mask. To wire out the base, a 1000 Å Al strip is deposited with another shadow mask. LiF layer of 28 Å is deposited on the thin Al film, followed by 3300 Å of PVK spun cast from toluene solution (7 wt %) to form the emitter. Gold is deposited as the emitter contact. The devices are packaged in a glove box and all electrical measurements are performed in ambient condition. The polymers are purchased from Aldrich. All metal layers are deposited in a chamber having a base pressure of 1.0×10^{-6} mbar. The device active area, defined by crossover between the Au and ITO electrode, is 4 mm². The thickness of each polymer layer is measured by Kosaka ET4000 surface profiler. Current-voltage curves are measured by semiconductor parameter analyzer.

3.2.3 Electrical characteristics

Figure 3.3 shows the characteristics of hot-carrier metal base transistor in the common-emitter configuration. The emitter Au electrode is commonly grounded and the ITO electrode is negatively biased at V_C with respect to Au. The collector current I_C does increase with the base current I_B . The common-emitter current gain β is 25 when V_C is -5 V. β is the average of five current gains at different I_B . Each current gain is given by $[I_C - I_C(I_B = 0)]/I_B$. However, for fixed I_B , $|I_C|$ increases with $|V_C|$ without saturation. This is probably due to the image-force barrier lowering at the BC junction and β increases with $|V_C|$. [103,104] In Fig. 3.4, the voltage drop across the EB and BC junctions are plotted as functions of V_C at fixed $I_B = -0.2$ μ A. The BC voltage drop $V_{BC} = V_B - V_C$ increases with $|V_C|$ while the EB voltage drop $V_{EB} = V_E - V_B$ is nearly a constant after $|V_C|$ exceeds 2 V. This behavior implies that further increase of $|V_C|$ mostly falls on the reverse biased BC junction as expected. Common-base measurement shows consistent results. When $|V_C|$ is -5 V and the base electrode is open, the I_C leakage current is 1.9 μ A as shown in Fig. 3.3. Since the reverse current for BC junction is of the order nA as shown in Fig. 3.2, the leakage current is believed to result from some unexpected path caused by residual mutual dissolution of PVK and P3HT outside the active area. I_C leakage can be in principle reduced to a few nA if process control is improved. Au migration into PVK layer during the evaporation may reduce the effective resistance of PVK layer, and consequently the device has a small turn-on voltage despite the large hole injection barrier at Au/PVK junction. Finally, from the atomic force microscope image of the base metal, the Al roughness is less than two nanometers and

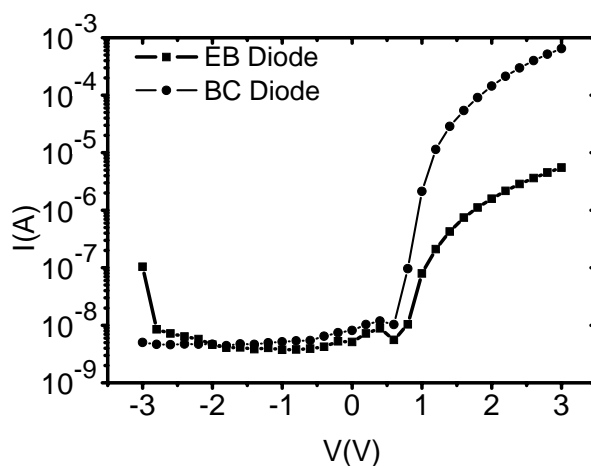


Figure 3.2 The I-V curves of emitter-base and base-collector diodes.

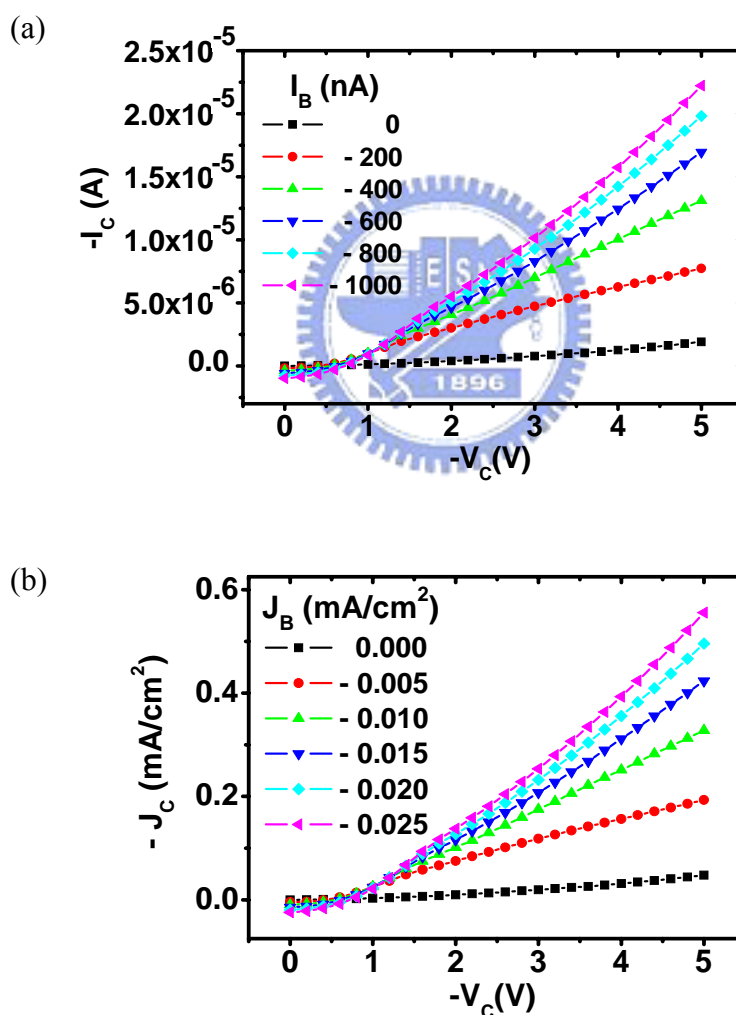


Figure 3.3 The characteristics of the polymer hot-carrier metal-base transistor in common-emitter configuration. (a) Unit: Ampere (b) Unit: milliampere per centimeter square

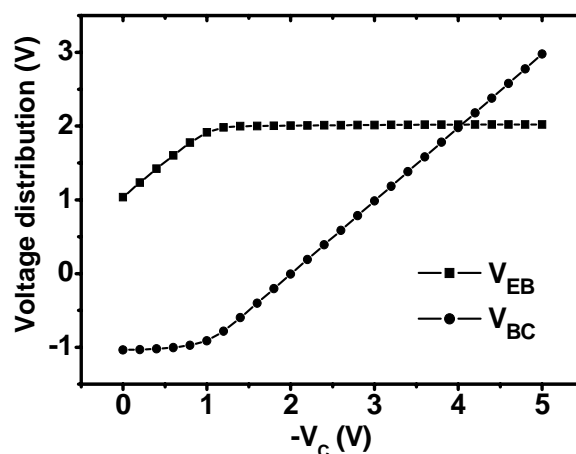


Figure 3.4 The characteristics of the polymer hot-carrier metal-base transistor in common-emitter configuration.

no pinholes can be seen. It shows that our metal-base hot-carrier transistor is not in fact a permeable base one.[99,105] The device reported in this letter is therefore the first organic hot-carrier transistor.

3.2.4 Summary of section 3.2

In summary, a solution-processed vertical polymer hot-carrier transistor is demonstrated to have current gain of 25. This device has high current output and low operation voltage. The active area can be made arbitrarily large and no lithography is needed. The use of LiF tunneling barrier not only improves the hot carrier kinetic energy and current gain but also serves as a protecting layer to prevent mutual dissolution between the polymers.

3.3 Polymer hot-carrier transistor with low bandgap emitter

3.3.1 Motivation

Previously a high bandgap organic semiconductor poly(9-vinylcarbazole) (PVK)

is selected for the emitter in order to maximize the energy barrier at the emitter-base junction, thus enhancing the hot carrier kinetic energy and reducing the base current.[70] Even though reasonable common emitter current gain β is achieved the high bandgap emitter comes at a great cost. The high bandgap implies a large barrier for the holes to be injected from the metal contact to the emitter valence band.[111] Au is used for the emitter electrode. Depending on the surface contamination level the work function of Au varies from 4.7 eV to 5.1 eV.[112] The ionization potential of PVK is 5.8 eV, implying a large hole injection barrier of 0.7 eV to 1.1 eV. The resulting collector density is therefore as low as 0.56 mA/cm^2 as shown in Fig. 3.3 (b). Similar low current density also occurs in hot-carrier transistor based on evaporated small molecules.[108-110]

In this section, we replace the high bandgap emitter by a low bandgap polymer poly(3-hexylthiophene) (P3HT) with ionization potential (IP) at 5.1 eV, which is much closer to the Au work function than PVK. In fact P3HT is also the material used for the collector. There is therefore no energy offset between emitter and collector valence band which is usually required for the hot carrier collection. Similar to the case of PVK emitter a thin layer of LiF is used as the tunneling barrier to enhance the relative energy. Unlike the PVK device where LiF is only auxiliary to create the hot carrier energy offset above the collector band edge, for P3HT emitter the energy offset depends entirely on the LiF layer. The prerequisite of hot-carrier transistor using low bandgap emitter is therefore that the tunneling barrier alone must be able to maintain a good common emitter current gain. It turns out that the common emitter current gain is not compromised even without the high bandgap emitter, indicating that the tunneling barrier is more crucial than the semiconductor band positions for the operation of the transistor. As for the collector current density, it increases dramatically from 0.56 mA/cm^2 for PVK emitter to several tens mA/cm^2 for P3HT

emitter. We demonstrate that this transistor is able to drive a polymer light-emitting diode with the same area up to brightness of thousands of cd/m^2 .

3.3.2 Device structure and fabrication

The device structure of the hot-carrier transistor in this work is ITO/PEDOT:PSS/P3HT(C)/Al(B)/Al₂O₃/LiF/P3HT(E)/Au. P3HT is used as both the emitter (E) and collector (C). PEDOT:PSS is poly(3,4-ethylenedioxythiophene) doped with polystyrene sulfonated acid, which is used to flatten the ITO surface and serve as the collector contact. The middle Al layer is the base (B), and the top Au layer is the emitter contact. Fig. 3.5 shows the structure as well as the energy band profile of hot-carrier transistor in the active mode. The hot carrier in the transistor is hole. The work function of Au and Al are 4.7 eV and 4.3 eV, respectively. As described above the holes injected from the emitter into the base are hot carriers because the large energy difference between the emitter valence band and the base Fermi level. α is the probability for the hot carrier to enter the collector valence band while $1 - \alpha$ is the probability for the carriers to relax to the base by energy loss. The β is defined as ratio between the collector current and base current J_C / J_B which is equal to $\alpha / (1 - \alpha)$. Apparently the larger the emitter IP, the higher the hot carriers are above the base Fermi level, and the higher the gain β is. Emitter with high IP value is therefore chosen in the previous study.[70] The thin LiF/Al₂O₃ layer is the tunneling barrier which further separates the emitter valence band and the base Fermi level by a voltage drop across it. The device is fabricated on cleaned ITO substrate, and a 300 Å PEDOT:PSS layer is spin coated. P3HT is then spin coated to form the 1200 Å collector layer. A thin Al film around 80 Å is evaporated (10 Å /s) as the base through a shadow mask, followed by a LiF layer of various thicknesses. The optimal Al₂O₃ layer is formed by air exposure for 3 minutes after Al deposition. The oxidation time

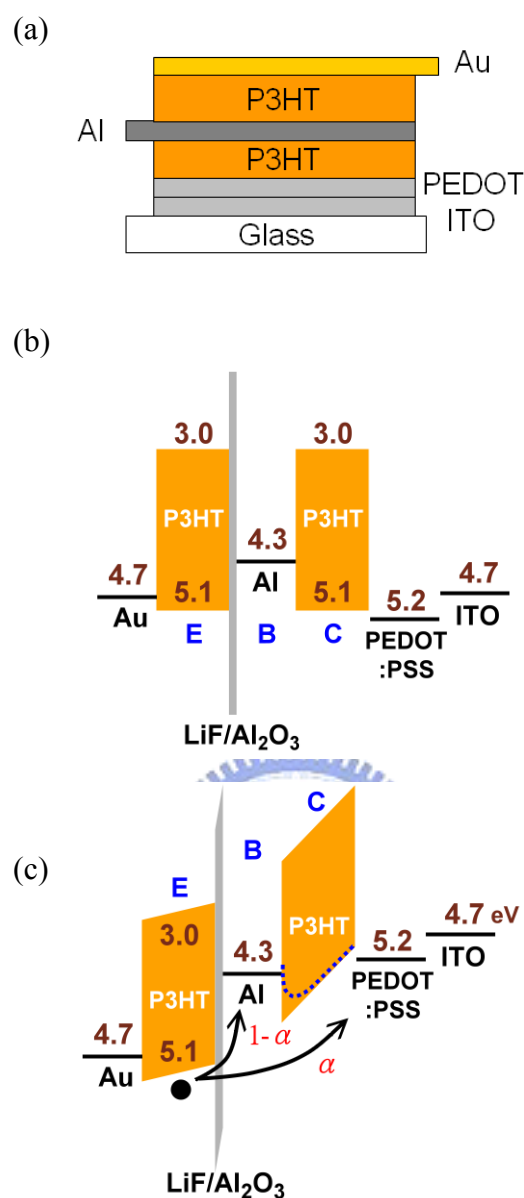


Figure 3.5 (a) The structures of polymer hot-carrier transistor with low bandgap emitter. (b) The energy band profile of metal-base hot-carrier transistor with low bandgap emitter. (c) The energy band profile of metal-base hot-carrier transistor in the active mode. The negatives of the actual energy are shown in order to illustrate the picture of holes better. The energies are indicated in eV.

for the Al is limited to be 3 minutes since a 15 Å Al can be completely oxidized in 5 minutes.[113] Another P3HT layer is spin coated from xylene (2 wt %) to form 320 Å emitter layer. Au is evaporated as the emitter contact. The active area is 2 mm². The devices are encapsulated by glass cap with UV glue in a glove box, and measured in

ambient condition. The sign convention throughout the text is that when holes leave from the base and collector, J_B and J_C are positive.

The work function of Au surface can be enhanced from 4.7 eV to 5.1 eV by UV/O₃ treatment to reduce the contamination.[112] However, the Au in our device is the topmost layer without any surface treatment, the work function of Au should remain close to its lower level of 4.7 eV. To confirm this we measure the diode with structure ITO/PEDOT/P3HT/Au. The I-V relation is highly asymmetric, implying that PEDOT is able to inject more holes than Au into P3HT. Since PEDOT work function is 5.1 eV the work function of Au is lower than 5.1 eV, consistent with the previous reports.[114] Even though there is still a moderate injection barrier from Au to P3HT, it is much smaller than the barrier between Au and PVK which is more than 0.7 eV.

3.3.3 The effect of the insulating layer thickness

Figure 3.6 shows the β of hot-carrier transistor with different LiF layer thickness with or without Al₂O₃ layer in the common-emitter configuration. The emitter voltage V_E is 0 V, collector voltage V_C is -5 V, and base current density J_B is 2 mA/cm². For transistor without Al₂O₃, β initially increases with increasing LiF thickness, and reaches a maximum $\beta = 0.6$ when LiF thickness is 10 Å. For LiF thickness higher than 10 Å, β decreases due to the insulating nature of LiF. For the transistor with Al₂O₃, β also has a maximum value of 1.6 when LiF thickness is 7 Å. The inset in Fig. 3.7 shows the atomic force microscopy (AFM) image of Al base on P3HT. No pinhole can be observed. In addition, the roughness of 2.6 nm is much smaller than the mean thickness of the Al base.

As LiF thickness increases, the tunneling barrier forms gradually, and the voltage drop across the LiF layer develops. Hence, the energy barrier at emitter-base junction is enlarged and the hot carrier loss to base reduced. However as the thickness is too

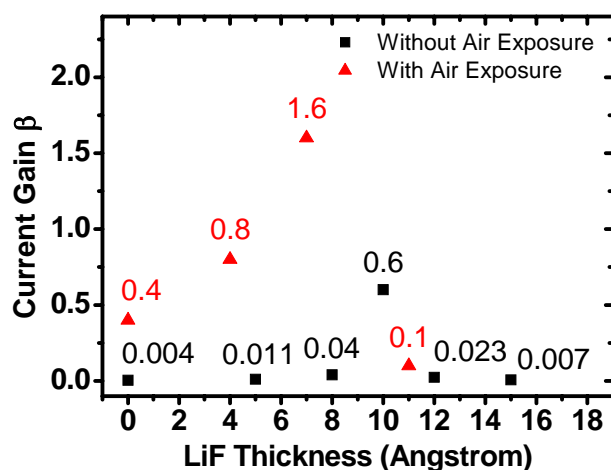


Figure 3.6 The current gain β as a function of LiF thickness of the hot-carrier transistor. The solid square (solid triangular) indicates the device without (with) exposure to air after Al deposition. The current gain is obtained in the common emitter configuration with V_E is 0 V, V_C is -5 V, and J_B is 2 mA/cm².

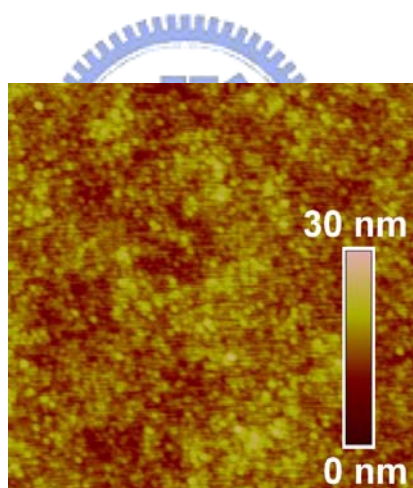


Figure 3.7 The AFM image of Al base on P3HT with roughness of 2.6 nm. The height scale is 30 nm and the dimensions of the image is 5×5 μm².

large the LiF layer becomes an insulator which blocks all carriers and the collector current density J_C becomes very small. The residual base current due to the reverse current of the base-collector diode then dominates and causes a small β . In general, β is much higher for devices with Al₂O₃ layer, and the maximal β occurs at smaller LiF thickness. The transistor with Al₂O₃ needs less LiF to achieve maximal β since there is an ultra thin Al₂O₃ before LiF deposition. The Al₂O₃ grown in air is dense with a

much better insulating property than LiF, so it may serve as a better tunneling barrier than LiF. Furthermore, the Al_2O_3 may prevent the reaction between Al and LiF which will release Li atom and reduce the thickness of the LiF.[115] Considering the small thickness of several Angstroms it is not likely that LiF will form a uniform layer without nucleation. However, similar to electron injection in organic light emitting diode, somehow, such a lands-like LiF layer has a great effect on device electrical performance.

3.3.4 The effect of the emitter-base diode current density

In addition to insulator thickness, β is also sensitive to the emitter thickness. A series of hot-carrier transistor with Al_2O_3 and 7 Å LiF, with various emitter thickness from 600 Å to 250 Å is fabricated. The emitter-base diode is fixed at a forward bias $V_{EB} = V_E - V_B$ of 4 V. The emitter-base diode current density J_{EB} increases from 2.7 to 80 mA/cm² as the emitter thickness decreases from 600 Å to 250 Å. Fig. 3.8 shows the relationship between β and J_{EB} . β is derived from the common-emitter characteristics with $V_E = 0$ V, $V_C = -10$ V, and $J_B = 2.5$ mA/cm². The β increases with increasing J_{EB} and decreasing emitter thickness. The highest $\beta = 8.8$ is obtained when J_{EB} is around 80 mA/cm² at 4 V. The base voltage V_B is recorded during the transistor operation to monitor the voltage distribution as shown in Fig. 3.9. Initially, V_{EB} increases with increasing $|V_C|$ then saturates. V_{EB} at $V_C = -10$ V and $J_B = 2.5$ mA/cm² decreases from 3.9 to 2.5 V with decreasing emitter thickness. The dependence of β on emitter thickness can be explained as follows. For thin thickness, a small V_{EB} is needed to obtain a specific J_B , so base-collector voltage $V_{BC} = V_B - V_C$ is larger for given V_C . The image-force lowering effect at the base-collector becomes strong as shown by the dotted line in Fig. 3.5. The effective barrier between the base and collector is therefore reduced further and hot carrier

collection more efficient.

3.3.5 Electrical characteristics

Under optimal conditions, the characteristics of the hot-carrier transistor using P3HT as both the emitter and collector is shown in Fig. 3.10. With the lower injection barrier from the Au anode, the collector current density J_C reaches as high as 31

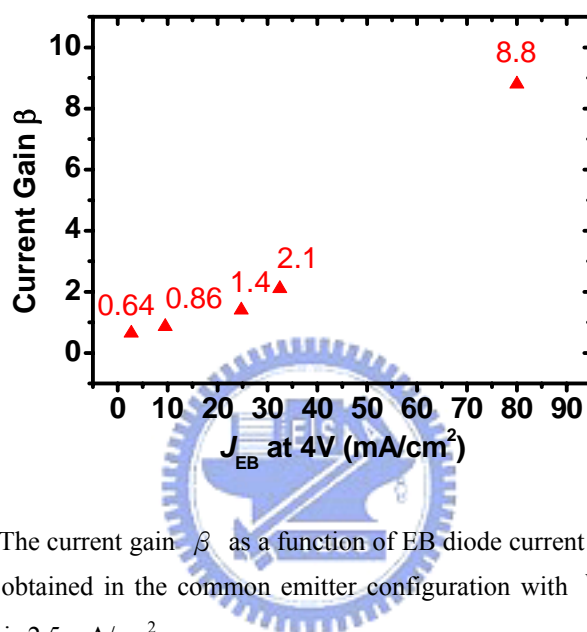


Figure 3.8 The current gain β as a function of EB diode current density at 4 V. The current gain is obtained in the common emitter configuration with V_E is 0 V, V_C is -5 V, and J_B is 2.5 mA/cm².

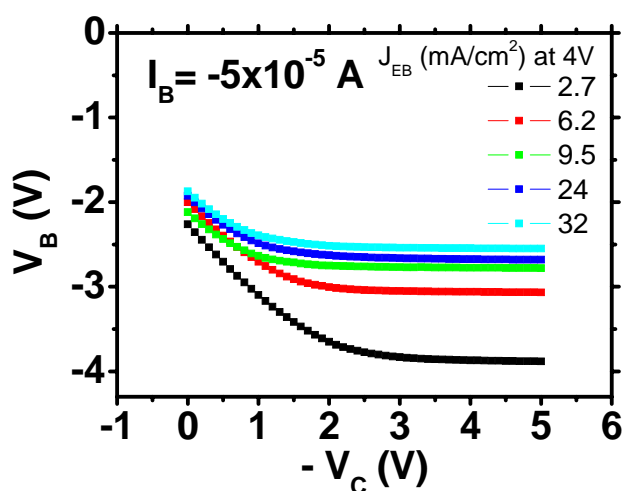


Figure 3.9 The base voltage of various devices with different emitter thickness and hence EB diode current density.

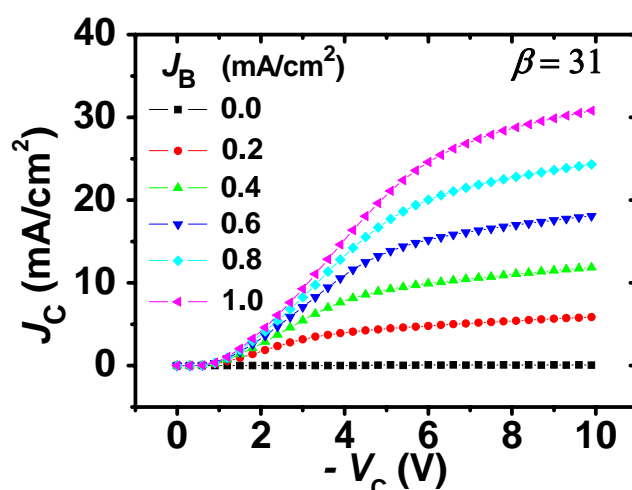


Figure 3.10 The characteristics of the polymer hot-carrier transistor in common emitter configuration. The emitter layer is P3HT.

mA/cm², a dramatic increase from the previous work using high bandgap emitter PVK by two orders of magnitude⁸. The β is 31. This value is similar to the case of PVK suggesting that the hot carrier collection is not compromised by the lower hot carrier energy as long as LiF layer is used. Even though there is no energy offset between the emitter and the collector semiconductor, Fig. 3.10 shows that the tunneling barrier alone is enough to produce a reasonable β with proper thickness. The transistor shows quite pronounced saturation as the collector voltage increases.

3.3.6 Frequency response

In addition to high β and current density, hot-carrier transistor has an intrinsic fast response because the effective channel length is defined by the film thickness which is only 150 nm. This length is much lower than the source-drain channel length of several microns for organic field-effect transistors. The carrier transit time across the channel is therefore much shorter. In fact, due to the higher vertical mobility, the operation frequency of polymer hot-carrier transistor is expected to exceed that of

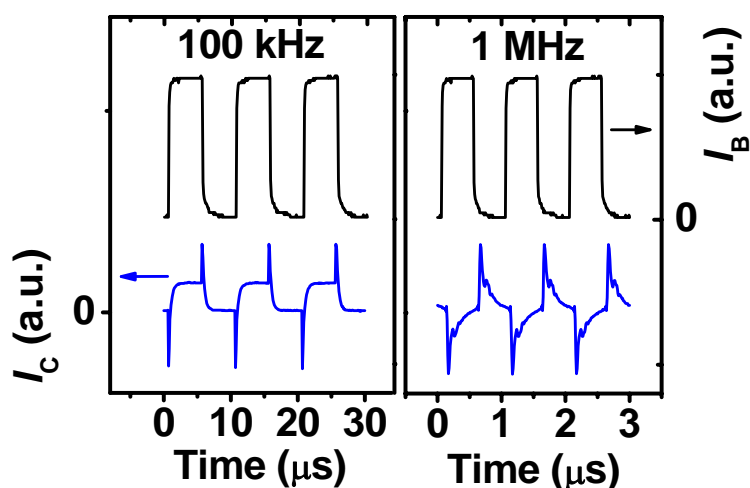


Figure 3.11 Frequency response of the hot-carrier transistor under modulation at 100 kHz and 1 MHz.

polymer light emitting diode (PLED). Fig. 3.11 shows the response of the transistor under modulation at 100 kHz and 1 MHz square wave applied between the base and emitter. The collector current is registered by the voltage across a 100Ω resistor in series. The collector current follows the square wave up to 100 kHz. At 1 MHz the output waveform is distorted but still responding. Polymer hot-carrier transistor is therefore promising for high speed applications in the radio frequency, such as radio-frequency identification.

3.3.7 Summary of section 3.3

In summary, we show that the high bandgap semiconductor is not necessary for the emitter in organic hot-carrier transistor in order to achieve a high common emitter current gain. Low bandgap polymer P3HT with the major advantage of easy current injection from the metal contact is used as the emitter and gives a high current density of 31 mA/cm^2 . The current gain maintains the high value of 31. The transistor can be operated at a high frequency.

3.4 Polymer hot-carrier transistor with a blend of low and high bandgap materials as emitter

3.4.1 Motivation

An ideal hot-carrier transistor has a high collector current and small base current. In Section 3.2, a high bandgap organic semiconductor poly(9-vinylcarbazole) (PVK) is selected for the emitter in order to maximize the energy barrier at the emitter-base junction.[70] Even though reasonable common emitter current gain β is achieved, the high bandgap emitter comes at a great cost. The high bandgap implies a large barrier for the holes to be injected from the metal contact to the emitter valance band.[111] Therefore, we replace the high bandgap emitter by a low bandgap polymer poly(3-hexylthiophene) (P3HT) with ionization potential (IP) at 5.1 eV. As shown in Section 3.3, a high current density of 31 mA/cm² and high current gain of 31 are achieved. In this section, we still try to enhance the output current density by studying the hot-carrier transistor whose emitter is a blend of low and high bandgap materials.

3.4.2 Device structure and fabrication

The device is fabricated on cleaned ITO substrate, and a 300 Å PEDOT:PSS layer is spin coated. P3HT is then spin coated to form the 1200 Å collector layer. A thin Al film around 80 Å is evaporated (10 Å /s) as the base through a shadow mask, followed by a LiF layer of various thicknesses. The optimal Al₂O₃ layer is formed by air exposure for 3 minutes after Al deposition. The oxidation time for the Al is limited to be 3 minutes since a 15 Å Al can be completely oxidized in 5 minutes. P3HT and PVK are blended in toluene solution (1:5 wt/wt) with the total polymer concentration of 6 wt % and spin-coated at 8000 rpm to form the emitter. Au is evaporated as the emitter contact. The active area is 2 mm². The devices are encapsulated by glass cap

with UV glue in a glove box, and measured in ambient condition. The sign convention throughout the text is that when holes leave from the base and collector, J_B and J_C are positive.

3.4.3 Electrical characteristics

The current density of emitter-base diode at $V_{EB} = 4$ V is 126 mA/cm^2 . This transistor is measured in the common-emitter configuration when $V_E = 0$ V, $V_C = -10$ V, and $J_B = 5 \text{ mA/cm}^2$. The collector current density J_C is 126 mA/cm^2 , β is 25, and on/off ratio is 468. When J_B increases to 40 mA/cm^2 , the output current density is as high as 428 mA/cm^2 , β is 11, and on/off ratio is 1751. The transistor characteristics is shown in Fig. 3.12. PVK:P3HT blend emitter give a surprisingly high current density, which is in fact much higher than in the organic light emitting diode. The previous limit of the current density in vertical type organic transistors is therefore completely removed. Unlike pure P3HT transistor in Fig. 3.10, the blend transistor in Fig. 3.12 somehow does not show a tendency for saturation. AFM image shows a rough surface with root-mean-square value of 20 nm. The roughness may increase the contact area between Au and emitter. In addition, some carriers could be injected stepwise from Au to P3HT, and then finally to PVK. The hot carriers in metal base from PVK have higher energy than those from P3HT, and are easier to cross the base-collector junction barrier and contribute to the collector current. Therefore, the output current density higher than 428 mA/cm^2 is achieved.

3.4.4 Connection between the polymer hot-carrier transistor and a polymer light-emitting diode

Now the current density of the hot-carrier transistor is high enough to drive a PLED, the ITO collector of the hot-carrier transistor and the ITO anode of the PLED are connected to demonstrate their integration as shown in Fig. 3.13. The PLED has

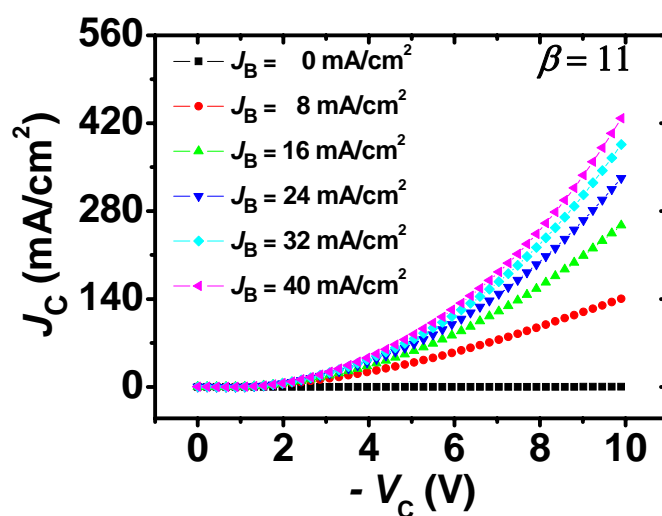


Figure 3.12 The characteristics of the polymer hot-carrier transistor in common emitter configuration. The emitter layer composed of P3HT and PVK in weight ratio 1:5.

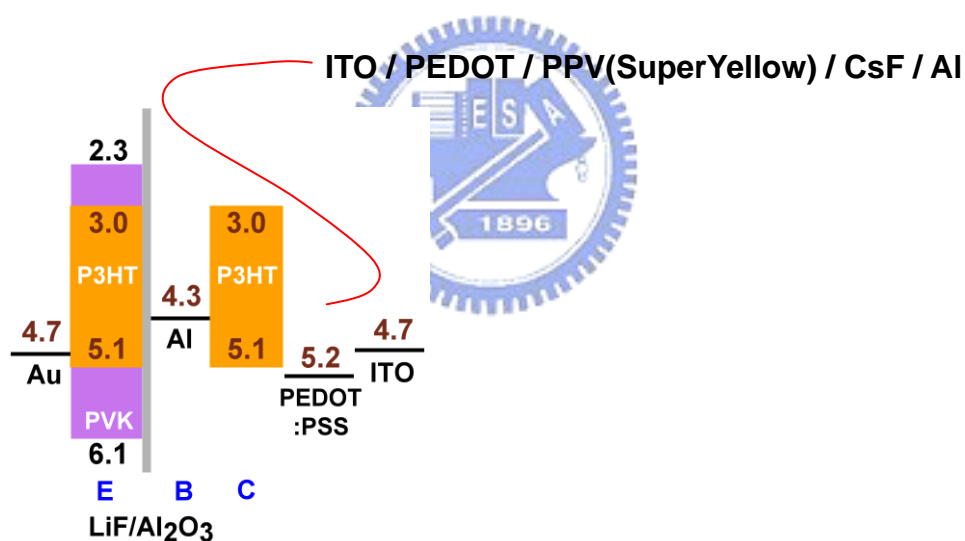


Figure 3.13 Connection between hot-carrier transistor and polymer light-emitting diode. The ITO collector of the hot-carrier transistor and the ITO anode of the PLED are connected to demonstrate their integration.

the structure ITO/PEDOT/PPV(SuperYellow)/CsF/Al. The Au electrode of hot-carrier transistor is grounded, and the cathode voltage of the PLED is kept constant at -10 V. The output current density, controlled by the J_B of hot-carrier transistor, modulates the PLED luminance. Fig. 3.14 shows the luminance of the PLED at various J_B . The

luminance of the PLED driven by the hot-carrier transistor can be over 3000 cd/m^2 , which is enough for most applications.

3.4.5 Summary of section 3.4

We show that the high bandgap semiconductor is not necessary for the emitter in organic hot-carrier transistor in order to achieve a high common emitter current gain. As blend of P3HT with high bandgap polymer PVK is used as the emitter, the current density reaches as high as several hundreds mA/cm^2 . Such current density is good enough to drive a polymer light-emitting diode to high brightness as demonstrated by their integration.

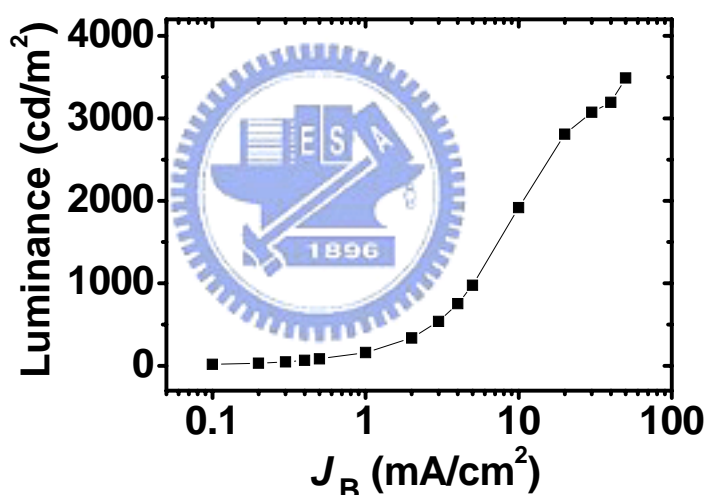


Figure 3.14 The luminance of the polymer light-emitting diode driven by the polymer hot-carrier transistor operated in various base current densities.

3.5 Summary of chapter 3

Metal-base hot-carrier transistor with high bandgap conjugated polymer emitter and collector is demonstrated in this chapter. The device is fabricated by multiple spin coating with the metal base sandwiched between two polymers. A thin insulating layer

of LiF is inserted between the emitter and base to enhance the hot carrier kinetic energy and reduce mutual dissolution. Using poly(9-vinylcarbazole) as the emitter, Al as the base, and poly(3-hexylthiophene) as the collector, common-emitter current gain of 25 is obtained with operation voltage as low as 5 V. Besides, vertical polymer hot-carrier transistor using the low bandgap material poly(3-hexylthiophene) as both the emitter and the collector are studied. The common emitter current gain is shown to depend on the LiF thickness and the emitter thickness, with maximal value at 31. Current density as high as 31 mA/cm^2 is achieved when collector voltage is -10 V . Furthermore, for the device using blend of poly(3-hexylthiophene) and high bandgap polymer poly(9-vinylcarbazole) as the emitter, the current density rises sharply to 428 mA/cm^2 . The brightness of 3000 cd/m^2 is obtained as a polymer light-emitting diode is driven by the transistor with the same area. The transistor can be operated at 100 kHz.



Chapter 4

Polymer space-charge-limited transistor

4.1 Introduction

4.1.1 Background

Electronic devices based on organic semiconductors provide attractive alternatives to inorganic devices due to their lower cost as well as the compatibility with flexible substrates. One of the key components in the organic electronic circuits is the polymer field-effect transistor (FET).[116,117] Many researches on polymer FET have demonstrated reasonable performance [15,118] and the possibility of integration with organic light-emitting diodes.[15-18] The characteristics of polymer FETs can be strengthened by increasing the mobility [53], utilizing a self-assemble monolayer as gate dielectrics [54] and reducing the channel lengths to the submicron [124]. Horizontal organic FETs with submicron channel lengths made by electron-beam lithography [56], nanoimprint lithography [57] and soft contact lamination [58] have been demonstrated. Vertical organic FETs, whose channel length was determined by the thickness of an insulating layer between source and

drain, have been made by solid-state embossing [59], excimer laser [60] and photolithography [61]. However, the inherently low mobility as well as the incompatibility between conventional submicron lithography and organic materials pose great limitation on the device performance and the fabrication process for polymer FET. The unique advantages of organic materials such as low-cost and large-area solution process are so far not fully explored for high-performance FET. Vertical non-field-effect transistors with multilayer structures give another route to circumvent the limits of both horizontal and vertical field-effect transistors. In vertical non-field-effect transistors, the channel length can be easily defined by the total thickness of the organic layers, and the current is modulated by a conductive layer embedded in the organic materials. Various device operating principles were proposed with different types of conductive layers such as a thin metal film [62,63,70,71], a strip-type metal film [64,65], a mesh gate electrode [66-68], and a porous conducting polymer network [69]. The remaining problems are the low current density, low on/off ratio as well as the complex fabrication process.

Take the organic static-induced transistor (SIT) as an example, it have a striped metal layer embedded in the thermally evaporated organic layer.[65,119] It has a similar structure with the vacuum tube triode, which consists of the cathode for electron emissions by heating, the anode for electron collection, and the grid for current modulation. In a vacuum tube triode both the grid and anode electrodes are able to control the potential within the device but the grid is much more effective in controlling the gradient near the cathode. When the grid is in large and negative bias, the electrons experience a negative gradient of potential after they are emitted from cathode. Effectively the electrons encounter a large energy barrier between cathode and anode, and consequently very few of them can be collected by the anode. On the contrary, if the grid is slightly negative biased or positively biased, it is possible for

the electrons to find a passage through the potential minimum between two grid wires. Despite similar structure, in SIT the current is modulated by a junction potential barrier while in vacuum tube triode the space-charge-limited current (SCLC) is modulated.[95] Another example is the “analog transistors” proposed by Schockley in 1952. It is the first solid-state device whose operation resembles that in the vacuum tube triode with current limited by the SCLC.[121]

4.1.2 Organization of this chapter

In this chapter, we demonstrated the polymer space-charge-limited transistor (SCLT) which functions similar to the vacuum tube triode. Characteristics of the polymer space-charge-limited transistor with low grid opening density on Al grid are shown in Section 4.2. After high grid opening density on the grid is obtained, high collector current density is achieved. Characteristics of polymer space-charge-limited transistor with high current density are discussed in Section 4.3.

4.2 Polymer space-charge-limited transistor with low current density

4.2.1 Motivation

SCLC is not the most common mode of transport in high-mobility inorganic semiconductors. However, in organic semiconductors, it is well known that the current is governed by SCLC. Therefore, conjugated polymer might be one candidate for the vertical non-FET analog transistor.[69,120] In this section, we present a vertical polymer version of solid-state vacuum tube triode with an embedded metal grid. A more transparent name “space-charge-limited transistor” is given to this device. The metal grid made of Al film with random openings functions similarly to

the grid in vacuum tube triode. The fabrication processes of polymer space-charge-limited transistor have both the advantages of short channel length and easy large-area solution processes. The carriers in the transistor are injected from the emitter, going through the openings on the metal grid and finally arriving at the collector. The potential distribution between emitter and collector can be controlled by the voltages of grid and collector. When the voltages of the grid and collector constitute a high barrier between the emitter and the opening, few carriers can arrive at the collector through the openings. On the other hand, if there is no barrier the carriers can go through the opening and reach the collector. The magnitude of the collector current is determined by the SCLC given by the potential difference between the emitter and the center of the opening. Collector current is modulated by the grid which controls the effective potential at the opening for fixed emitter and collector potentials.

4.2.2 Device structure and fabrication

The multilayer structure of the polymer space-charge-limited transistor is indium tin oxide (ITO) glass/PEDOT:PSS/P3HT/Al grid/P3HT/Al, as shown in Fig. 4.1 (a). P3HT is poly(3-hexylthiophene) which is used as the semiconducting polymer between the electrodes. PEDOT:PSS is poly(3,4-ethylenedioxythiophene) doped with polystyrene sulfonated acid. PEDOT:PSS with a work function of 5.2 eV serves as an Ohmic contact for hole injection into the highest occupied molecular orbital (HOMO) of P3HT at 5.1 eV as shown in Fig. 4.1 (b). The injected holes can pass through the openings on Al grid and finally arrive at Al collector as the transistor is on. The lowest unoccupied molecular orbital (LUMO) of P3HT is 3 eV, which is 1.3 eV higher than the Al work function of 4.3 eV to suppress unwanted electron current from Al to P3HT. Two differences between vacuum tube triode and the present

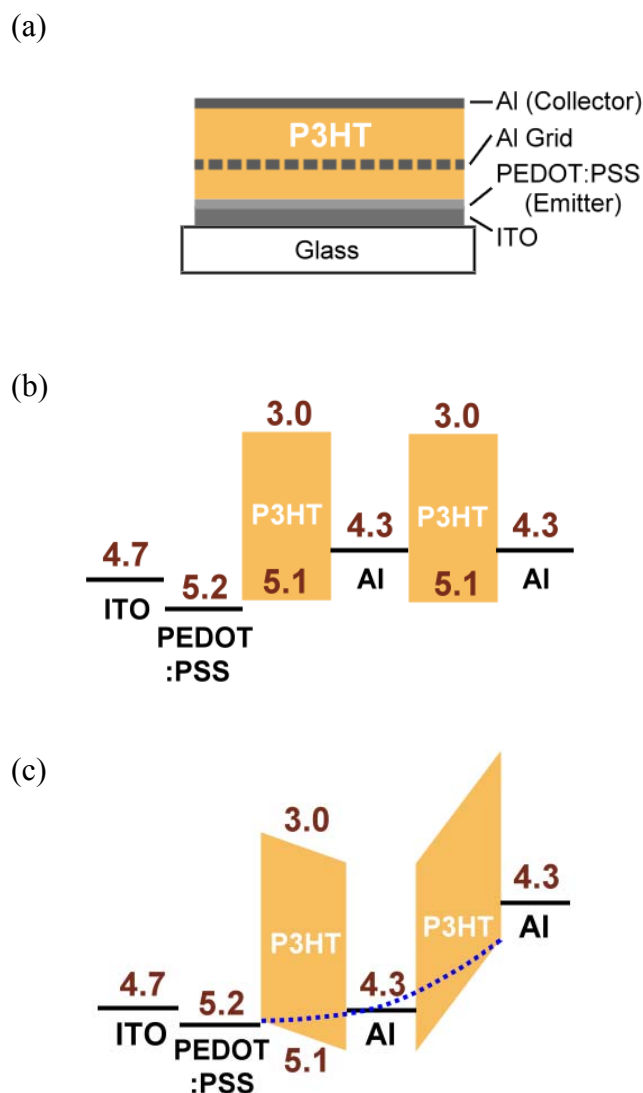


Figure 4.1 (a) Device structure of the polymer space-charge-limited transistor. (b) The energy band profile of the polymer space-charge-limited transistor. (c) The energy band profile of the polymer space-charge-limited transistor in operation. The dotted line is the potential profile along a path passing through the metal grid. The negatives of the actual energy are shown in order to illustrate the picture of holes better. The energies are indicated in eV.

polymer space-charge-limited transistor shall be mentioned. First, the carrier is hole in polymer space-charge-limited transistor while the carrier is electron in vacuum tube triode. Second, the carrier injection in polymer space-charge-limited transistor is via Ohmic contact, while in vacuum tube triode it is via thermionic emission of heated cathode. The basic operation principle of the transistor is illustrated in Fig. 4.1 (c) and

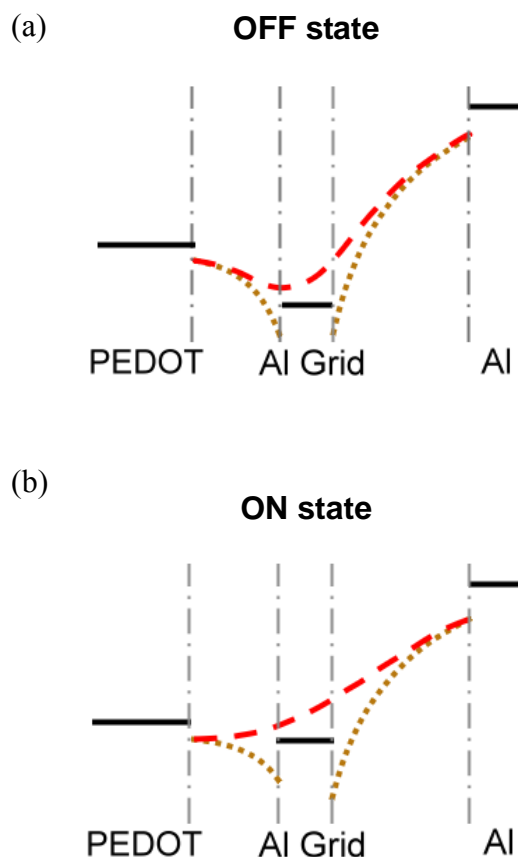


Figure 4.2 The potential profile for the (a) off and (b) on states of the transistor. The dash line is along the channel through the grid opening, while the dotted line is along the grid electrode. The solid line is the Fermi level of Al and PEDOT.

Fig. 4.2. The dotted line is the potential profile along a path passing through the metal grid, while the dash line is the profile along a path through the opening. As the transistor is off, no hole is collected due to the barrier between the emitter and opening. As the transistor is on, there is a SCLC between the emitter and opening.

The device is fabricated on patterned ITO glass substrate cleaned in ultrasonic bath. A layer of 500 Å PEDOT:PSS is spin coated onto ITO as the hole injection layer. After baking in vacuum at 200 °C for 10 min, the substrate is transferred to a glove box. P3HT is spin coated from chloroform solution (1 wt %) on the PEDOT:PSS layer, and then baked at 120 °C for 30 min in vacuum. A spin rinsing [122,123] with xylene is used to remove the remaining soluble part of P3HT, and a thin P3HT layer

of about 200 Å is obtained. To fabricate Al grid with openings, polystyrene spheres are used as shadow mask. Ethanol solution (0.1 wt %) of polystyrene spheres with various diameters is spin coated on P3HT, followed by 300 Å Al evaporated as the Al grid. After removing the polystyrene spheres by submerging the sample in ethanol for 20 s with ultrasonic agitation, an Al film with openings at the positions of the spheres is formed. A layer of 450 Å P3HT is then spin coated from xylene solution (1 wt %) on the sample, followed by depositing an Al film of 300 Å to complete the device. Ethanol was used to dilute the polystyrene spheres because its alkyl group improves the adhesion between polymer and polystyrene solution. The device active area is 1 mm².

4.2.3 Spin-coated polystyrene spheres as shadow mask

The AFM images of the surface of Al grid after removal of polystyrene spheres of 2000 and 5000 Å are shown in Figs. 4.3(a) and 4.3(b), respectively. The sizes of the openings are almost identical to the diameter of polystyrene spheres, which are removed without causing mechanical damages to the Al grid and the underlying spin-rinsed P3HT film. The spin-rinsed P3HT is intended to provide three advantages. First, the thickness of spin-rinsed P3HT film is usually less than 200 Å, which makes the Al grid much closer to the emitter than the collector. This geometry, similar to the vacuum tube triode, facilitates the Al grid to easily control the potential distribution near the emitter. Second, after the P3HT is spin rinsed with xylene, the film is not easy to be dissolved by xylene in the subsequent processes. This does not only prevent the possible dissolution when spin coating P3HT from xylene on Al grid but also the possible shorting between the emitter and Al grid caused by deformation. Third, the spin-rinsed P3HT film is robust during the removal of polystyrene spheres by ultrasonic agitation.

4.2.4 Device characteristics

Figure 4.4 shows the characteristics of polymer space-charge-limited transistor with hole diameter of 2000 Å on Al grid. I_C , J_C and V_C are the collector current, collector current density, and collector voltage, respectively. The ITO electrode is commonly grounded and the Al collector is negatively biased at V_C with respect to ITO. The negative J_C means that holes are driven toward the collector through the grid. The J_C has apparent modulation by the grid voltage V_G . As shown in Fig. 4.4(d), the grid current density J_G is in the order of 10^{-5} mA/cm² when different V_G are applied. To avoid large J_G , V_G is restricted to be not more negative than -0.85 V which is the built-in potential between PEDOT:PSS and Al. A large J_G is

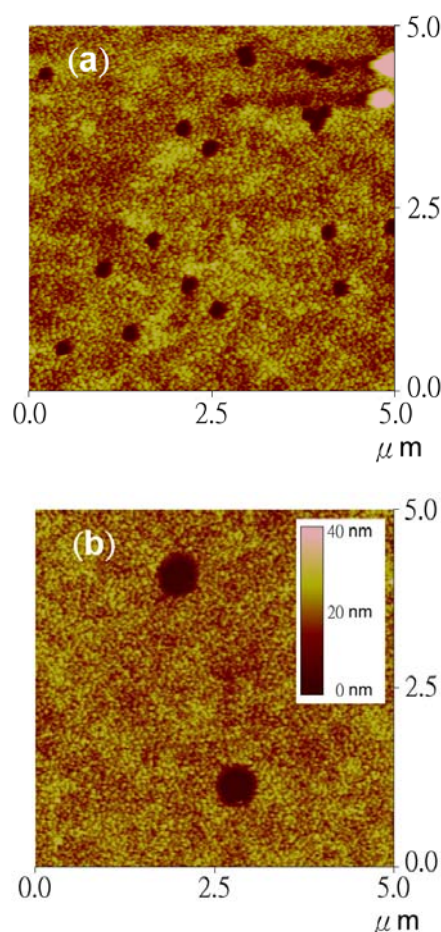


Figure 4.3 The AFM images of the Al grid after removal of polystyrene spheres with diameter of (a) 2000 Å and (b) 5000 Å. Note the aggregate at the upper right corner of (a).

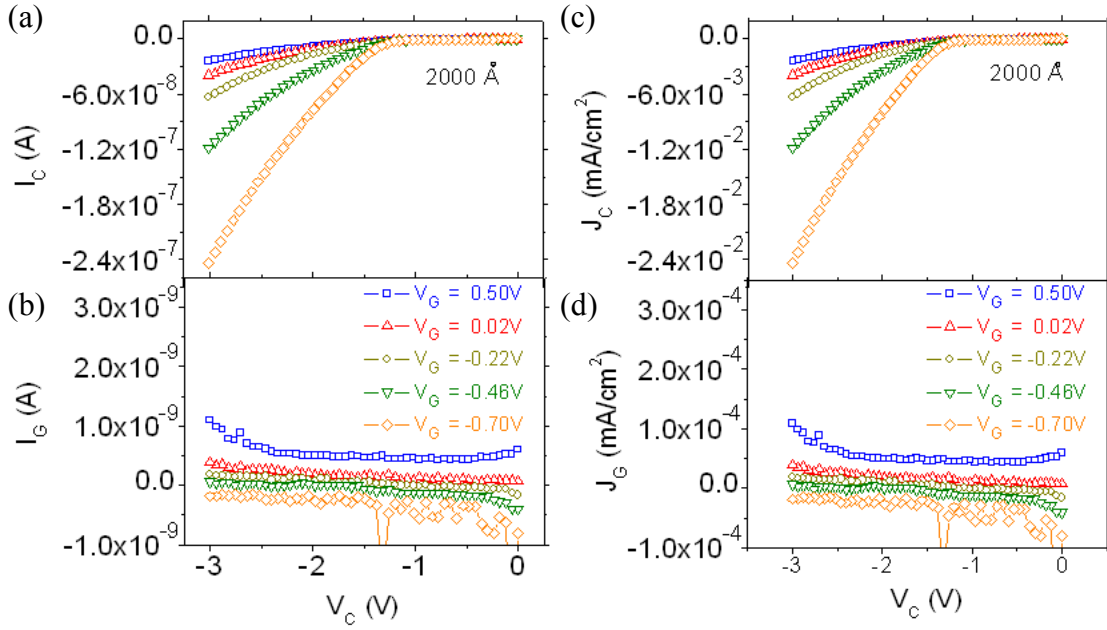


Figure 4.4 (a) Collector current I_C and (b) grid current I_G as a function of collector voltage V_C at different grid bias V_G of device with 2000 Å openings on Al grid. Same data represent in current density are also shown. (c) Collector current density J_C and (d) grid current density J_G as a function of collector voltage V_C .

obtained when negative V_G is applied beyond -0.9 V. The current gain, defined by $\partial I_C / \partial I_G$, is 506 when V_C is -3 V. The transconductance $g_m = \partial I_C / \partial V_G$ is 3.21×10^{-6} S, calculated from the slope of the $I_C - V_G$ curve in the range from -0.75 to -0.81 V. The off current can be reduced by continuing to increase V_G until the occurrence of a large leakage current between the grid and collector. In principle, lower off current can be achieved by reducing the aggregate of polystyrene spheres, which introduce the big holes on the Al grid film shown in the upper right corner of Fig. 4.3(a). In order to verify the presumption that this device works in the same way as in vacuum tube triode, we look for signature of the SCLC behavior. The collector current for the vacuum tube triode is given by $I_C = C(\mu V_G + V_C)^n$. μ is the grid amplification factor.[95] The linear combination of grid and collector potential $\mu V_G + V_C$ is the effective potential at the opening. $n = 3/2$ for ballistic SCLC in

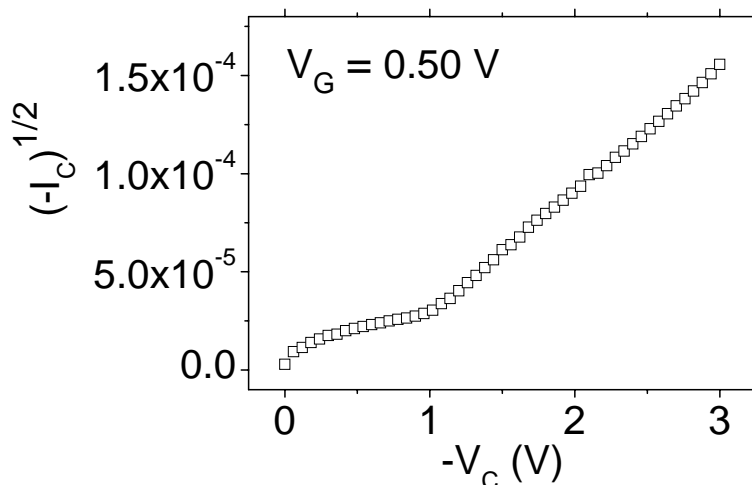
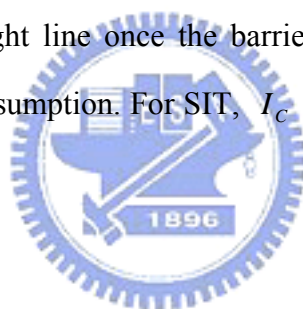


Figure 4.5 $(-I_C)^{1/2}$ against $-V_C$ when $V_G=0.5V$.

vacuum and $n = 2$ for diffusive SCLC in solid state. Plotting $I_C^{1/2}$ against V_C in the Fig. 4.5 indeed gives a straight line once the barrier at the opening is suppressed, confirming the key SCLC presumption. For SIT, I_C would depend exponentially on V_C . [95]



4.2.5 The effect of the opening diameter and density

The diameter and density of the openings are also crucial to the properties of polymer space-charge-limited transistor. As demonstrated in Fig. 4.6(a), the $J_C - V_C$ curves of the device with opening diameter of 1000 Å are overlapped with positive V_G . On the other hand, curves corresponding to the device with opening diameter of 5000 Å separate from each other but with a high off current as shown in Fig. 4.6(b). The current is difficult to be turned off because of the region around the center of the opening is too far from the Al grid, thus the potential barrier is only enhanced slightly by grid potential ($\mu \ll 1$) before the leakage current between the reverse-biased grid and collector occurs. Therefore the optimal opening diameter falls in the range of 1000 and 5000 Å. Figures 4.6(c) and 4.6(d) show the characteristics of polymer

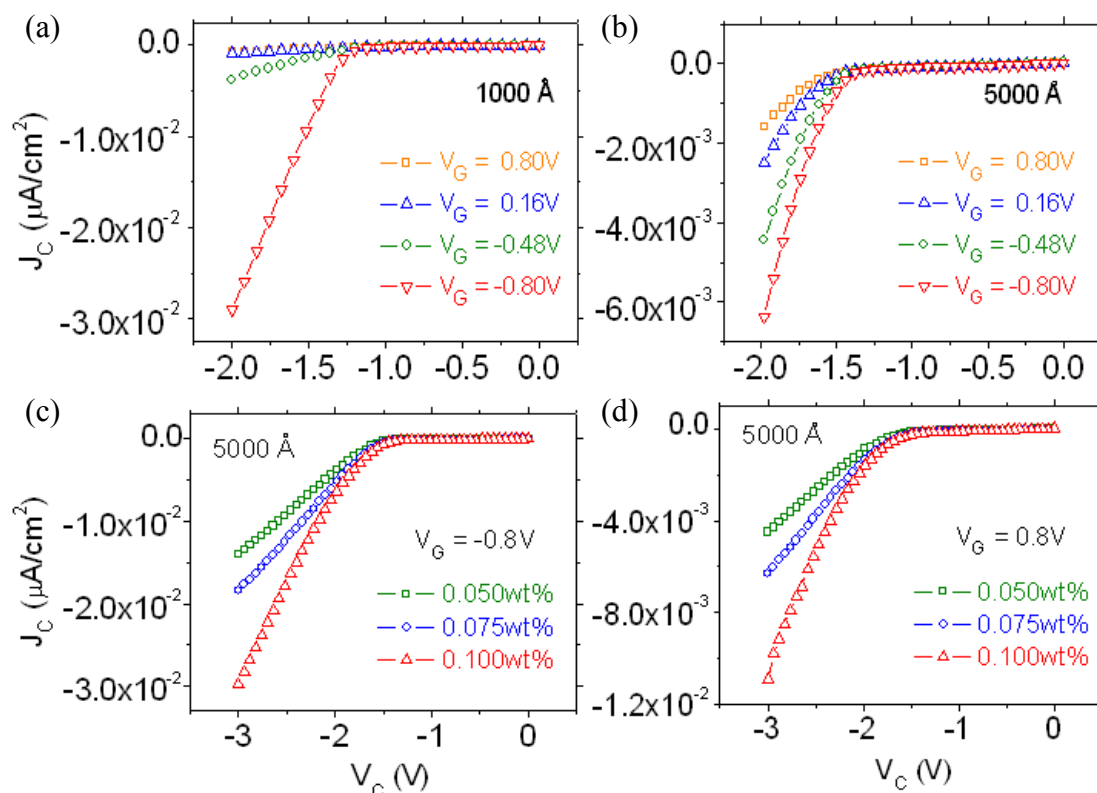


Figure 4.6 The characteristics of the polymer space-charge-limited transistor with (a) 1000 Å and (b) 5000 Å opening diameter on Al grid. The characteristics of the polymer space-charge-limited transistor with different concentration of polystyrene spheres used in fabrication process when V_G is (c) -0.8 V and (d) 0.8 V.

space-charge-limited transistor with different opening density when V_G is -0.8 and 0.8 V. Higher J_C is obtained with higher concentration of polystyrene sphere solution in the fabrication process of Al grid. This indicates that by using the higher concentration of polystyrene sphere solution the higher opening density is obtained, which in turn leads to more current paths and higher J_C . The way to achieve high polystyrene sphere density without aggregation like the case shown in Fig. 4.3(a) will be the key issue for further study.

4.2.6 Summary of section 4.2

In summary, a solution-processed vertical polymer space-charge-limited transistor is demonstrated. A nonlithographic method is introduced for Al grid

fabrication with different opening diameters. The operating voltage is as low as 3 V. The transconductance is 3.21×10^{-6} S and the current gain is 506. Such device concept has the potential advantages of easy large-area solution process, high current, low voltage, and being lithography-free.

4.3 Polymer space-charge-limited transistor with high current density

4.3.1 Motivation

Previously, we demonstrated the polymer space-charge-limited transistor (SCLT) which functions similar to the vacuum tube triode, as shown in Section 4.2. A metal with random openings made by non-lithographic method is used as the grid. The output current density is however only about 0.01 mA/cm^2 due to the difficulty in realizing high opening density. In this work we solve that difficulty and the current density is significantly raised by two orders of magnitudes to as high as 1 mA/cm^2 , which is nearly enough to drive a high-efficiency phosphorescent organic LED with the same area.

4.3.2 Device structure and fabrication

The schematic device structure and the energy band diagram are shown in Fig. 4.7. Poly(3,4-ethylenedioxythiophene):poly(styrenesulfonate) (PEDOT:PSS), with a work function of 5.2 eV, was used as an Ohmic contact for hole injection into the highest occupied molecular orbital (HOMO) of poly(3-hexylthiophene) (P3HT) at 5.1 eV. As the transistor is on, the injected holes can pass through the openings on Al grid and collected by Al collector electrode. The Al grid, functions similarly to the grid in vacuum tube triode, is an Al film with a high density of random submicron openings.

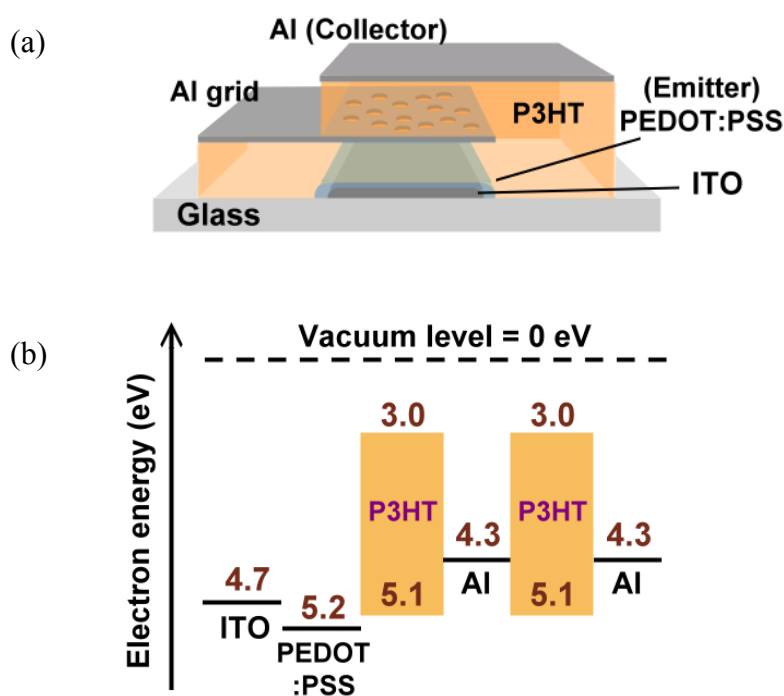


Figure 4.7 (a) Device structure of polymer SCLT with an Al grid with random submicron openings. (b) Energy band diagram of polymer SCLT. The energies are indicated in eV. The solid line is the Fermi level of Al and PEDOT:PSS. The LUMO and HOMO energy for P3HT are 3 and 5.1 eV. The thickness between PEDOT and Al grid is 200 Å, and 300 Å between grid and Al collector.

The polystyrene spheres are used as the shadow mask for Al deposition to form Al grid, and the openings are formed at the positions of the spheres. The current density is proportional to the opening density. We form Al grid with high opening density using controlled assembly of polystyrene spheres on hydrophobic polymer surface, resulting a much higher current density.

The device is fabricated on a cleaned indium-tin-oxide (ITO) glass substrate with a layer of 400 Å PEDOT:PSS. After baking in glove box at 200 °C for 10 min, P3HT is spin coated from chlorobenzene solution (1.5 wt %) on the PEDOT:PSS layer and anneal at 200 °C for 10 min. A spin rinsing with xylene is used to remove the remaining soluble part of P3HT, even though the P3HT annealing condition has been chosen to have an almost fixed thickness after spin rinsing. After depositing the polystyrene spheres on the P3HT surface with the method described in the next

section, the 150 Å Al grid is evaporated. After removing the polystyrene spheres by an adhesive tape, a layer of 300 Å P3HT is spin coated from xylene solution (1.3 wt %). An Al film of 300 Å is finally deposited to complete the device. The device active area is 1 mm².

4.3.3 High density polystyrene spheres as shadow mask

A variety of self-assembly strategies of polystyrene spheres have been developed for hydrophilic surface to form two dimensional colloidal arrays [67,68,125,126]. A major problem to achieve a high density of separated colloid spheres is the hydrostatic attraction among the spheres. Fujimoto et al [67] rinsed the samples in 98 °C water to avoid the sphere aggregation on the hydrophilic glass substrate. However, for the hydrophobic surface of the polymer like P3HT, modifications of these strategies are necessary. We use ethanol to dilute the polystyrene spheres (Sigma-Aldrich) for decreasing the contact angle since its alkyl group improves the adhesion between polymer and polystyrene ethanol solution. The polystyrene spheres are absorbed on the P3HT film surface by submerging the film in a polystyrene spheres ethanol solution for tens of seconds. The key procedure in the fabrication is that the substrate is then transferred to a beaker with boiling isopropanol solution for ten seconds. Similar to the method of Fujimoto et al [67], the substrate is finally blown dry immediately in a unidirectional nitrogen flow. After the Al deposition as Al grid, the polystyrene spheres are removed by an adhesive tape (Scotch, 3M) without damage to the metal. The atomic force microscopy (AFM, Digital Instruments D3100) images of the Al grid with 1000 Å and 2000 Å opening diameter are shown in Fig. 4.8. The boiling isopropanol treatment is a critical step to achieve a high density yet separated array of holes, required for vacuum tube triode as well as SCLT. When the substrate is submerged in polystyrene solution, the charged polystyrene spheres are absorbed on

the P3HT surface without aggregation due to the electrostatic repulsion force. Without the boiling isopropanol treatment, the polystyrene spheres are easy to aggregate during the drying process and cause unwanted non-uniform and connected distribution (Fig. 4.8(f)). This may be attributed to the capillary force which pulls spheres into aggregates before the spheres are immobile when the solvent is vaporized. The importance of the boiling isopropanol treatment is presumed to increase the evaporation rate of the solvent during the nitrogen blow dry such that the spheres do not have enough time to move to one another and form aggregate during evaporation. Another possible advantage of the boiling solvent is that it partially melts the spheres and glues the spheres on the surface. With the boiling isopropanol treatment, the opening density on the Al grid indeed increases dramatically, and the openings remain separated. The opening density on the Al grid increases with increasing solution concentration and submerging time (Fig. 4.8(a)-(e)). However, the amount of openings with irregular shape and size also increases (Fig. 4.8(e)). This may be due to the high capillary force between spheres with very short distance when the sphere density is high, or due to the unabsorbed spheres in the fluid over the film. One way to remove these unabsorbed spheres is gently rinsing the surface with ethanol or isopropanol before boiling isopropanol treatment. In spite of some occurrence of the unwanted irregular openings, the condition to prepare Al grid with maximum opening density with minimum unwanted openings can be found by tuning the solution concentration and submerging time. The benefit of this method is the possibility to process large areas in a short processing time without photolithography.

4.3.4 Electrical characteristics

The characteristics of polymer SCLT with opening diameters of 1000 Å and 2000 Å on Al grid are shown in Fig. 4.9(a) and 4.9(c). First note there is one major

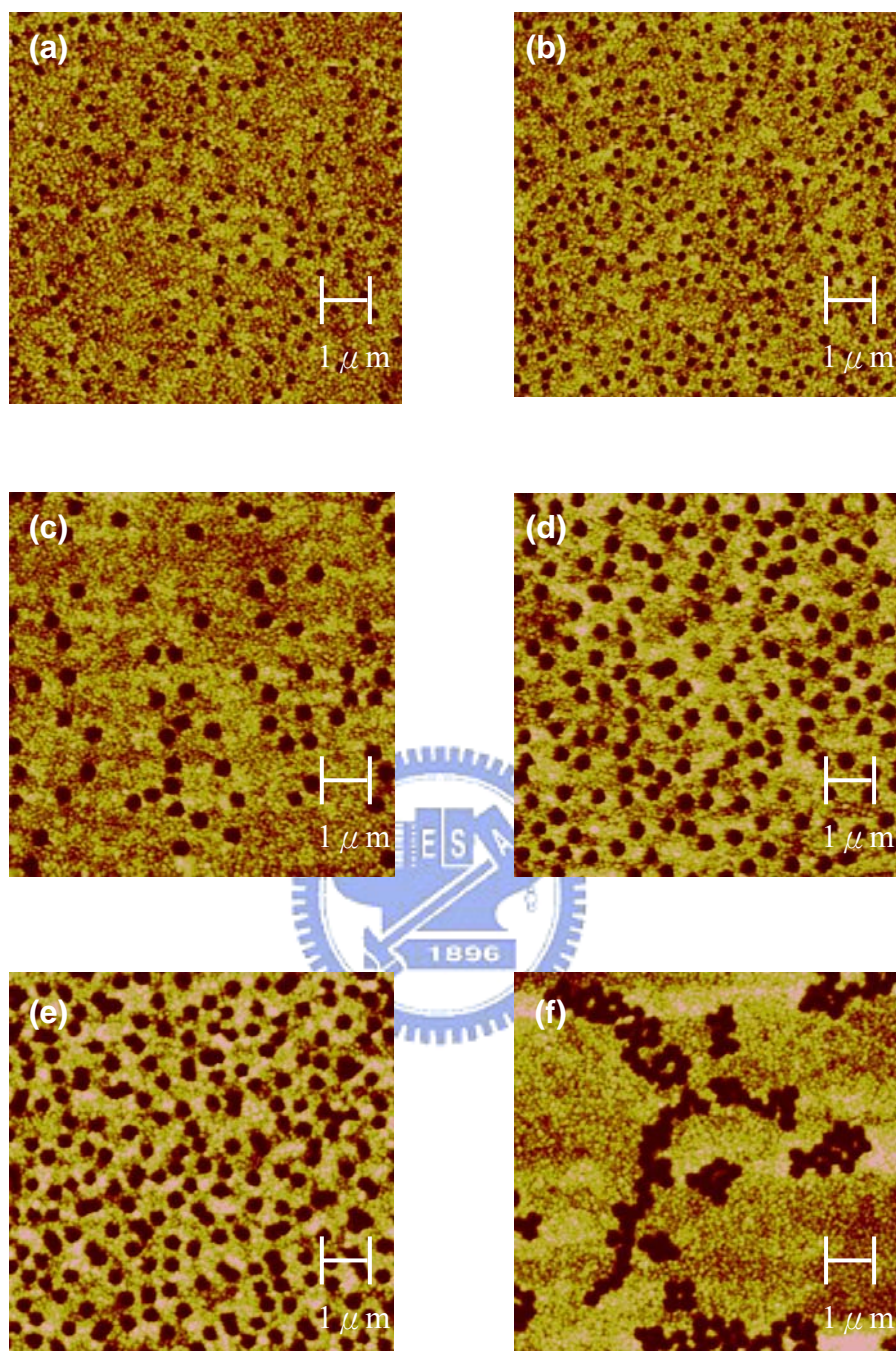


Figure 4.8 Al grid with opening diameter of 1000 Å prepared by submerging the substrate in (a) 0.05 wt.%, and (b) 0.1 wt.% polystyrene solutions for 20 s with the boiling isopropanol treatment. Al grid with opening diameter of 2000 Å prepared by submerging the substrate in (c) 0.08 wt.%, (d) 0.24 wt.% and (e) 0.4 wt.% polystyrene solutions for 40 s with the boiling isopropanol treatment. (f) Same condition in (e) but without the boiling isopropanol treatment. The height scale is 30 nm for each image and the dimensions of the image is $5 \times 5 \mu\text{m}^2$.

difference on the grid current density J_G between vacuum tube and SCLT. The grid electrode in vacuum tube is not heated so the possibility for the electrons to enter the vacuum by thermal excitation from the grid is practically zero. There is therefore no need to consider the current gain which is defined as the ratio between the collector current and grid current. However in SCLT the carriers in the Al grid are blocked only by the Schottky barrier of 0.5 eV between Al and P3HT. In fact the grid current is the reverse current of the Al/P3HT Schottky diode which is small but not zero. The current gain is therefore an important value to be maximized. As shown in Fig. 4.9(b) and 4.9(d), the grid current density J_G of our devices is in the order of 10^{-9} A which is much smaller than J_C . The current gain J_C/J_G is as large as 10^4 . For fixed collector voltage the collector current J_C is modulated by the grid voltage V_G . The emitter is the common ground. V_G is limited to be no more negative than -1 V otherwise the emitter-grid diode would turn on and cause large J_G . The positive V_G is used to introduce energy barrier for holes at the openings, and the off current can be reduced by increasing V_G until a large leakage current between the grid and collector occurs. The on/off ratio of J_C is 123 and 116 at $V_G = -4$ V, respectively, for transistors with opening diameters of 1000 Å and 2000 Å on Al grid. The highest J_C output is 1.14 mA/cm² in Fig. 4.9(c), for active area of 1 mm². Note the total output current can be easily scaled up by using a larger area. In order to look for the signature of SCLC, the device characteristics in double logarithmic scale with fixed V_G are shown in the inset of Fig. 4.9(a) and 4.9(c). Three regions belonging to ohmic, trap filling and SCLC can be distinguished [127]. The slope of $\log I - \log V$ is equal to 1 for ohmic conduction, while the slope is equal to 2 for SCLC. The dashed lines with slope equal to 1 and 2 are drawn in the inset of Fig. 4.9(a) and 4.9(c) for indication. Indeed, the current follows the SCLC once the barrier at the opening is suppressed by a negative enough V_G . At low voltage there is always a small ohmic

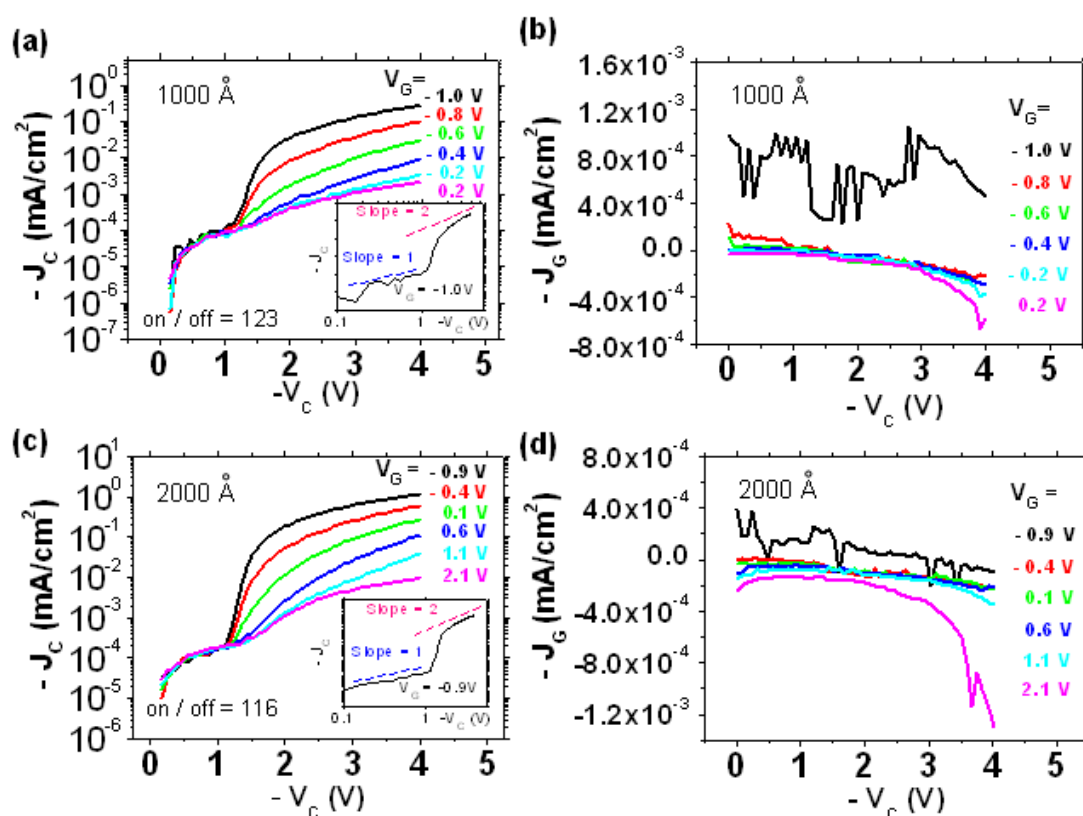


Figure 4.9 The electric characteristics of the polymer SCLT with various grid voltages applied. The ITO electrode is commonly grounded and the Al collector is negatively biased at V_C with respect to ITO. The negative collector current I_C means the holes are collected by the Al collector and flows out from the transistor. The gate current I_G is no more than a few nA for all measurements. (a) The collector current as a function of the collector voltage. During the fabrication procedure, the 0.05 wt.% solution of polystyrene spheres with diameters of 1000 Å is used. The submerging time is 20 s. The inset shows the characteristics in double logarithmic of the device with V_G equal to -1 V. (b) The grid current as a function of the collector voltage of the transistor with same fabrication procedure described in (a). (c) The collector current as a function of the collector voltage. During the fabrication procedure, the 0.08 wt.% solution of polystyrene spheres with diameters of 2000 Å is used. The submerging time is 40 s. The inset shows the characteristics in double logarithmic of the device with V_G equal to -0.9 V. (d) The grid current as a function of the collector voltage of the transistor with same fabrication procedure described in (c).

current. The polymer diode has a turn-on voltage where the current switches from a small leakage ohmic current into a quadratic SCLC current. The turn-on voltage is

determined by both the level of the leakage and the difference between the work functions of the cathode and anode. For our diode it is about 1 V as shown in Fig. 4.9.

4.3.5 Operation mechanism

The operation mechanism of the polymer SCLT can be understood as the quadratic space-charge-limited current between the emitter and the opening modulated by the grid potential. As in vacuum tube, the potential at the center of the opening is a linear combination of grid and collector potential $\mu V_G + V_C$, the factor μ depends on the device geometry and increases with the ratio between the opening diameter and the grid-collector distance. The SCLC between the emitter and the opening is therefore approximately $C\varepsilon\mu(\lambda V_G + V_C)^2/L^3$, where ε is the polymer dielectric constant and L is the emitter-grid distance. If the potential across the opening were uniform, the factor C would be the standard SCLC value of $9/8$. The overall effect of non-uniform potential in our case can be absorbed into a numerical factor C . Because of the higher electric field the space between the grid and the collector does not limit the collector current so the emitter-opening current given above is actually the output current.

The above analysis is based on the assumption that all the space charge and potential profiles are determined by the injected carriers instead of background doping. The active semiconductor P3HT is an intrinsic semiconductor without intentional doping. It is well known the main source of unintentional doping of P3HT is oxygen. The samples are fabricated in our glove box with oxygen level below 1 ppm. There are reports on the doping level of P3HT around 10^{15} cm^{-3} without particular attention on oxygen doping.[128] The sample fabrication process is carefully controlled to minimize the oxygen and water contamination. The water and oxygen level inside the glove box are both below 1 ppm. Dehydrated ethanol ($\leq 0.2\%$ water, Riedel-de-Haën)

is used for the polystyrene sphere deposition. The vacuum in the grid evaporation chamber is 10^{-7} torr, so most of the adsorbed oxygen molecules during ethanol immersion are expected to be removed by the high vacuum. Moreover the sample is annealed at $200\text{ }^{\circ}\text{C}$ in vacuum after the spin coating of the second P3HT film. It is known that thermal treatment will significantly de-dope P3HT.[129] We therefore believe our doping level is below 10^{15} cm^{-3} . Even for 10^{15} cm^{-3} the calculated Debye-Huckel screening length is 700 \AA which is larger than the total thickness of the SCLT. The electric field provided by the collector voltage is therefore not screened. The quadratic $I_C - V_C$ relation indicates that the space charge is dominated by the injection carrier. This is also an evidence that the doping is not important for the device operation here.

The grid control of the current can be further illustrated by looking at the spatial distribution of the current across the opening. In general only some region near the center of the opening has negative potential for the holes to pass through. Near the edge the effect of the grid is so strong that a potential barrier forms despite of the negative potential of the collector. The current is therefore confined in an area controlled by the grid potential. As the transistor is in the on state, there is no barrier in all the area. The emitter-collector path through A position at the center and the path through B position near the edge of the opening have the potential profiles as the curves (x) and (y) in Fig. 4.10(b) respectively. Assuming that the collector current is roughly a superposition of the currents of many small diodes given by the paths through different positions, the small diodes at position A contributing to a high current (A^{ON}) and those at position B are just about to be turned on (B^{ON}), as indicated in Fig. 4.10(c). On the other hand as the device is in the off state, the grid potential is positive and there is a potential barrier at the B position as the curve (z) in Fig. 4.10(b), and the small diodes there is reverse biased (B^{OFF}). As for A position, if it also has the

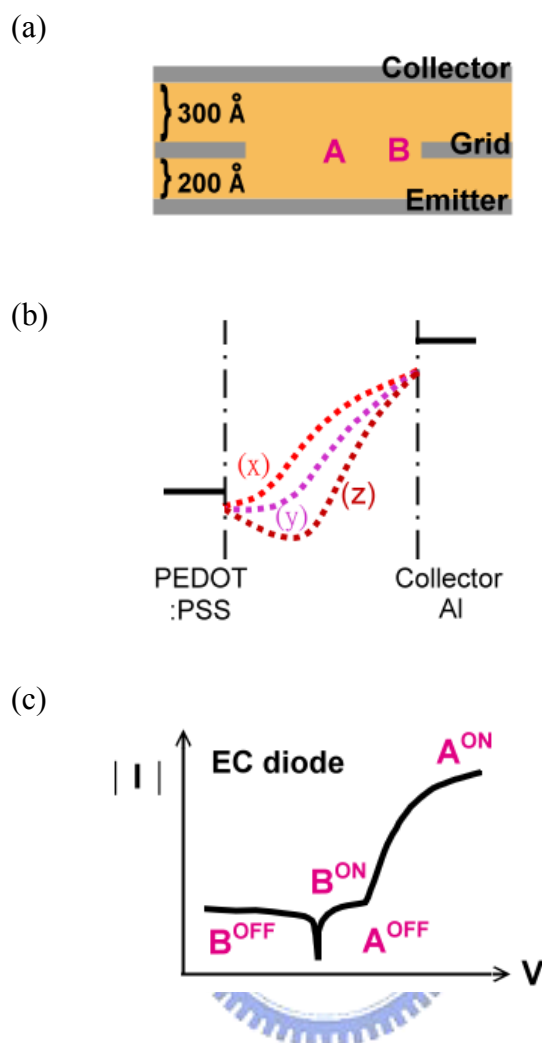


Figure 4.10 (a) The device structure near one opening of polymer SCLT. Position A is at the center of the opening, while position B is near the grid. (b) The potential profile along the emitter–collector path through the opening when V_C is fixed at a negative value. (x), (y), (z) are the potential profile along the path for various conditions. Curve (x) is a potential profile without energy barrier for hole as in the case of a simple emitter–collector diode without the grid. Curve (z) is a potential profile with energy barrier for hole for a positive enough grid potential V_G . The barrier for hole diminishes while V_G drops from positive to negative as indicated by (y). Different position in the opening has different potential profile, which result from different $\lambda V_G + V_C$. (c) The schematic current–voltage curve of EC diode with the structure ITO/PEDOT/P3HT/Al. There is a turn-on voltage for the forward bias direction. The path through position A in on or off state are denote as A^{ON} or A^{OFF} in the diode IV curve. The double-sided arrow means off-state could be either reverse bias or small forward bias before turn-on. The state of the path through B is also shown. Because of the proximity to the positive biased grid B path can never be fully turned on as A.

potential profile like curve (z) in Fig. 4.10(b), the off current comes from small diodes at position A will be small. However, if the potential profile is as the curve (y), there will be an undesirable leakage current from the barely-on small diode at A (A^{OFF}). Theoretically an even more positive grid potential can always drive it into curve (z), but in practice breakdown of the grid/polymer Schottky junction may happen first.

4.3.6 Summary of section 4.3

In summary, we demonstrate the vertical polymer space-charge-limited transistor with high current density, high on/off ratio, high current gain, and low operation voltage. A non-lithography method is introduced for the desired high opening density on the metal grid embedded in the polymer. This non-field-effect device opens a new possibility for high-performance organic electronics with easy large-area solution process and vertical integration with organic light-emitting diodes without demanding a very high carrier mobility.



4.4 Summary of chapter 4

A polymer non-field-effect transistor in a vertical architecture with an Al grid embedded in a polymer sandwiched between another two electrodes is demonstrated in this chapter. A metal grid is sandwiched between poly(3-hexylthiophene) to form a solid-state version of vacuum tube triode, where the vertical space-charge-limited current is modulated by the grid potential. The Al grid contains random submicron openings formed by a nonlithographic method. The multilayer polymer structure is made by spin coating. This device modulates the space-charge-limited current of a unipolar polymer diode with the Al grid. For the transistor with low opening density, the current density is around 0.01 mA/cm^2 . The operating voltage of the polymer space-charge-limited transistor is 3 V, and the current gain of 506 is obtained. The

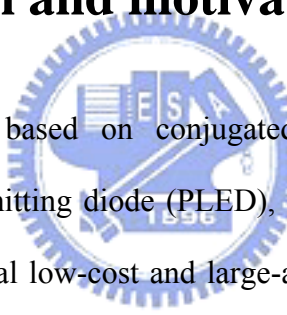
characteristics of the transistor can be tuned by the diameters and the density of the openings on the grid. Similar to the vacuum tube triode, the current follows a power law voltage dependence. For the transistor with high opening density, the current density higher than 1 mA/cm^2 is achieved. The operating voltage of the device is as low as 4 V, the on/off ratio is higher than one hundred, and the current gain is 104.



Chapter 5

Light-emitting polymer space-charge-limited transistor

5.1 Introduction and motivation



Semiconductor devices based on conjugated polymers have been widely explored for polymer light-emitting diode (PLED), field-effect transistor (FET), and solar cell, due to their potential low-cost and large-area solution process. One of the promising applications of the polymer devices is the thin, flexible, and light-weight active-matrix display.[130] Unlike liquid-crystal display which is voltage-controlled, in polymer display a PLED in each pixel is controlled by a driving transistor which supplies the current.[131] The current output of the transistor must be very stable and uniform. Currently poly-crystalline silicon FET suffers from uniformity problem, while amorphous silicon and organic FET have rather low carrier mobility and long-term stability problems.[132] In addition, FET is a horizontal device while PLED is a vertical device, so they can only be placed side by side and the aperture ratio of the pixel is limited by the size of the FET. One possible way to replace the conventional combination of LED driven by FET is the organic light-emitting transistor which combines the electrical switching and the light generation capabilities

in a single device.[133-136] Under appropriate bias conditions, both electrons and holes are injected from the electrodes into the transistor channel and recombine radiatively to generate light. However, so far the applications of light-emitting transistor is hindered because the emission efficiency is rather low, and the emission zone is in a narrow line pattern which is unfavorable for display applications.[134] In this work, a non-FET polymer light-emitting transistor is demonstrated by vertically integrating a top-emitting PLED on a polymer vertical metal-base transistor. The vertical transistor is used to modulate the current and therefore the luminance of the PLED. The grid base voltage variation of 1.8 V is enough to turn on and off the light emitting transistor. Uniform luminance over 1000 cd/m^2 is achieved, fulfilling the requirement for display panel. The current efficiency of the light-emitting transistor is 10 cd/A at yellow emission. The aperture ratio is basically 100 % because the light emitted upward is not shielded by the vertical metal-base transistor underneath with roughly the same area. Light generation in vertical transistor was reported before [137,138], but these early works show very poor luminance and low on/off ratio. The high luminance in this work is achieved by a newly developed vertical polymer light-emitting transistor, the space-charge-limited transistor (SCLT).

Organic vertical metal-base transistors [64,65,68-73,95,99,101,106-110,119,120] with various architectures and operation principles have been developed to overcome the limits of conventional horizontal organic field-effect transistors such as low mobility, long channel length, high operation voltage, and the low operation frequency. The channel length of vertical metal-base transistor is defined by the thickness of the organic layer, and the output current is modulated by a base electrode embedded in the organic semiconductor. Two types of vertical metal-base transistors, namely the hot-carrier transistor [70,71] and space-charge-limited transistor [72,73], show promising performance. In this work the polymer space-charge-limited

transistor is vertically integrated with a PLED. The transistor is in fact a solid-state version of the vacuum tube triode. The carriers are injected from the emitter into the semiconductor, passing through the openings on the metal grid base and finally arriving at the collector. The potential distribution and current flow between emitter and collector is controlled by the voltages of grid. Because of the emitter-collector distance is only tens of nanometers high current output and high speed can be achieved even for low carrier mobility typical for PLED, thus solving the problems of organic field-effect transistors for current output and speed. The fabrication is even simpler than field-effect transistor as no photo-lithography is needed. In this work, the output current of the transistor is enhanced from 1 mA/cm^2 to 27 mA/cm^2 by polymer annealing and surrounding the grid by insulators. In addition the high current output and potentially high speed, SCLT shows far better stability than organic FET. Due to the current channel confinement organic FET characteristics is easily affected by the chemical and physical defects at the gate dielectric-semiconductor interface, SCLT is free from the unpredictable conditions at the dielectric interface because its current is uniformly distributed in the bulk like organic light-emitting diodes.

5.2 Device structure and fabrication

The device structure of the polymer space-charge-limited transistor with an silicon monoxide insulating layer on the aluminum grid is shown in Fig. 5.1. A 400 \AA layer of poly(3,4-ethylenedioxythiophene) doped with polystyrene sulfonated acid (PEDOT:PSS) is spin-coated onto the indium tin oxide (ITO) glass substrate to flatten the ITO surface and serve as the emitter for holes. A layer of 200 \AA P3HT is then spin coated from chlorobenzene solution (1.5 wt %). After annealing at $200 \text{ }^\circ\text{C}$ for 10 min, a spin rinsing with xylene is used to remove the remaining soluble part of P3HT.

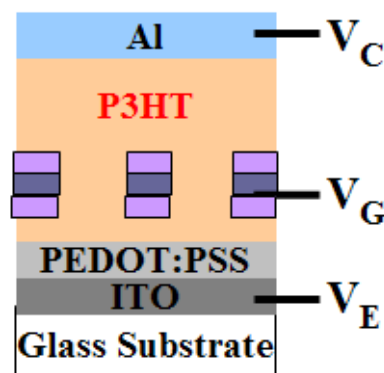


Figure 5.1 Device structure of the polymer space-charge-limited transistor.

The substrate is submerged into 2000 Å (1000 Å) polystyrene spheres ethanol solution with 0.24 wt % (0.4 wt %) for 40 seconds, and then transferred into a beaker with boiling isopropanol solution for 10 s. The substrate is immediately blown dry in a unidirectional nitrogen flow to form two dimensional colloidal arrays without aggregation. After 150 Å Al grid is evaporated as grid, the sample is annealed in high vacuum (10^{-6} torr). 500 Å SiO is evaporated to prevent large leakage current from grid to collector. After the polystyrene spheres are removed by an adhesive tape, another layer of 800 Å P3HT is spin coated from xylene solution (3 wt %). A 400 Å Al collector is finally deposited to complete the polymer space-charge-limited transistor with active area 3 mm². For the light-emitting transistor as shown in Fig. 5.2 and 5.3, the fabrication procedure of the vertical transistor is the same as described above, while the procedures of the PLED are described below. A 30 Å MoO₃ anode is deposited on the Al collector with same shadow mask, followed by spin coating 450 Å PEDOT:PSS from an aqueous solution diluted by isopropanol in equal volume. A surfactant (Zonyl FSN) with 2 wt % is added into the diluted solution to facilitate aqueous PEDOT:PSS solution to be spin on a substrate coated with hydrophobic polymer. Poly(para-phenylene vinylene) polymer derivative (Super Yellow by Merck) is spin coated from toluene as light-emitting layer of 100 nm. The semi-transparent

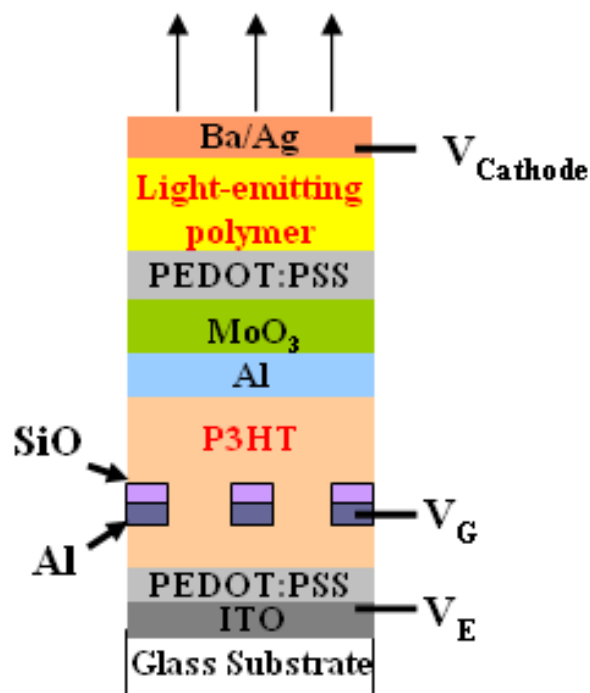


Figure 5.2 Device structure of the top-emitting polymer light-emitting transistor.

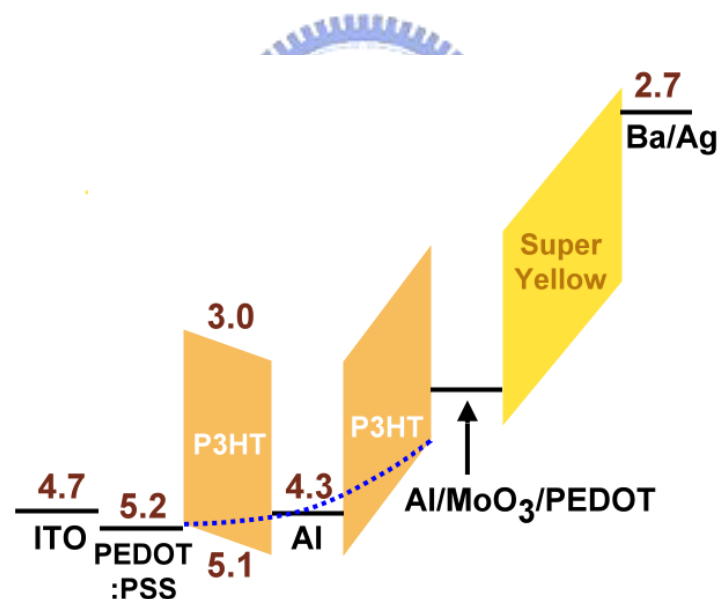


Figure 5.3 Energy profile of the top-emitting polymer light-emitting transistor.

cathode Ba(100 Å)/Ag(150 Å) is then deposited to complete the device with an active area of 4 mm². Due to convenience in mask alignment the LED area is slightly larger than the transistor area of 3 mm². The PEDOT:PSS layer prevents the transistor from being dissolved by the solution of the light-emitting polymer.

5.3 Electrical and optical characteristics

5.3.1 High performance polymer space-charge-limited transistor

The polymer space-charge-limited transistor is in a diode sandwich structure with a third metal base electrode inserted into the semiconductor to control the vertical carrier flow between the emitter and the collector. The collector is always forward-biased relative to the emitter. The space-charge-limited current through the grid opening is modulated when the carriers are expelled back to the emitter by the reversely biased emitter-grid diode. The output current density of the vertical transistor can be enhanced by reducing the polymer layer thickness between PEDOT:PSS and the Al base, using polymer with high vertical mobility, and improving the mobility by optimizing the polymer processing conditions. In this work, additional high vacuum annealing after Al grid deposition is used for increasing the P3HT mobility and current density of ITO/PEDOT:PSS/P3HT/Al diode. The transistor output current can be enhanced from 1 mA/cm² to as high as 27 mA/cm². The improved polymer space-charge-limited transistor with grid opening diameters of 2000 Å is shown in Fig. 5.4. J_C and V_C are the collector current density and collector voltage, respectively. The ITO electrode is commonly grounded and the Al collector is negatively biased at V_C . Various grid voltages is applied to Al grid base to modulate the current. The negative collector current density J_C means the holes flow from the transistor and are collected by the Al collector. To have small grid current density J_G grid voltage V_G is limited to be no more negative than -1 V. Otherwise the emitter-grid diode would turn on. The off-current of the transistor is

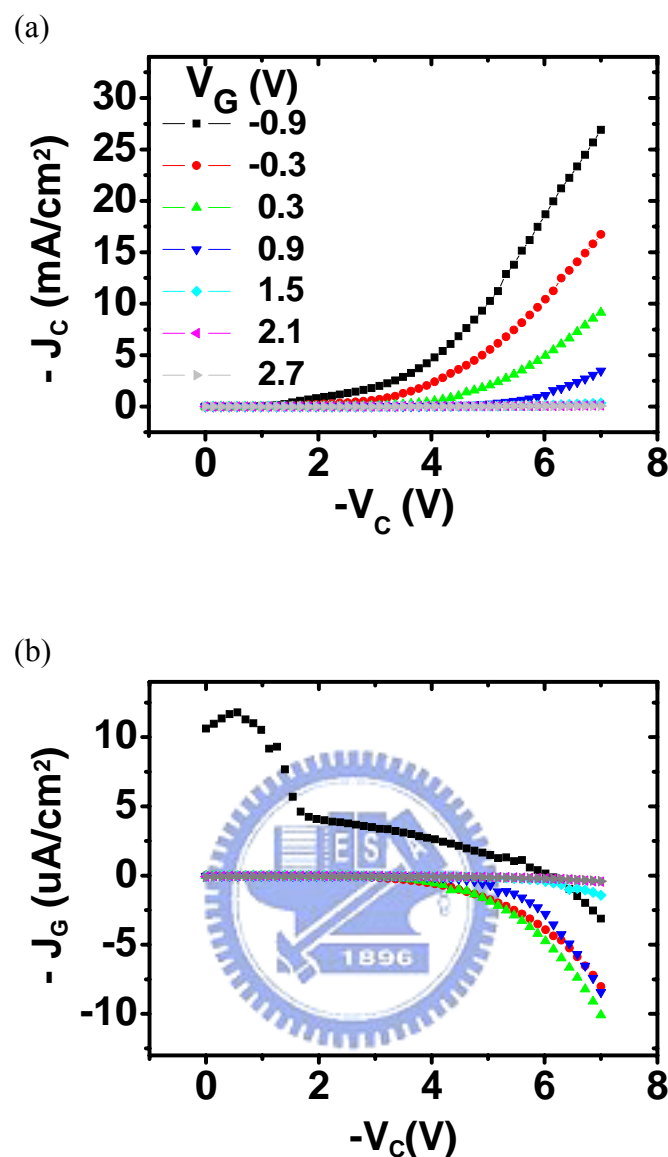


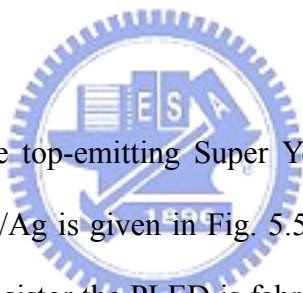
Figure 5.4 The electric characteristics of the polymer space-charge-limited transistor with 2000 °A openings on Al grid. (a) Collector current density J_C and (b) grid current density J_G as a function of collector voltage V_C at various grid bias V_G .

reduced by increasing V_G until a large reverse breakdown current between the grid and collector occurs. An insulating SiO layer is deposited on Al grid to reduce the grid leakage current from Al grid to collector. Such SiO layer allows a higher collector bias and higher output current before grid diode breaks down. When V_C is -7 V and V_G is -0.9 V, the transistor output current density is about 27 mA/cm² and

on/off ratio is 386. The maximum on/off ratio is 428 when V_C is reduced to -6 V. J_G as a function of V_C is also shown in Fig. 5.4(b). The grid current, which is the reverse current of the Al/P3HT Schottly diode. The current gain, defined as J_C/J_G , is around 10^4 . The annealing procedure is expected to have two results. First, annealing in high vacuum causes oxygen dedoping of P3HT. Second, annealing helps the polymer chains to reorganize to have a high mobility and high current density. The collector current density of 27 mA/cm² is about the same as PLED under normal operation. The transistor is therefore able to drive an PLED vertically stacked with roughly the same area.

5.3.2 Light-emitting polymer space-charge-limited

transistor



The characteristics of the top-emitting Super Yellow PLED with the structure PEDOT:PSS/Super Yellow/Ba/Ag is given in Fig. 5.5. The current efficiency is 10.6 cd/A. In the light-emitting transistor the PLED is fabricated on top of the Al collector of SCLT with a MoO₃ layer in between. The electrical characteristics of the polymer light-emitting transistor with opening diameter of 1000 Å and 2000 Å on Al grid are shown in Fig. 5.6(a) and 5.6(b), respectively. This structure is effectively a PLED connected in series to a variable resistor which modulates the PLED current and therefore luminance. The ITO emitter electrode is commonly grounded and various V_G is applied to the Al grid base. The voltage applied to the semi-transparent cathode $V_{Cathode}$ is varied from 0 to -12 V.

Voltage V_C of the Al collector in the SCLT component is floating and determined by the voltage drop across the PLED. It spontaneously matches the currents of the space-charge-limited transistor component and the PLED component.

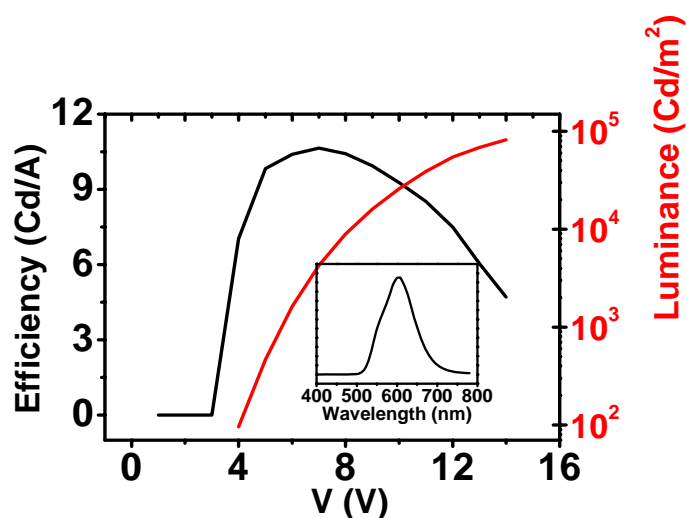


Figure 5.5 The efficiency and luminance of the top-emitting polymer light-emitting diode.

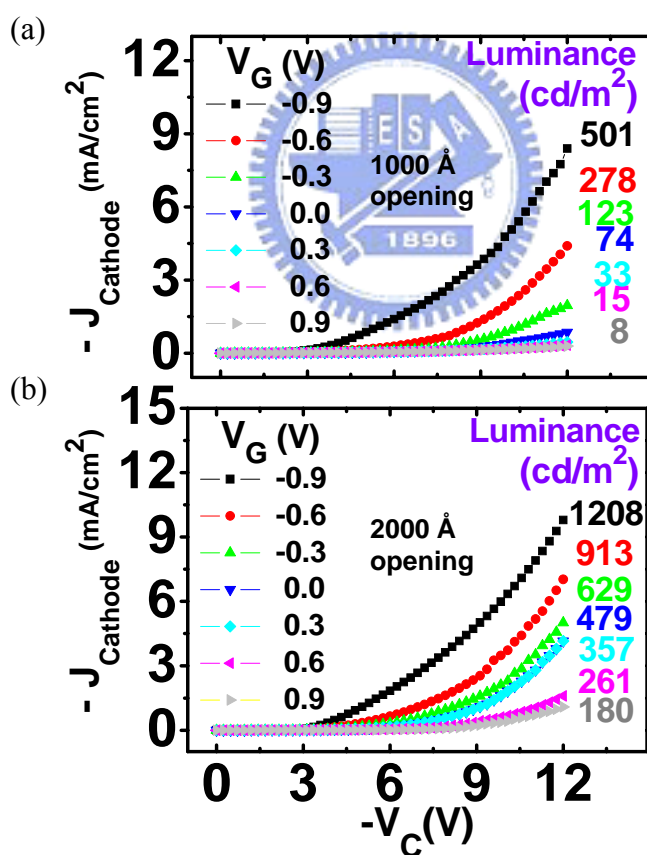


Figure 5.6 The electric characteristics of the polymer light-emitting transistor with (a) 1000 Å and (b) 2000 Å openings on Al grid. The luminance at varies V_G while V_{Cathode} is -12 V are also demonstrated.

The luminance at various V_G for $V_{Cathode}$ at -12 V is shown in Fig. 5.6(a) and 5.6(b). The maximum luminance around 500 cd/m² and 1200 cd/m² is achieved for polymer light-emitting transistor with grid opening diameters of 1000 Å and 2000 Å, respectively. The minimum luminance can be turned off by increasing V_G until large leakage current occurs. This device not only fulfills the minimum luminance requirement for the display panel, but also achieves by far the highest luminance among various light-emitting transistor principles. The on-off contrast of the luminance is yet to be improved. The residual off-luminance can not be switched off by the grid voltage before grid diode breakdown. A stronger insulation of the grid is needed to withstand a more positive grid voltage.

The structure and operation principle of the polymer light-emitting transistor above is different from previous report on static induction transistor [137,138], where the light is emitted inside the channel of the vertical transistor. In our device the light emission and driving are separated into different components of the device with a floating electrode between them. The performance of each component is therefore not compromised by the integration with the other component. The composite electrode Al/MoO₃/PEDOT:PSS layer have two advantages. First, the electrons injected from the cathode will not reach P3HT due to high Schottky barrier between Al and the conduction band of P3HT (see Fig. 5.1). The efficiency and color of the light emission are therefore not ruined by the unwanted recombination in P3HT. Second, the electrons injected from the cathode will not arrive at the Al grid and cause a large J_G and poor current gain.

5.4 Summary of chapter 5

Polymer light-emitting transistor is realized by vertically stacking a top-emitting

polymer light-emitting diode on a polymer space-charge-limited transistor. The transistor modulates the current flow of the light-emitting diode by the metal-grid base voltage. The performance of the polymer space-charge-limited transistor is enhanced by annealing and insulator on grid metal to have high output current density and high current gain. The active semiconductor of the transistor is poly(3-hexylthiophene). Yellow poly(para-phenylene vinylene) derivative is used as the yellow emitting material. As the cathode is fixed at -12 V and the grid base voltage varies from 0.9 V to -0.9 V the light emission is turned on and off with on luminance up to 1208 cd/m². The current efficiency of the light-emitting transistor is 10 cd/A. This transistor has low voltage, high light-emission aperture ratio, and high luminance good enough for display applications.



Chapter 6

Conclusions

Organic semiconductor has been a major world-wide research area since 1990 with great promises to revolutionize the optoelectronic technology. Now the organic light-emitting diode become rather mature and has entered the commercial market. Contrary to OLED, the progress of organic transistors is relatively slow and the gap between research and real applications remain wide. In our view vertical transistors are the ideal concepts for organic and the newly developed oxide semiconductors with the advantages of easy fabrication, high performance, and high stability. It has the great chance to close the gap between research and applications of organic electronic devices. Vertical polymer metal-base transistors were proposed and realized in this thesis to overcome basic obstacles of organic field-effect transistor.

Polymer hot-carrier transistor is demonstrated in Chapter 3. For the hot-carrier transistor with high bandgap conjugated polymer emitter, common-emitter current gain of 25 is obtained with operation voltage as low as 5 V. For the hot-carrier transistor with low bandgap conjugated polymer emitter, maximum common-emitter current gain of 31 and current density as high as 31 mA/cm² is achieved when collector voltage is -10 V. Furthermore, for the device using blend of low and high bandgap polymer as the emitter, the current density rises to 428 mA/cm². The brightness of 3000 cd/m² is obtained as a polymer light-emitting diode is driven by

the transistor with the same area. The transistor can be operated at 100 kHz.

Polymer space-charge-limited transistor is shown in Chapter 4. A metal grid is sandwiched between poly(3-hexylthiophene) to form a solid-state version of vacuum tube triode, where the vertical space-charge-limited current is modulated by the grid potential. The characteristics of the transistor can be tuned by the diameters and the density of the openings on the grid. For the transistor with high opening density, the current density higher than 1 mA/cm^2 is achieved. The operating voltage of the device is 4 V, the on/off ratio is higher than one hundred, and the current gain is 104.

For transistors shown in Chapter 3 and Chapter 4, the active area of vertical metal-base transistors is defined by the overlap of the electrodes. The only thing to do to achieve higher output current is to increase the active area, which can be easily achieved by widening electrodes. Besides, in polymer field-effect transistor, oxygen molecules are easily trapped at the dielectric surface and cause a large off-current of the organic field-effect transistor. The threshold voltage of the polymer field-effect transistor is also affected by the carrier trapping sites at the interface due to various chemical and physical defects. There is no such instability for organic vertical transistor, since the current is not confined near the interface. Indeed the vertical polymer metal-base transistors are highly reproducible and show stable characteristics over long period time. Furthermore, there is a strong reason for us to believe that the lifetime of vertical polymer metal-base transistor should be even better than organic light-emitting diodes because the metal-base transistors are hole-only sandwich devices. In bi-polar device a low workfunction metal cathode like Ca or Li is used for electron injection. Such metals are sensitive to oxygen and moisture. In the hole-only vertical polymer metal-base transistors, there are no low workfunction metals for electron injection. The projected lifetime of organic vertical transistor is expected to be no less than the organic light-emitting diodes. The lifetime of OLED has been

shown to be over 100,000 hours which is more than enough for most applications.

Finally, a light-emitting polymer space-charge-limited transistor is demonstrated in Chapter 5. It is realized by vertically stacking a top-emitting polymer light-emitting diode on a polymer space-charge-limited transistor. The performance of the polymer space-charge-limited transistor is enhanced by annealing and insulator on grid metal to have high output current density and high current gain. The transistor modulates the current flow of the light-emitting diode by the metal-grid base voltage. Luminance up to 1208 cd/m^2 is achieved. The light emission is turned on and off with the grid base voltage varies from -0.9 V to 0.9 V . The current efficiency of the light-emitting transistor is 10 cd/A . This transistor has low voltage, high light-emission aperture ratio, and high luminance good enough for display applications.



References

- [1] H. Shirakawa, E. J. Louis, A. G. MacDiarmid, C. K. Chiang and A. J. Heeger, "Synthesis of electrically conducting organic polymers: halogen derivatives of polyacetylene, (CH)_x", J. Chem. Soc., Chem. Commun., Vol. 1977, pp. 578-580, 1977.
- [2] http://nobelprize.org/nobel_prizes/chemistry/laureates/2000/
- [3] R. H. Friend, R. W. Gymer, A. B. Holmes, J. H. Burroughes, R. N. Marks, C. Taliani, D. D. C. Bradley, D. A. Dos Santos, J. L. Bredas, M. Logdlund, W. R. Salaneck, "Electroluminescence in conjugated polymers", Nature, Vol. 397, pp. 121-128, 1999.
- [4] Y. Ohmori, M. Uchida, K. Muro, and K. Yoshino, "Blue Electroluminescent Diodes Utilizing Poly(alkylfluorene)", Jpn. J. Appl. Phys., Vol. 30, pp. L1941-L1943, 1991.
- [5] D. Braun, G. Gustafsson, D. McBranch, and A. J. Heeger, "Electroluminescence and electrical transport in poly(3-octylthiophene) diodes", J. Appl. Phys., Vol. 72, pp. 564-568, 1992.
- [6] K. Sethuraman, S. Ochiai, K. Kojima, and T. Mizutani, "Performance of poly(3-hexylthiophene) organic field-effect transistors on cross-linked poly(4-vinyl phenol) dielectric layer and solvent effects", Appl. Phys. Lett., Vol. 92, pp. 183302, 2008.
- [7] M. Pope, H. P. Kallmann, and P. Magnante, "Electroluminescence in Organic Crystals", J. Chem. Phys., Vol. 38, pp. 2042-2043, 1963.
- [8] C. W. Tang and S. A. VanSlyke, "Organic electroluminescent diodes", Appl. Phys. Lett., Vol. 51, pp. 913-915, 1987.
- [9] C. W. Tang and S. A. VanSlyke, "Degradation mechanism of small molecule-based organic light-emitting devices", Science, Vol. 283, pp. 1900-1902, 1999.
- [10] W. L. Yu, J. Pei, Y. Cao, and W. Huang, "Hole-injection enhancement by copper phthalocyanine (CuPc) in blue polymer light-emitting diodes", J. Appl. Phys., Vol. 89, pp. 2343-2350, 2001.
- [11] Y. Hamada, N. Matsusue, H. Kanno, H. Fujii, T. Tsujioka, and H. Takahashi, "Improved Luminous Efficiency of Organic Light-Emitting Diodes by Carrier

- Trapping Dopants”, Jpn. J. Appl. Phys., Vol. 40, pp. L753-L755, 2001.
- [12] D. J. Gundlach, J. E. Royer, S. K. Park, S. Subramanian, O. D. Jurchescu, B. H. Hamadani, A. J. Moad, R. J. Kline, L. C. Teague, O. Kirillov, C. A. Richter, J. G. Kushmerick, L. J. Richter, S. R. Parkin, T. N. Jackson, and J. E. Anthony, “Contact-induced crystallinity for high-performance soluble acene-based transistors and circuits”, Nature Mater., Vol. 7, pp. 216 - 221, 2008.
- [13] S. Steudel, K. Myny, V. Arkhipov, C. Deibel, S. D. Vusser, J. Genoe, and P. Heremans, “50 MHz rectifier based on an organic diode”, Nature Mater., Vol. 4, pp. 597-600, 2005.
- [14] J. B. Chang, V. Liu, V. Subramanian, K. Sivula, C. Luscombe, A. Murphy, J. Liu, and J. M. J. Frechet, “Printable polythiophene gas sensor array for low-cost electronic noses”, J. Appl. Phys., Vol. 100, pp. 014506, 2006.
- [15] H. Sirringhaus, N. Tessler, and R. H. Friend, “Integrated Optoelectronic Devices Based on Conjugated Polymers”, Science, Vol. 280, pp. 1741-1744, 1998.
- [16] A. Dodabalapur, Z. Bao, A. Makhija, J. G. Laquindanum, V. R. Raju, Y. Feng, H. E. Katz, and J. Rogers, “Organic smart pixels”, Appl. Phys. Lett., Vol. 73, pp. 142-144, 1998.
- [17] K. L. Tzeng, H. F. Meng, M. F. Tzeng, Y. S. Chen, C. H. Liu, S. F. Horng, Y. Z. Yang, S. M. Chang, C. S. Hsu, and C. C. Chi, “One-polymer active pixel”, Appl. Phys. Lett., Vol. 84, pp. 619-621, 2004.
- [18] Z. L. Li, S. C. Yang, H. F. Meng, Y. S. Chen, Y. Z. Yang, C. H. Liu, S. F. Horng, C. S. Hsu, L. C. Chen, J. P. Hu, and R. H. Lee, “Patterning-free integration of polymer light-emitting diode and polymer transistor”, Appl. Phys. Lett., Vol. 84, pp. 3558-3560, 2004.
- [19] J. H. Burroughes, D. D. C. Bradley, A. R. Brown, R. N. Marks, K. Mackay, R. H. Friend, P. L. Burns, and A. B. Holmes, “Light-emitting diodes based on conjugated polymers”, Nature, Vol. 347, pp. 539-541, 1990.
- [20] F. F. So and S. R. Forrest, “Evidence for exciton confinement in crystalline organic multiple quantum wells”, Phys. Rev. Lett., Vol. 66, pp. 2649-2652, 1991.
- [21] G. He, O. Schneider, D. Qin, X. Zhou, M. Pfeiffer, and K. Leo, “Very high-efficiency and low voltage phosphorescent organic light-emitting diodes based on a p-i-n

- junction”, J. Appl. Phys., Vol. 95, pp. 5773-5777, 2004.
- [22] S. R. Tseng, S. C. Lin, H. F. Meng, H. H. Liao, C. H. Ye, H. C. Lai, and S. F. Horng, “General method to solution-process multilayer polymer light-emitting diodes”, Appl. Phys. Lett., Vol. 88, pp. 163501, 2006.
- [23] R. N. Marks, J. J. M. Halls, D. D. C. Bradley, R. H. Friend and A. B. Holmes, “The photovoltaic response in poly(p-phenylene vinylene) thin-film devices”, J. Phys.: Condens. Matter, Vol. 6, pp. 1379-1394, 1994.
- [24] K. M. Coakley, and M. D. McGehee, “Conjugated Polymer Photovoltaic Cells”, Chem. Mater., Vol. 16, pp. 4533-4542, 2004.
- [25] N. S. Sariciftci, D. Braun, C. Zhang, V. I. Srdanov, A. J. Heeger, G. Stucky, and F. Wudl, “Semiconducting polymer-buckminsterfullerene heterojunctions: Diodes, photodiodes, and photovoltaic cells”, Appl. Phys. Lett., Vol. 62, pp. 585-587, 1993.
- [26] J. J. M. Halls, C. A. Walsh, N. C. Greenham, E. A. Marseglia, R. H. Friend, S. C. Moratti, and A. B. Holmes, “Efficient photodiodes from interpenetrating polymer networks”, Nature, Vol. 376, pp. 498-500, 1995.
- [27] G. J. de A. A. Soler-Illia, A. Louis, and C. Sanchez, “Synthesis and Characterization of Mesostructured Titania-Based Materials through Evaporation-Induced Self-Assembly”, Chem. Mater., Vol. 14, pp. 750-759, 2002.
- [28] P. C. A. Alberius, K. L. Frindell, R. C. Hayward, E. J. Kramer, G. D. Stucky, and B. F. Chmelka, “General Predictive Syntheses of Cubic, Hexagonal, and Lamellar Silica and Titania Mesostructured Thin Films”, Chem. Mater., Vol. 14, pp. 3284-3294, 2002.
- [29] H. Sirringhaus, T. Kawase, R. H. Friend, T. Shimoda, M. Inbasekaran, W. Wu, and E. P. Woo, “High-Resolution Inkjet Printing of All-Polymer Transistor Circuits”, Science, Vol. 290, pp. 2123-2126, 2000.
- [30] A. Facchetti, “Semiconductors for organic transistors”, Materials Today, Vol. 10, pp. 28-37, 2007.
- [31] A. Salleo, “Charge transport in polymeric transistors”, Materials Today, Vol. 10, pp. 38-45, 2007.
- [32] Y. D. Parka, J. A. Lima, H. S. Leea, and K. Cho, “Interface engineering in organic transistors”, Materials Today, Vol. 10, pp. 46-54, 2007.

- [33] H. E. Katz, "Organic molecular solids as thin film transistor semiconductors", J. Mater. Chem., Vol. 7, pp. 369-376, 1997.
- [34] A.R. Brown, C.P. Jarrett, D.M. de Leeuw, and M. Matters, "Field-effect transistors made from solution-processed organic semiconductors", Synth. Metal., Vol. 88, pp. 37-55, 1997.
- [35] F. Garnier, "Thin-film transistors based on organic conjugated semiconductors", Chem. Phys., Vol. 227, pp. 253-262, 1998.
- [36] G. Horowitz, "Organic Field-Effect Transistors", Adv. Mater., Vol. 10, pp. 365-377, 1998.
- [37] C.D. Dimitrakopoulos, and P.R.L. Malenfant, "Organic Thin Film Transistors for Large Area Electronics", Adv. Mater., Vol. 14, pp. 99-117, 2002.
- [38] H. Sirringhaus, P. J. Brown, R. H. Friend, M. M. Nielsen, K. Bechgaard, B. M. W. Langeveld-Voss, A. J. H. Spiering, R. A. J. Janssen, E. W. Meijer, P. Herwig, and D. M. de Leeuw, "Two-dimensional charge transport in self-organized, high-mobility conjugated polymers", Nature, Vol. 401, pp. 685-688, 1999.
- [39] R. J. Kline, M.D. McGehee, E.N. Kadnikova, J. Liu, and J.M.J. Frechet, "Controlling the Field-Effect Mobility of Regioregular Polythiophene by Changing the Molecular Weight", Adv. Mater., Vol. 15, pp. 1519-1522, 2003.
- [40] Y. D. Parka, D. H. Kima, Y. Janga, J. H. Choa, M. Hwanga, H. S. Leea, J. A. Lima, and K. Cho, "Effect of side chain length on molecular ordering and field-effect mobility in poly(3-alkylthiophene) transistors", Org. Electron., Vol. 7, pp. 514-520, 2006.
- [41] R. J. Kline, M. D. McGehee, and M. F. Toney, "Highly oriented crystals at the buried interface in polythiophene thin-film transistors", Nat. Mater., Vol. 5, pp. 222-228, 2006.
- [42] J. J. Apperloo, R. A. J. Janssen, M. M. Nielsen, and K. Bechgaard, "Doping in Solution as an Order-Inducing Tool Prior to Film Formation of Regio-Irregular Polyalkylthiophenes", Adv. Mater., Vol. 12, pp. 1594-1597, 2000.
- [43] Y. D. Park, J. H. Cho, D. H. Kim, Y. Jang, H. S. Lee, K. Ihm, T. H. Kang, and K. Cho, "Energy-Level Alignment at Interfaces Between Gold and Poly(3-hexylthiophene) Films with Two Different Molecular Structures", Electrochem. Solid-State Lett., Vol.

- 9, pp. G317-G319, 2006.
- [44] H. Sirringhaus, P. J. Brown, R. H. Friend, M. M. Nielsen, K. Bechgaard, B. M. W. Langeveld-Voss, A. J. H. Spiering, R. A. J. Janssen, and E. W. Meijer, "Microstructure–mobility correlation in self-organized, conjugated polymer field-effect transistors", *Synth. Metal.*, Vol. 111-112, pp. 129-132, 2002.
- [45] T. W. Kelly, P. F. Baude, C. Gerlach, D. E. Ender, D. Muires, M. A. Hasse, D. E. Vogel, and S. D. Theiss, "Recent Progress in Organic Electronics: Materials, Devices, and Processes", *Chem. Mater.*, Vol. 16, pp. 4413-4422, 2004.
- [46] M. Halik, H. Klauk, U. Zschieschang, G. Schmid, P. S. Onomarenko, S. Kirchmeyer, and W. Weber, "Synthesis of Vertical High-Density Epitaxial Si(100) Nanowire Arrays on a Si(100) Substrate Using an Anodic Aluminum Oxide Template", *Adv. Mater.*, Vol. 15, pp. 917-920, 2003.
- [47] H. Meng, J. Zheng, A. J. Lovinger, B.-C. Wang, P. G. V. Patten, and Z. Bao, "Oligofluorene-Thiophene Derivatives as High-Performance Semiconductors for Organic Thin Film Transistors", *Chem. Mater.*, Vol. 15, pp. 1783-1787, 2003.
- [48] A. R. Murphy, J. M. J. Frecht, P. Chang, J. Lee, and V. Subramanian, "Organic Thin Film Transistors from a Soluble Oligothiophene Derivative Containing Thermally Removable Solubilizing Groups", *J. Am. Chem. Soc.*, Vol. 126, pp. 1596-1597, 2004.
- [49] H. Meng, F. Sun, M. B. Goldfinger, F. Gao, D. J. Londono, W. J. Marshall, G. S. Blackman, K. D. Dobbs, and D. E. Keys, "2,6-Bis[2-(4-pentylphenyl)vinyl]anthracene: A Stable and High Charge Mobility Organic Semiconductor with Densely Packed Crystal Structure", *J. Am. Chem. Soc.*, Vol. 128, pp. 9304-9305, 2006.
- [50] M. M. Payne, S. R. Parkin, J. E. Anthony, C.-C. Kuo, and T. N. Jackson, "Organic Field-Effect Transistors from Solution-Deposited Functionalized Acenes with Mobilities as High as $1 \text{ cm}^2/\text{V}\cdot\text{s}$ ", *J. Am. Chem. Soc.*, Vol. 127, pp. 4986-4987, 2005.
- [51] D. H. Kim, D. Y. Lee, H. S. Lee, W. H. Lee, Y. H. Kim, J. I. Han, and K. Cho, "High-Mobility Organic Transistors Based on Single-Crystalline Microribbons of Triisopropylsilylethynyl Pentacene via Solution-Phase Self-Assembly", *Adv. Mater.*,

- Vol. 19, pp. 678-682, 2007.
- [52] B. H. Hamadani, D. J. Gundlach, I. McCulloch, and M. Heeney, "Undoped polythiophene field-effect transistors with mobility of $1 \text{ cm}^2/\text{V}\cdot\text{s}$ ", *Appl. Phys. Lett.*, Vol. 91, pp. 243512, 2007.
- [53] I. McCulloch, M. Heeney, C. Bailey, K. Genevicius, I. MacDonald, M. Shkunov, D. Sparrowe, S. Tierney, R. Wagner, W. Zhang, M. L. Chabinye, R. J. Kline, M. D. McGehee, and M. F. Toney, "Liquid-crystalline semiconducting polymers with high charge-carrier mobility", *Nature Mater.*, Vol. 5, pp. 328-333, 2006.
- [54] M. Halik, H. Klauk, U. Zschieschang, G. Schmid, C. Dehm, M. Schütz, S. Maisch, F. Effenberger, M. Brunnbauer, and F. Stellacci, "Low-voltage organic transistors with an amorphous molecular gate dielectric", *Nature*, Vol. 431, pp. 963-966, 2004.
- [55] H. Klauk, U. Zschieschang, J. Pflaum, and M. Halik, "Ultralow-power organic complementary circuits", *Nature*, Vol. 445, pp. 745-748, 2007.
- [56] Y. Zhang, J.R. Petta, S. Ambily, Y. Shen, D.C. Ralph, and G.G. Malliaras, "30 nm Channel Length Pentacene Transistors", *Adv. Mater.*, Vol. 15, pp. 1632-1635, 2003.
- [57] M. D. Austin, and S. Y. Chou, "Fabrication of 70 nm channel length polymer organic thin-film transistors using nanoimprint lithography", *Appl. Phys. Lett.*, Vol. 81, pp. 4431-4433, 2002.
- [58] J. Zaumseil, T. Someya, Z. Bao, Y.-L. Loo, R. Cirelli, and J. A. Rogers, "Nanoscale organic transistors that use source/drain electrodes supported by high resolution rubber stamps", *Appl. Phys. Lett.*, Vol. 82, pp. 793-795, 2003.
- [59] N. Stutzmann, R. H. Friend, and H. Sirringhaus, "Self-Aligned, Vertical-Channel, Polymer Field-Effect Transistors", *Science*, Vol. 299, pp. 1881-1884, 2003.
- [60] R. Parashkov, E. Becker, G. Ginev, T. Riedl, M. Brandes, H.-H. Johannes, and W. Kowalsky, "Organic vertical-channel transistors structured using excimer laser", *Appl. Phys. Lett.*, Vol. 85, pp. 5751-5753, 2004.
- [61] R. Parashkov, E. Becker, S. Hartmann, G. Ginev, D. Schneider, H. Krautwald, T. Dobbertin, D. Metzdorf, F. Brunetti, C. Schildknecht, A. Kammoun, M. Brandes, T. Riedl, H.-H. Johannes, and W. Kowalsky, "Vertical channel all-organic thin-film transistors", *Appl. Phys. Lett.*, Vol. 82, pp. 4579-4580, 2003.
- [62] M. S. Meruvia, I. A. Hümmelgen, M. L. Sartorelli, A. A. Pasa, and W. Schwarzacher,

- “Organic-metal-semiconductor transistor with high gain”, Appl. Phys. Lett., Vol. 84, pp. 3978-3980, 2003.
- [63] K. I. Nakayama, S. Y. Fujimoto, and M. Yokoyama, “High-current and low-voltage operation of metal-base organic transistors with LiF/Al emitter”, Appl. Phys. Lett., Vol. 88, pp. 153512, 2006.
- [64] K. Kudo, D. X Wang, M. Iizuka, S. Kuniyoshi, and K. Tanaka, “Schottky gate static induction transistor using copper phthalocyanine films”, Thin Solid Films, Vol. 331, pp. 51-54, 1998.
- [65] Y. Watanabe, and K. Kudo, “Flexible organic static induction transistors using pentacene thin films”, Appl. Phys. Lett., Vol. 87, pp. 223505, 2005.
- [66] N. Hirashima, N. Ohashi, M. Nakamura, and K. Kudo, “Fabrication of organic vertical-type field-effect transistors using polystyrene spheres as evaporation mask”, IPAP Conf. Series, Vol. 6, pp. 158-169, 2005.
- [67] K. Fujimoto, T. Hiroi, and M. Nakamura, “Organic static induction transistors with nano-hole arrays fabricated by colloidal lithography”, e-J. Sci. Nanotech., Vol. 3, pp. 327-331, 2005.
- [68] K. Fujimoto, T. Hiroi, K. Kudo, and M. Nakamura, “High-performance, vertical-type organic transistors with built-in nanotriode arrays”, Adv. Mater., Vol. 19, pp. 525-530, 2007.
- [69] Y. Yang, and A. J. Heeger, “A new architecture for polymer transistors”, Nature, Vol. 372, pp. 344-346, 1994.
- [70] Y. C. Chao, S. L. Yang, H. F. Meng, and S. F. Horng, “Polymer hot-carrier transistor”, Appl. Phys. Lett., Vol. 87, pp. 253508, 2005.
- [71] Y. C. Chao, M. H. Xie, M. Z. Dai, H. F. Meng, S. F. Horng, and C. S. Hsu, “Polymer hot-carrier transistor with low bandgap emitter”, Appl. Phys. Lett., Vol. 92, pp. 093310, 2008.
- [72] Y. C. Chao, H. F. Meng, and S. F. Horng, “Polymer space-charge-limited transistor”, Appl. Phys. Lett., Vol. 88, pp. 223510, 2006.
- [73] Y. C. Chao, H. F. Meng, S. F. Horng, and C. S. Hsu, “Polymer hot-carrier transistor with low bandgap emitter”, Org. Electronics, Vol. 9, pp. 310-316, 2008.
- [74] L. B. Smilowitz, “Conjugated polymers: modern electronic materials”, IEEE

- Circuits and Devices Magazine, Vol. 10, pp. 19-23, 1994.
- [75] H. G. Kiess, Conjugated conducting polymers, Springer-Verlag, New York, 1992.
- [76] A. J. Heeger, S. Kivelson, J. R. Schrieffer, and W. P. Su, "Solitons in conducting polymers", Rev. Mod. Phys., Vol. 60, pp. 781-850, 1988.
- [77] A. J. Heeger, "Charge storage and charge transport in conducting polymers: solitons, polarons and bipolarons", Phil. Trans. R. Soc. Lond. A, Vol. 314, pp. 17-35, 1985.
- [78] S. M. Sze, Semiconductor Devices: Physics and Technology, Wiley, New York, 2002.
- [79] A. B. Walker, A. Kambili, and S. J. Martin, "Electrical transport modelling in organic electroluminescent devices", J. Phys.: Condens. Matter, Vol. 14, pp. 9825-9876, 2002.
- [80] S. M. Sze, Physics of Semiconductor Devices, Wiley, New York, 1981.
- [81] Ehrenreich, Solid State Physics, Academic Press, New York, 1995.
- [82] K. C. Kao, and W. Hwang, Electrical transport in solids : with particular reference to organic semiconductors, Pergamon Press, New York, 1981.
- [83] M. A. Lampert, and P. Mark, Current Injection in Solids, Academic Press, New York, 1970.
- [84] J. Millman, Vacuum-tube and semiconductor electronics, McGRAW-HILL, New York, 1958.
- [85] N. F. Mott, and R. W. Gurney, Electronic processes in ionic crystals, Clarendon Press, Oxford, 1940.
- [86] M. Pope, and C. E. Swenberg, Electronic processes in organic crystals and polymers, Oxford University Press, Oxford, 1999.
- [87] W. Brutting, S. Berleb, and A. G. Muckl, "Device physics of organic light-emitting diodes based on molecular materials", Org. Electron., Vol. 2, pp. 1-36, 2001.
- [88] P. N. Murgatroyd, "Theory of space-charge-limited current enhanced by Frenkel effect", J. Phy. D: Appl. Phys., Vol. 3, pp. 151-156, 1970.
- [89] H. A. Al Attar, and A. P. Monkman, "Dopant Effect on the Charge Injection, Transport, and Device Efficiency of an Electrophosphorescent Polymeric Light-Emitting Device", Adv. Funct. Mater., Vol. 16, pp. 2231-2242, 2006.
- [90] J. Shinar, Organic light-emitting devices, Springer, New York, 2004.

- [91] S. R. Forrest, D. D. C. Bradley, and M. E. Thompson, "Measuring the efficiency of organic light-emitting devices", Adv. Mater., Vol. 15, pp. 1043-1048, 2003.
- [92] L. S. Hung, and C. H. Chen, "Recent progress of molecular organic electroluminescent materials and devices", Mater. Sci. Eng., R, Vol. 39, pp. 143-222, 2002.
- [93] B. Geffroy, P. Roy, and C. Prat, "Organic light-emitting diode technology: materials, devices and display technologies", Polym. Int., Vol. 55, pp. 572-582, 2006.
- [94] G. Horowitz, "Organic field-effect transistors", Adv. Mater., Vol. 10, pp. 365-377, 1998.
- [95] K. K. Ng, Complete guide to semiconductor devices, IEEE Press, New York, 2002.
- [96] M. Jacob, Vacuum-tube and semiconductor electronics, McGRAW-HILL, New York, 1958.
- [97] D. Voss, "Cheap and cheerful circuits", Nature, Vol. 407, pp. 442 - 444, 2000.
- [98] D. V. Geppert, "A metal-base transistor", Proc. IRE, Vol. 50, pp. 1527-1528, 1962.
- [99] M. S. Meruvia, I. A. Hümmelgen, M. L. Sartorelli, A. A. Pasa, and W. Schwarzacher, "Pseudo-metal-base transistor with high gain", Appl. Phys. Lett., Vol. 86, pp. 263504, 2005.
- [100] L. P. Ma, J. Liu, S. M. Pyo, and Y. Yang, "Organic bistable light-emitting devices", Appl. Phys. Lett., Vol. 80, pp. 362-364, 2002.
- [101] L. P. Ma and Y. Yang, "Unique architecture and concept for high-performance organic transistors", Appl. Phys. Lett., Vol. 85, pp. 5084-5086, 2004.
- [102] S. M. Sze, C. R. Crowell, G. P. Carey, and E. E. LaBate, "Hot-Electron Transport in Semiconductor-Metal-Semiconductor Structures", J. Appl. Phys., Vol. 37, pp. 2690-2695, 1966.
- [103] C. R. Crowell, and S. M. Sze, "Electron-optical-phonon scattering in the emitter and collector barriers of semiconductor-metal-semiconductor structures", Solid-State Electron., Vol. 8, pp. 979-990, 1965.
- [104] C. R. Crowell, and S. M. Sze, "Quantum-Mechanical Reflection of Electrons at Metal-Semiconductor Barriers: Electron Transport in Semiconductor-Metal-Semiconductor Structures", J. Appl. Phys., Vol. 37, pp. 2683-2689, 1966.
- [105] D. D. Rathman, "Optimization of the doping profile in Si permeable base

- transistors for high-frequency, high-frequency, high-voltage operation”, IEEE Trans. Electron Devices, Vol. 37, pp. 2090-2098, 1990.
- [106] S. Fujimoto, K. Nakayama, and M. Yokoyama, “Fabrication of a vertical-type organic transistor with a planar metal base”, Appl. Phys. Lett., Vol. 87, pp. 133503, 2005.
- [107] M. Yi, S. Yu, C. Feng, T. Zhang, D. Ma, M. S. Meruvia, and I. A. Hümmelgen, “High gain in hybrid transistors with vanadium oxide/tris(8-hydroxyquinoline) aluminum emitter”, Org. Electron., Vol. 8, pp. 311-316, 2007.
- [108] S. S. Cheng, C. Y. Yang, Y. C. Chuang, C. W. Ou, M. C. Wu, S. Y. Lin, and Y. J. Chan, “Influence of thin metal base thickness on the performance of CuPc vertical organic triodes”, Appl. Phys. Lett., Vol. 90, pp. 153509, 2007.
- [109] T. M. Ou, S. S. Cheng, C. Y. Huang, M. C. Wu, I. M. Chan, S. Y. Lin, and Y. J. Chan, “All-organic hot-carrier triodes with thin-film metal base”, Appl. Phys. Lett., Vol. 89, pp. 183508, 2006.
- [110] C. Y. Yang, T. M. Ou, S. S. Cheng, M. C. Wu, S. Y. Lin, I. M. Chan, and Y. J. Chan, “Vertical organic triodes with a high current gain operated in saturation region”, Appl. Phys. Lett., Vol. 89, pp. 183511, 2006.
- [111] S. C. Tse, S. W. Tsang, and S. K. So, “Polymeric conducting anode for small organic transporting molecules in dark injection experiments”, J. Appl. Phys., Vol. 100, pp. 063708, 2006.
- [112] S. Rentenberger, A. Vollmer, E. Zojer, R. Schennach, and N. Koch, “UV/ozone treated Au for air-stable, low hole injection barrier electrodes in organic electronics”, J. Appl. Phys., Vol. 100, pp. 053701, 2006.
- [113] F. Li, H. Tang, J. Andereg, and J. Shinar, “Fabrication and electroluminescence of double-layered organic light-emitting diodes with the Al₂O₃/Al cathode”, Appl. Phys. Lett., Vol. 70, pp. 1233-1235, 1997.
- [114] W. Osikowicz, M. P. de Jong, S. Braun, C. Tengstedt, M. Fahlman, and W. R. Salaneck, “Energetics at Au top and bottom contacts on conjugated polymers”, Appl. Phys. Lett., Vol. 88, pp. 193504, 2006.
- [115] S. E. Shaheen, G. E. Jabbour, M. M. Morrell, Y. Kawabe, B. Kippelen, N. Peyghambarian, M.F. Nabor, R. Schlaf, E. A. Mash, and N. R. Armstrong, “Bright

- blue organic light-emitting diode with improved color purity using a LiF/Al cathode”, J. Appl. Phys., Vol. 84, pp. 2324-2327, 1998.
- [116] B. Crone, A. Dodabalapur, Y.-Y. Lin, R. W. Filas, Z. Bao, A. LaDuca, R. Sarpeshkar, H. E. Katz, and W. Li, “Large-scale complementary integrated circuits based on organic transistors”, Nature, Vol. 403, pp. 521-523, 2000.
- [117] L. L. Chua, R. H. Friend, and P. K. H. Ho, “Organic double-gate field-effect transistors: Logic-AND operation”, Appl. Phys. Lett., Vol. 87, pp. 253512, 2005.
- [118] J. Park, S. Y. Park, S.-O. Shim, H. Kang, and H. H. Lee, “A polymer gate dielectric for high-mobility polymer thin-film transistors and solvent effects”, Appl. Phys. Lett., Vol. 85, pp. 3283-3285, 2004.
- [119] K. Kudo, S. Tanaka, M. Iizuka, and M. Nakamura, “Fabrication and device characterization of organic light emitting transistors”, Thin Solid Films, Vol. 438, pp. 330-333, 2003.
- [120] J. McElvain, M. Keshavarz, H. Wang, F. Wudl, and A. J. Heeger, “Fullerene-based polymer grid triodes”, J. Appl. Phys., Vol. 81, pp. 6468-6472, 1997.
- [121] W. Shockley, “Transistor electronics: Imperfections, unipolar and analog transistors”, Proc. IRE, Vol. 40, pp. 1289-1313, 1952.
- [122] J. S. Kim, R. H. Friend, I. Grizzi, and J. H. Burroughes, “Spin-cast thin semiconducting polymer interlayer for improving device efficiency of polymer light-emitting diodes”, Appl. Phys. Lett., Vol. 87, pp. 023506, 2005.
- [123] S. A. Choulis, V.-E. Choong, M. K. Mathai, and F. So, “The effect of interfacial layer on the performance of organic light-emitting diodes”, Appl. Phys. Lett., Vol. 87, pp. 113503, 2005.
- [124] J. Z. Wang, Z. H. Zheng, H. W. Li, W. T. S. Huck, H. Sirringhaus, “Dewetting of conducting polymer inkjet droplets on patterned surfaces”, Nature Mater., Vol. 3, pp. 171-176, 2004.
- [125] Y. Xia, B. Gates, Y. Yin, and Y. Lu, “Monodispersed Colloidal Spheres: Old Materials with New Applications”, Adv. Mater., Vol. 12, pp. 693-713, 2000.
- [126] C. Werdinius, L. Österlund, and B. Kasemo, “Nanofabrication of Planar Model Catalysts by Colloidal Lithography: Pt/Ceria and Pt/Alumina”, Langmuir, Vol. 19, pp. 458 - 468, 2003.

- [127] Z. Chiguvare, and V. Dyakonov, “Trap-limited hole mobility in semiconducting poly(3-hexylthiophene)”, Phys. Rev. B, Vol. 70, pp. 235207, 2007.
- [128] E. J. Meijer, A. V. G. Mangnus, C. M. Hart, D. M. de Leeuw, and T. M. Klapwijk, “Frequency behavior and the Mott–Schottky analysis in poly(3-hexyl thiophene) metal–insulator–semiconductor diodes”, Appl. Phys. Lett., Vol. 78, pp. 3902-3904, 2001.
- [129] B. Mattis, P. Chang, and V. Subramanian, “Performance recovery and optimization of poly(3-hexylthiophene) transistors by thermal cycling”, Synth. Met., Vol. 156, pp. 1241-1248, 2006.
- [130] T. K. Chuang, M. Troccoli, P. C. Kuo, A. Jamshidi-Roudbari, M. K. Hatalis, I. Biaggio, and A. T. Voutsas, “Top-emitting 230 dots/in. active-matrix polymer light-emitting diode displays on flexible metal foil substrates”, Appl. Phys. Lett., Vol. 90, pp. 151114, 2007.
- [131] L. Zhou, A. Wanga, S. C. Wu, J. Sun, S. Park, and T. N. Jackson, “All-organic active matrix flexible display”, Appl. Phys. Lett., Vol. 88, pp. 083502, 2006.
- [132] M. L. Chabynec, F. Endicott, B. D. Vogt, D. M. DeLongchamp, E. K. Lin, Y. Wu, P. Liu, and B. S. Ong, “Effects of humidity on unencapsulated poly(thiophene) thin-film transistors”, Appl. Phys. Lett., Vol. 88, pp. 113514, 2006.
- [133] A. Dodabalapur, H. E. Katz, L. Torsi, and R. C. Haddon, “Organic heterostructure Field-effect transistors”, Science, Vol. 269, pp. 1560-1562, 1995.
- [134] J. Zaumseil, R. H. Friend, and H. Sirringhaus, “Spatial control of the recombination zone in an ambipolar light-emitting organic transistor”, Nature Mater., Vol. 5, pp. 69-74, 2006.
- [135] F. Cicoira, and C. Santato, “Organic Light Emitting Field Effect Transistors: Advances and Perspectives”, Adv. Funct. Mater., Vol. 17, pp. 3421-3434, 2007.
- [136] C. A. Di, G. Yu, Y. Q. Liu, X. J. Xu, D. C. Wei, Y. B. Song, Y. M. Sun, Y. Wang, and D. B. Zhu, “Organic Light-Emitting Transistors Containing a Laterally Arranged Heterojunction”, Adv. Funct. Mater., Vol. 17, pp. 1567-1573, 2007.
- [137] Z. Xu, S. H. Li, L. Ma, G. Li, and Y. Yang, “Vertical organic light emitting transistor”, Appl. Phys. Lett., Vol. 91, pp. 092911, 2007.
- [138] K. Kudo, “Organic light emitting transistors”, Current Appl. Phys., Vol. 5, pp.

337-340, 2005.

